Tsunami Impact on a Coastal Building and Effect of Spatial Configuration of the Building on Acting Tsunami Force

Chathura Manawasekara

Supervised by

Prof. Norimi Mizutani

Costal and Ocean Engineering Laboratory

Department of Civil Engineering

Nagoya University

Japan

ACKNOWLEDGEMENT

First of all, I would like to convey my sincere gratitude to my supervisor Prof. Norimi Mizutani for the encouragement, supervision and support all throughout the study period which immensely helped me to understand the subject and improve myself. I am also thankful to Assoc. Prof. Koji Kawasaki and Assoc. Prof. Tomoaki Nakamura for their kind and generous support for the study, in both material and knowledge wise.

I would like to extend my gratitude to the dissertation committee, which consist of Prof. Norimi Mizutani (Head), Prof. Tetsuro Tsujimoto, Assoc. Prof. Koji Kawasaki, Assoc. Prof Tomoaki Nakamura of Nagoya University and Prof. Takehisa Saito of Kanazawa University, for their valuable comments, suggestions, review and guidance for this study.

I also appreciate the supporting and friendly environment and the excellent research facilities at Coastal and Ocean Engineering Laboratory of Nagoya University which chaired by Prof. Norimi Mizutani. At the same time, I was able to learn the subject and improve my abilities through numerous laboratory activities like weekly seminars and discussions. I also thankful to Information and Communication Headquarters of Nagoya University for their consistent support, in accessing super computing system.

I acknowledge the sincere support from Dr. Masami Kiku and Mr. Kazuki Suzuki of Coastal and Ocean Engineering Laboratory in cases of technical and general difficulties and accessing computer facilities. I also appreciate the cooperation and help from Mr. Satoru Aoki and Dr. Gyeong-Song Yeom in the study and thankful to all the lab members of Coastal and Ocean Engineering laboratory for their sincere friendship and support.

I also grateful to Japanese Government for providing me the financial support to study in Japan, through Monbukagakusho Scholarship programme.

At the same time, I deeply appreciate the unconditional friendship and support of Mr. Chinthaka, Mr. Kensuke Kamata, Mr. Enhyou, Ms. Maw maw Win & Ms. Nadia Orion of Nagoya University, in my trouble and happiness.

Last for but not least, I like to express my heartily gratitude to my parents, sister and brother for understanding me and providing all the encouragement and support to study abroad.

ABSTRACT

Tsunami Impact on a Coastal Building and Effect of Spatial Configuration of the Building on Acting Tsunami Force

Recent tsunami events of December 2004 Indian Ocean tsunami and March 2011 Tohoku earthquake tsunami have highlighted the magnitude of the destruction associated with the great waves. Vast damage to the coastal buildings in those events has raised the question of capability of coastline buildings to withstand against tsunami wave force. In most of the cases it was evident that the wreckage of the destroyed buildings has increased the damage to the surrounding buildings. On the other hand, well-constructed coastline buildings have the added advantage of using as a tsunami evacuation structures and as well as a frontline barrier for tsunami.

This study mainly focuses on simulating the interaction between tsunami and the coastline buildings. Even though numbers of past studies have been carried out on this area, there are still doubts on the understanding the tsunami interaction with structures because of its dynamic and complex behavior, and in design the infrastructure accordingly. Understanding the response of a coastline building and the variation in acting tsunami force with regards to the structural arrangement and configuration of the building, under tsunami event will provide a clear guidance to effective design, especially in the construction of structures like tsunami evacuation buildings. At the same time, the reliability of existing tsunami force estimation formula in estimating the tsunami force on three-dimensional building is discussed and suggested modifications are presented.

LS-DYNA, three dimensional nonlinear finite element modeling code is used and Arbitrary Lagrangian and Eulerian (ALE) algorithms are applied in the tsunami-structure modeling. Fluid-structure interaction is discussed. The failure mechanism of basic structural components of a reinforced concrete building is analyzed in order to develop a process to understand the tsunami interaction with comprehensive building in the future.

Keywords*: Tsunami force, fluid-structure interaction, ALE algorithms, structural failure*

Table of Contents

Chapter 1

INTRODUCTION

1.1 Background and Motivation

Near-coast areas are the most common and favored areas for living all around the world. According to the statistics, Hinrichsen (1999) indicated that, by 1998, nearly about 3.2 billion of the world human population works and lives in a 200 km wide coastal strip. Accordingly, most of the important and functional infra-structures are also located within the area. Therefore, any sort of vulnerability of the coastal community for the disastrous situations, has always drawn the attention and been under tremendous concern.

Especially, the sensitivity of the coastal community to the natural disasters in the kind of tsunami has proven to be very high with past events. The December 2004 Indian Ocean and the March 2011 Tohoku earthquake tsunamis have exposed the vulnerability of the coastal communities in a large coastal strip of Indian and Pacific Oceans. In addition, highly populated countries such as Indonesia and Japan have regularly suffered by tsunami mainly due to their geographical location to the under-sea earthquake sources. By 1997 out of the total population of 126 million in Japan, nearly 80% (~100 million) are considered to live in coastal area (Hinrichsen, 1999). Even though the probability of occurrence for a natural event like tsunami lies in the lower side, the concentrated coastal population and physical properties have increased the possible damage. Especially, with the devastation caused by the 2011 Tohoku earthquake tsunami, large attention is paid upon the protection of such coastal communities and serious questions have been raised on the reliability of existing techniques and methods on the defense against tsunami. Meanwhile, with the current

predictions of Tokai, Tonankai and Nankai earthquakes (Fig. 1.1), which will affect large portion of the Pacific coastal belt of Japan, including major commercial and industrial cities such as Nagoya and Osaka, the urgency has been increased on the re-evaluation of existing damage estimation and safety methods in the protection against tsunami.

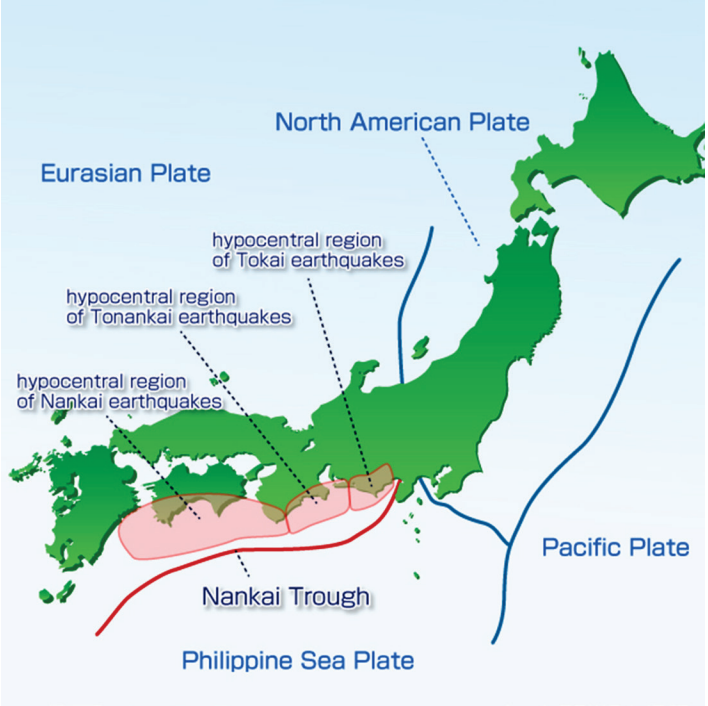

Fig. 1.1 Tectonic plates around Japan and possible future earthquake regions
(Source: http://www.jamstec.go.jp/donet/rendou/en/about/)

Since the highly populated coastal areas generally consist of buildings and other infra-structures, it has become a great concern that effective use of such structures in an event of tsunami in terms of maintaining the stability and minimizing the damage to the structure itself. Fig. 1.2 shows the damage to the coastal city of Rikuzentakata (Iwate prefecture, Japan) following the event of 2011 Tohoku earthquake tsunami. It is clearly visible the complete washout of the city and the topographical change of the area at the incident.

Majority of the coastline protection structures that had been installed and the coastline buildings were proven to be ineffective during the tsunami event and vast amount of damage was observed from frontline coastal protection structure to primary wooden house, as far as coastal structures are concerned. It was also evident that the

large amount of floating debris and wreckage which came with the on-land tsunami flow has increased the damage in the up-ward areas from the coast.

Fig. 1.2. Coastal city of Rikuzentakata, Iwate prefecture before (above) and after (below) 2011 Tohoku tsunami (Picture courtesy of Google Earth / GeoEye)

At the same time, with narrow and limited evacuation time due to the near tsunami source has forced to find the shelters within the flat coastland and resistance and stability of coastal buildings under such conditions had been valued. Especially, the damage and failure of reinforced concrete structures under tsunami loading have increased the wreckage and also have degrade the possibility of effective evacuation.

Fig. 1.3 shows some damage to the coastal buildings observed during the 2011 Tohoku earthquake tsunami event.

Fig. 1.3. Damage to the coastal buildings during 2011 Tohoku tsunami (left: Yuriage, Miyagi Prefecture, right: Taro, Iwate prefecture)

Various types of failures to the buildings have been observed and Nishiyama et al. (2011) categorized the damage to the reinforced concrete buildings during the 2011 Tohoku earthquake tsunami, through the results observed in the field surveys. They classified damage to the reinforced concrete buildings mainly into six categories as, collapse of first floor, overturning, movement and wash away, tilting by scouring, fracture of the wall and debris impact. The damage statistics in the tsunami inundated area in 2011 Tohoku earthquake tsunami which extracted from this particular study are shown in Table 1.2.

1.2 Literature Review

Considering the resistance of coastal buildings against tsunami, number of past studies has been carried out to estimate the acting tsunami force on the structures. Asakura et al. (2000) did experimental study on wave force acting on on-shore structures due to tsunami. Based on the experiments, they proposed an empirical formula to estimate the maximum tsunami wave pressure acting on the structures (Eq. 1.1). Cabinet office of Japanese government (2006) published a design guideline for tsunami evacuation buildings and in the guideline, the acting tsunami pressure is calculated considering the hydrostatic pressure distribution for a flow depth three times than of maximum tsunami inundation depth, based on Asakura et al. (2000).

$$p_{max}(z) = (3\eta_{max} - z)\rho g \tag{1.1}$$

Table 1.1. Damage statistics in tsunami inundated area in 2011 Tohoku earthquake tsunami (Nishiyama, 2011)

Prefecture	City, Town, Village	Human Damage			House Damage			
		Dead	Missing	Injury	Complete Destruction or Missing	Partial Damage	Below Partial Damage	Fire
Aomori	Hachinohe	1	1	17	250	769		2
	Hashikami	0	0	0	12	8	1	
	Total	1	1	17	262	777	1	2
Iwate	Hirono	0	0	0	10	16	5	
	Kuji	2	2	8	65	210		
	Noda	38		17	309	169		1
	Hudai	0	1	1				
	Tanohata	14	19	8	225	45	4	
	Miyako	420	124	33	3,669	1,006	176	6
	Yamada	597	256	Unknown	2,789	395	120	2
	Otsuchi	796	653	Unknown	3,677			2
	Kamaishi	881	299	Unknown	3,188	535	120	
	Ofunato	331	118	Unknown	3,629		Unknown	2
	Rikuzentakata	1,546	569	Unknown	3,159	182	27	
	Total	4,625	2,041	67	20,720	2,558	452	13
Miyagi	Kesen-numa	1,004	410	Unknown	8,533	2,313	3,248	8
	Minamisanriku	550	437	Unknown	3,167	144	Unknown	5
	Onagawa	535	414	2	2,939	337	640	5
	Isinomaki	3,153	890	Unknown	19,065	3,354	10,199	23
	Higashimatsushima	1,044	104	Unknown	4,589	4,672	2,471	1
	Matsushima	2	0	37	213	1,321	1,184	2
	Rifu	1	1	1	59	508	1,732	
	Shiogama	20	1	10	682	2,784	3,973	8
	Shichigahama	66	6	Unknown	729	460	1,067	
	Tagajo	188	3	Unknown	1,662	2,993	5,097	15
	Sendai	704	33	2,276	19,922	41,344	56,347	39
	Natori	911	82	Unknown	2,786	922	8,060	12
	Iwanuma	183	1	293	720	1,545	2,403	1
	Watari	256	5	44	2,459	1,032	1,985	3
	Yamamoto	670	23	90	2,200	1,042	1,086	2
	Total	9,287	2,410	2,753	69,725	64,771	99,492	124
Fukushima	Shinchi	107	3	3	548	Unknown		
	Soma	454	5	71	1,049	643	3,092	
	Minamisoma	633	38	59	4,682	975		
	Namie	141	43					
	Futaba	29	6	1	58	5		
	Okuma	73	1		30			
	Tomioka	19	6					
	Naraha	11	2	5	50			
	Hirono	2	1		Unknouwn	Unknown		
	Iwaki	308	39	4	6,585	18,931	21,800	3
	Total	1,777	144	143	13,002	20,554	24,892	3
Ibaraki	Kitaibaraki	5	1	188	339	1,569	5,745	3
	Takahagi	1		19	131	728	3,213	
	Hitachi			166	403	3,016	11,229	4
	Tokai	4		5	56	104	3,150	2
	Hitachinaka	2		27	79	720	5,863	1
	Oarai	1		6	10	268	1,087	
	Hokota			15	96	524	4,863	3
	Kajima	1			368	1,726	2,567	4
	Kamisu			6	139	1,660	3,011	3
	Total	14	1	432	1,621	10,315	40,728	20
Chiba	Choshi			19	23	105	1,938	
	Asahi	13	2	12	336	931	2,358	
	Total	13	2	31	359	1,036	4,296	0
Sum Total		15,717	4,599	3,443	105,689	100,011	169,861	162

where, p_{max} is the maximum tsunami wave pressure $(0 \leq z/\eta_{max} \leq 3)$; z is the height from the ground level; $\eta_{max}$is the maximum inundation depth; ρ is the mass per unit volume of water; and g is the gravitational acceleration. The basic idea of the method is to invisibly include the dynamic effects in to hydrostatic pressure calculations.

Ikeno et al. (2001) introduced an equation for tsunami wave pressure estimation without soliton fission. In the experiment, pressure was estimated by a bore wave generated by dam break scenario while a still water level was maintained at outside the tank at the beginning. Ohmori (2000) performed a time history analysis for the experiment data from Asakura (2000) and proposed an equation to estimate the tsunami force, which consists of drag force, inertia force, impulse force and hydraulic gradient force.

In considering the damage to the coastal buildings, Shuto (1993) presented a estimation of damage to the coastal houses in terms of tsunami height and type of house (Fig. 1.4). The estimation was based on the collected data of post-tsunami surveys in the past. The types of houses were considered in the study were (i) wood, (ii) stone, brick and concrete block, (iii) stone and steel, (iv) reinforced concrete and (v) iron. However this output was presented with limited number of data for the reinforced concrete structures.

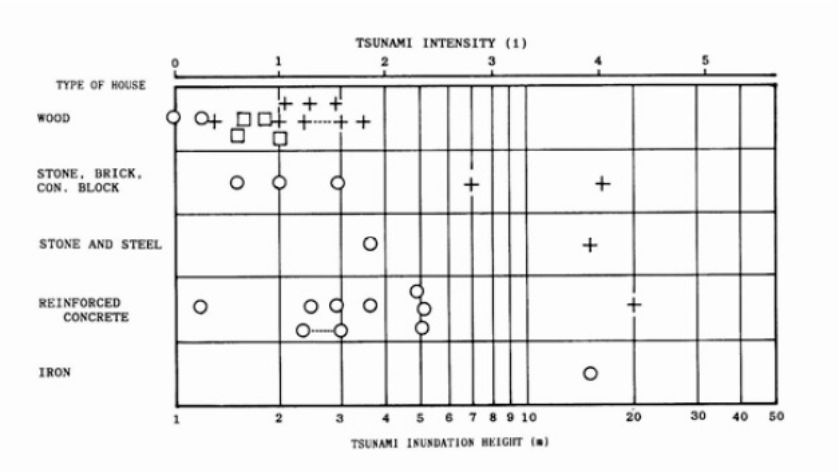

Fig. 1.4. Classification of damage to houses. Circles - withstand, Squares - partially damaged, Crosses - washed away (Shuto, 1993).

Iizuka and Matsutomi (2000) tried to express the damage to houses in terms of drag force (Eq. 1.2) estimated from the difference between front and rear inundation

heights (Table 1.1). Drag force was evaluated based on the damages of houses due to the recent past tsunami, occurred in Japan.

$$F_d = \frac{1}{2}\rho C_D U^2 H_f B_h \tag{1.2}$$

where, F_d is the horizontal drag force; C_D is the drag coefficient (= 1.1~2.0) ; U is the velocity in inland; ρ is the mass per unit volume of water; H_f is the inundation depth in front of the building/house; B_h is the width of the structure.

Table 1.2. Damage to houses in terms of inundation depth (H_f), current velocity (U) and drag force (F_d).

Type of Building	Partially destroyed			Completely destroyed		
	H_f (m)	U (m/s)	F_d (kN/m)	H_f (m)	U (m/s)	F_d (kN/m)
Reinforced concrete building	-	-	-	> 7.0	> 9.1	332~603
Concrete block building	3.0	6.0	60.7~111	7.0	9.1	332~603
Wooden house	1.5	4.2	15.6~27.4	2.0	4.9	27.4~49.0

Out of all these tsunami force estimation methods, it can be noted Asakura et al. (2000) estimation as more convenient application due to its simplicity as a function of inundation depth. In addition, Nakano (2008) conducted post-tsunami damage survey following the 2004 Indian Ocean Tsunami disaster to verify Asakura's formula with the real damage observations. In the study, the lateral strengths of structures in the affected areas, the tsunami load computed by the design formula considering tsunami inundation depth and the observed damage were compared. It has been found that the design coefficient (which is 3) given in the design formula compares well with the criteria between damaged and survived structures in the tsunami affected areas, even though the estimation by the design formula can be unreliable due to the on-site effects such as effect of floating debris. However, hydraulic experiment study conducted by Fujima et al. (2009) suggested that the integrating maximum wave pressure envelope may cause maximum tsunami force to be overestimated, because of the irregularity of the wave when it hit the structure which causes standing-wave pressure at different points to peaks at different time. Three tsunami force estimation equations were proposed in the study. Further, Nakamura (2013) estimated tsunami-

induced wave pressure and force acting on an instrumented specimen fronted by macro-roughness elements, through a numerical study. Study showed that the arrangement of macro-roughness elements can increase the inundation depth in front of the specimen which can increase the acting maximum wave pressure on the specimen. This particular study has an special concern which the arrangement of coastal buildings can affect the acting maximum tsunami force on the nearby buildings.

Arikawa (2009) conducted real scale physical model experiments in the large Hydro-Geo flume in Port and Airport Research Institute, Japan, to examine the failure process of wooden and concrete walls under tsunami force. In the study, it was found that the failure of the wooden wall under impulsive tsunami loading is explosive and tsunami also destroy the reinforced concrete wall with the thickness from 6 to 10 mm. The study also revealed that, unlike wooden wall concrete wall failed partially resulting in a punched-out hole near the bottom and if the strength of the concrete wall is small, the failure pattern will be bending or punching shear. However, when the strength of the concrete wall is increasing, the failure mode was found to be shifting from local failure to whole destruction. The study also highlighted the importance of understanding the wall failure process in design considerations against tsunami.

Sakakiyama et al. (2009) performed an experiment study to assess the tsunami force acting on oil tanks and the buckling of oil tanks due to tsunami pressure was evaluated using a general-purpose nonlinear finite element analysis program ABAQUS. Further, Yim and Zhang (2009) developed a multiphysics multiscale finite-element based nonlinear computational wave basin model using LS-DYNA. Predictive capability of the model was calibrated using laboratory fluid-structure interaction experiments. Good quantitative predictions have been observed from the simulation. The study also highlighted the high computational load of LS-DYNA when perform Arbitrary Lagrange Eulerian (ALE) simulations and necessity to take actions to reduce computational cost. Meanwhile, Yeom et al. (2009) proposed a drift collision coupled model consisting of LS-DYNA and successfully analyzed the collision process of containers drifting due to run-up tsunami.

1.3 Study Objectives

As it is described above, current tsunami force estimating methods have certain drawbacks when it comes to the practical applications. The currently recommended design formula of Asakura et al. (2000) has been defined based upon the physical experiments for two-dimensional structures. Therefore, the current study aims to assess the effectiveness of this design formula for three-dimensional structures. At the same time, the acting tsunami force on a building such as tsunami evacuation structure can be varied upon the structural configuration and arrangement of structural components. Therefore, the variation of tsunami force under such effect of building configurations are aim to assess through both laboratory experiments and numerical simulation.

Further attention is paid upon developing a fluid-structure interaction model using Arbitrary Lagrangian Eulerian (ALE) method in nonlinear finite element code LS-DYNA to understand tsunami interaction with structures. Available experimental results are used in the verification of re-producing ability of the developed scheme. The failure of a reinforced concrete structure under tsunami loading is simulated with the developed computational scheme. The study aims at providing a sound contribution for the development of a design guideline for buildings such as tsunami shelters.

Therefore, the basic study objectives can be summarized as follows,

a) Assess the effect of spatial configurations of a building on the acting tsunami force.
b) Study the effectiveness of existing tsunami force estimation formula in estimating the acting tsunami force on three-dimensional structures.
c) Conduct tsunami-structure interaction simulation to study the failure of reinforced concrete structure under tsunami loading and assess the applicability of numerical model for real scale situations.

1.4 Thesis Outline

The present study investigates the effect of spatial configuration of a coastal building in the estimation of acting tsunami force and simulates the tsunami-structure

interaction in order to understand the acting tsunami force and structural failure under tsunami loading.

Chapter 2 discusses the background of the numerical study. Three-dimensional numerical model developed by Lee et al. (2010) was used for the numerical analysis to estimate the behavior of acting tsunami force on three-dimensional rigid structure, which is discussed in detail under Chapter 4. Three-dimensional nonlinear finite element model LS-DYNA is used in the failure analysis of reinforced concrete structure under tsunami loading. The tsunami-structure interaction model is coupled with the three-dimensional numerical model developed by Nakamura & Yim (2011) in order to reduce the extensive computational cost of LS-DYNA simulation.

In Chapter 3, the 1:50 scaled laboratory experiments conducted in order to assess the tsunami interaction with multi-story building, is discussed. The effect variation of tsunami inflow condition and the configurations of the building, in the estimation of acting tsunami forced are assessed and presented in the chapter.

Chapter 4 discusses the numerical study conducted in the aim of evaluating the acting tsunami force on three-dimensional structure. The commonly used tsunami force estimation equation (Eq. 1.1) by Asakura et al. (2000), which is based on the two-dimensional laboratory experiments, is modified for a three-dimensional structure, considering the blockage ratio. Three-dimensional numerical model developed by Lee et al. (2010) is used for the numerical analysis and results are presented.

In Chapter 5, the failure of reinforced concrete structure under tsunami loading is discussed. Three-dimensional nonlinear finite element model LS-DYNA is used in the tsunami-structure interaction analysis and Arbitrary Lagrange Eulerian (ALE) method is used in solving the fluid-structure interaction (FSI). The three-dimensional numerical model developed by Nakamura & Yim (2011) is coupled with the FSI model in order to reduce the computational cost and the reproducibility of the combined model is verified comparing with the full-scale laboratory experiments conducted by Arikawa (2009). The developed model is applied to study the tsunami force acting on the lateral walls of enclosed structure and results are discussed.

Finally, in Chapter 6 the conclusions and discussion with the recommendations for the future research are presented.

Chapter 2

NUMERICAL METHODS

2.1 General

As it is explained in the previous chapter, a primary objective of this study is to simulate the tsunami-structure interaction and examine the behavior of tsunami force acting on structures, which will eventually leads to understand the failure mechanism of concrete structures due to tsunami loading. Because of the complexity of the phenomena and the continuous change of fluid domain with time and the moving interface, fluid-structure interaction simulations have been quite challenging for the researchers. So far, the finite element analysis (FEA) which is the practical application of finite element method (FEM) has become the most recognized approach especially in structural analysis due to numerical stability and its ability to accurately represent complex physical quantities. Three-dimensional finite element code LS-DYNA (Hallquist, 2006) is employed in the current study. Compared to the other well-known commercial structural analysis software such as SAP2000, ANSYS, MSC.DYTRAN, ABAQUS, etc., LS-DYNA has shown more reliable with fluid-structure interaction (FSI) modeling capabilities. The software was originally developed by the Lawrence Livermore National Laboratory as DYNA3D (Hallquist, 1976) and later Livermore Software Technology Corporation was founded to continue the development of DYNA3D as a commercial version which re-named as LS-DYNA. The model has been undergone number of improvements and modifications with time and mostly used in impact analysis simulation such as bird impact (Huertas-Ortecho, 2006), bomb blast impact (Borvik et al., 2009), vehicle collision (El-Tawil et al., 2005), etc. The current study employs the Arbitrary Lagrangian Eulerian (ALE) solution method which has much better edge in FSI modeling because of its combined

advantage of both Lagrangian algorithms and Eulerian algorithms. In this particular way it helps to minimize the drawbacks of each individual method in the simulation.

2.2 Lagrangian Description

In Lagrangian description each node in the computational domain follows the material during the motion. Therefore, elements and materials translate, rotate, and deform together (Fig. 2.1; top raw). It allows easy tracking of interface and free surface of the materials and mostly applied in structural mechanic simulations. Since the material does not cross element boundaries, the mass of material within element remain unchanged during the simulation. The major drawback of the description is its inability to follow large distortions of the computational domain without special treatments.

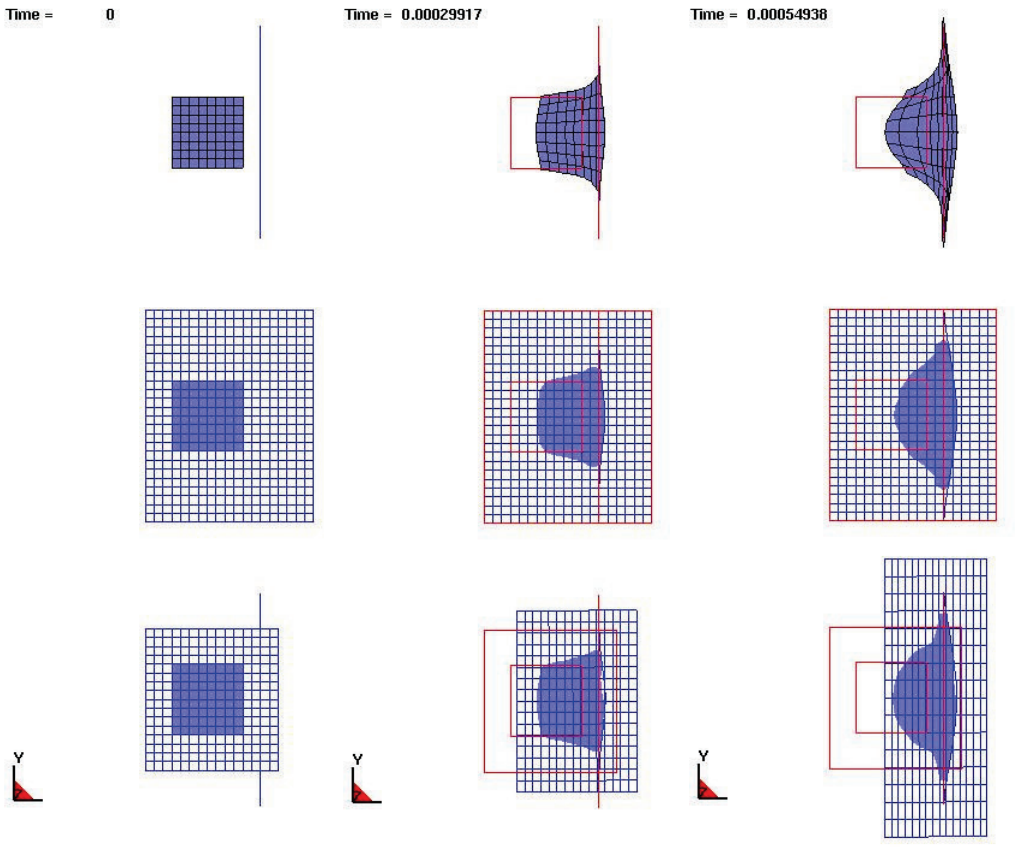

Fig. 2.1. Water projectile (blue) strikes a fixed plate simulation in Lagrangian (top raw), Eulerian (middle raw) and ALE descriptions. (Day, 2009)

2.3 Eulerian Description

In Eulerian description, a computational mesh is fixed in the space and the material moves with respect to the grid. Therefore materials are allowed to cross element boundaries and it can move and deform within the fixed mesh (Fig. 2.1; middle raw). Because of its ability to handle large distortions of the continuum motion with relative ease, Eulerian algorithms are widely used in fluid dynamic simulations. Generally, computational cost is relatively high because of precise interface definition and high resolution requirement for the details of flow.

2.4 Arbitrary Lagrange Eulerian (ALE) Description

ALE description basically consists of three types of domains in space (Souli, 2010), which are called as spatial domain, material domain and reference domain (Fig. 2.1; bottom raw). The spatial domain (the domain which general problem takes place) is generally in motion and the material domain is to be considered as the domain occupied at time t=0 by the material particles which occupy the spatial domain at time t. Meanwhile, the reference domain is defined as a fixed domain throughout the computation. Therefore, basically both spatial and material domains are in motion with respect to the reference domain. Nodes in the spatial domain can be moved with the material (as Lagrangian description) or can be set fixed (as Eulerian description) or can be moved in some arbitrary specified way. Because of this ability, ALE algorithms can handle large distortions of the materials with much ease than that of purely Lagrangian method and can handle more resolution than that of purely Eulerian method. Based on these reasons it can be clearly noted that the ALE method is more effective in simulating fluid-structure interaction problems.

2.4.1 Governing Equations

The material derivative for the ALE description (Souli et al., 2000) can be introduced as,

$$\frac{\partial f(X_i,t)}{\partial t} = \frac{\partial f(x_i,t)}{\partial t} + w_i \frac{\partial f(x_i,t)}{\partial x_i} \tag{2.1}$$

where X is Lagrangian coordinate and x is Eulerian coordinate. $w_i = v_i - u_i$ is introduced as relative velocity, where v is the velocity of the material and u is the velocity of the mesh. Governing equations for the ALE formulation can be described as follows, equation for the mass conservation,

$$\frac{\partial \rho}{\partial t} = -\rho \frac{\partial v}{\partial x_i} - w_i \frac{\partial \rho}{\partial x_i} \tag{2.2}$$

Navier-Stokes equation for fluids, which governs the motion,

$$\frac{\partial v}{\partial t} = -\left(\frac{\partial \sigma_{ij}}{\partial x_j} + \rho b_i\right) - \rho w_i \frac{\partial v_i}{\partial x_j} \tag{2.3}$$

Stress tensor σ_{ij} in Eq. (2.3) can be introduced as,

$$\sigma_{ij} = -p\delta_{ij} + \mu\left(\frac{\partial v_i}{\partial x_j} + \frac{\partial v_j}{\partial x_i}\right) \tag{2.4}$$

Equation for the conservation of total energy,

$$\frac{\partial E}{\partial t} = -\left(\sigma_{ij} v_{i,j} + \rho b_i v_j\right) - \rho w_j \frac{\partial E}{\partial x_j} \tag{2.5}$$

where ρ is the density of fluid; μ is the coefficient of kinematic viscosity; p is the pressure; b_i is the body force and E is the energy.

2.5 Fluid-Structure Coupling

A penalty coupling method is applied in the current study, at the fluid-structure interface which Lagrange mesh behaves as a moving boundary for the fluid. Following the construction of coupling interfaces on both Lagrangian and ALE fluid sides, a penetration based algorithm is executed to estimate the interaction force. A penalty force which is proportional to the relative displacement d_i between two interfaces is applied on each interface for the separation until it satisfies a certain acceptable pre-declared maximum penetration requirement. This method is simply equivalent to placing springs at the each coupling point for the interaction and once the penalty spring stiffness γ_i is known the penalty force p_i can be estimated as,

$$p_i = \gamma_i d_i \tag{2.6}$$

The algorithm flow chart for fluid-structure interaction analysis is shown in Fig. 2.2.

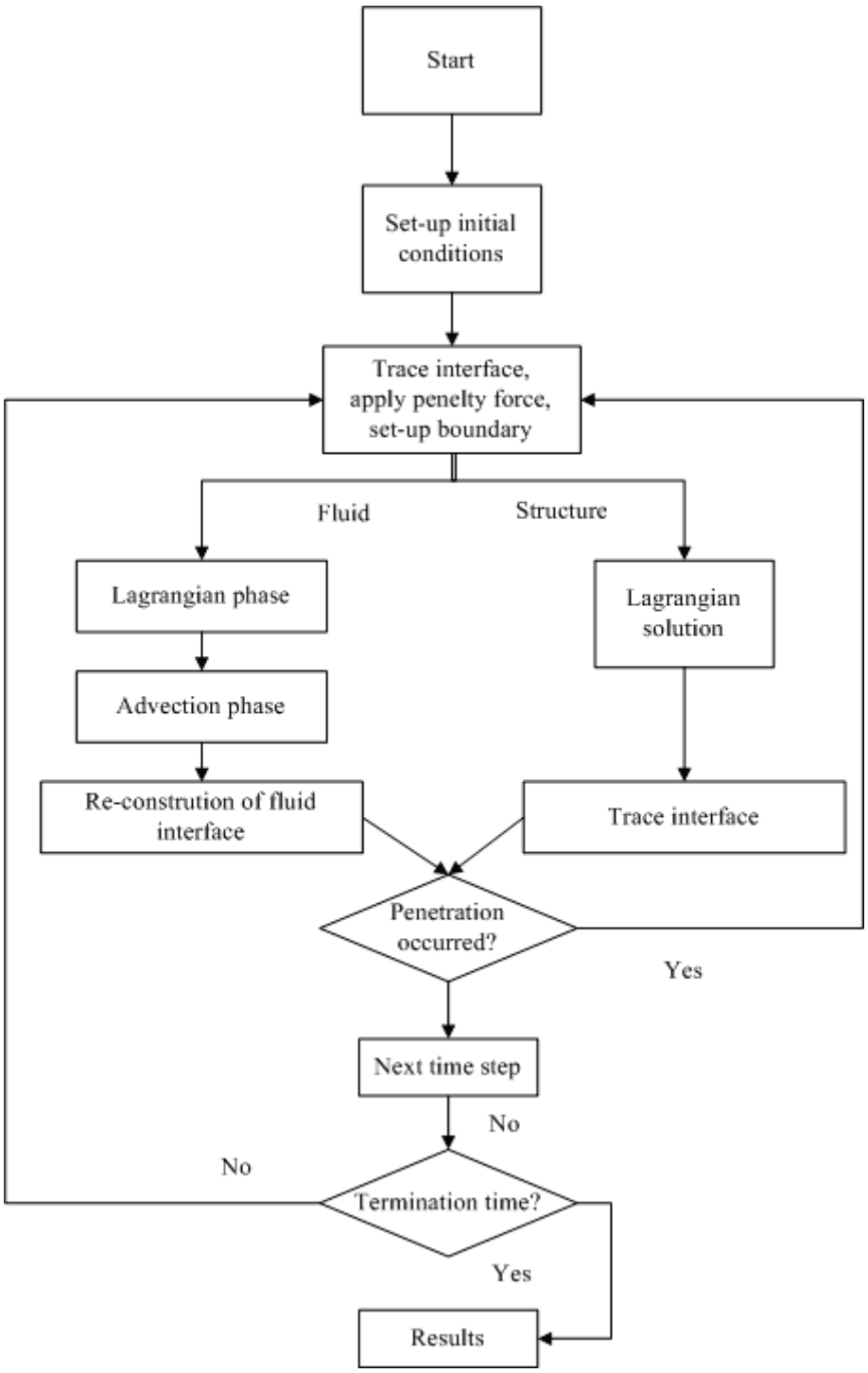

Fig. 2.2. Fluid-structure interaction algorithm flow chart

2.6 Sub Model for Tsunami Generation and Propagation

ALE fluid-structure interaction (FSI) calculations in LS-DYNA is often time consuming (Lin, 2002). Because of this computationally intensive behavior, appropriate computational techniques should be adopted to perform a comprehensively effective simulation. Yim and Zhang (2009) developed a half-basin model, optimizing symmetric basin geometry to reduce required simulation time, which eventually reduced the simulation time by an average of 26%. In the current study, a three-dimensional nonlinear fluid model developed by Nakamura and Yim (2011) was adopted as a sub model for tsunami generation and propagation. The model coupled with the FSI model at a location prior to the interaction while considering the recommendations by Yeom (2010). Even though the initial model includes the effect of porosity of solid, current study utilized only pure fluid (m = 1) and impermeable solids (m = 0) conditions for the simulation.

2.6.1 Governing equations

Continuity equation (2.7), generalized Navior-Stokes equation (2.8) and advection equation of the volume of fluid (VOF) function (2.9) are as follows

$$\frac{\partial(mv_j)}{\partial x_j} = q^* \tag{2.7}$$

$$\begin{aligned}\{m + C_A(1-m)\}\frac{\partial v_i}{\partial t} + \frac{\partial(mv_i v_j)}{\partial x_j} \\ = -\frac{m}{\hat{\rho}}\frac{\partial p}{\partial x_i} - mg_i + \frac{m(f_i^s + R_i)}{\hat{\rho}} + \frac{\partial(-m\tau_{ij}^a + 2m\hat{\nu}D_{ij})}{\partial x_j} + Q_i \\ + m\beta_{ij}v_j\end{aligned} \tag{2.8}$$

$$m\frac{\partial F}{\partial t} + \frac{\partial(mv_j F)}{\partial x_j} = Fq^* \tag{2.9}$$

where p is the pressure; m is the porosity (m = 1 & m = 0 are used for pure fluids and impermeable solids respectively), v_i is the flow velocity vector; x_i is the position vector; t is the time; $g_i = g\delta_{i3}$ is the gravitational acceleration vector, in which g is the gravitational acceleration and δ_{i3} is the Kronecker delta; $\hat{\rho} = F\rho_w + (1-F)\rho_a$ is

the density, in which ρ_w, ρ_a are the densities of water and air respectively; $\hat{v} = Fv_w + (1-F)v_a$ is the fluid kinematic molecular viscosity, in which v_w, v_a are the kinematic molecular viscosities of water and air respectively; C_A is the added mass factor; $q^* = q(y,z;t)/\Delta x_s$ is the wave generation source, in which $q(y,z;t)$ and Δx_s are the source density and x-directional mesh width at a source position $(x = x_s)$; f_s^i is the surface tension force based on the Continuum Surface Force (CSF) model; R_i is the laminar and turbulent drag force vector due to porous media; τ_{ij} is the turbulent stress based on the DTM (Dynamic Two-parameter mixed Model); $D_{ij} = \left(\partial v_i/\partial x_j + \partial v_j/\partial x_i\right)$ is the strain rate tensor; Q_i is the wave source vector and β_{ij} is the artificial damping factor matrix. The surface tension force f_i^s and wave source vector Q_i are expressed as follows:

$$f_i^s = \sigma\kappa\frac{\partial F}{\partial x_i}\frac{\hat{\rho}}{\bar{\rho}} \tag{2.10}$$

$$Q_i = v_i q^* - \frac{2}{3}\frac{\partial(\hat{v}q^*)}{\partial x_i} \tag{2.11}$$

where σ is the surface tension coefficient; κ is the local surface curvature; and $\bar{\rho} = (\rho_w + \rho_a)/2$ is the fluid density at the air-water interface. In the current study following values are used for the physical constants considered in the model; the gravitational acceleration $g = 9.81\ \mathrm{m/s^2}$; the water density $\rho_w = 9.92 \times 10^2\ \mathrm{kg/m^3}$; the air density $\rho_a = 1.18\ \mathrm{kg/m^3}$; the kinematic molecular viscosity of water $v_w = 8.93 \times 10^{-7}\ \mathrm{m^2/s}$; the kinematic molecular viscosity of air $v_a = 1.54 \times 10^{-5}\ \mathrm{m^2/s}$ and the surface tension $\sigma = 7.20 \times 10^{-2}\mathrm{N/m}$, whose values were adopted at $25.0\ ^0\mathrm{C}$ and $1.01 \times 10^5\mathrm{Pa}$ (National Astronomical Observatory of Japan, 2003). The reproducing of the turbulent flows in the direct numerical simulation is restricted to low Reynolds numbers because of the need to resolve all spatial scales of turbulence (Salvetti and Banerjee, 1995). In the large eddy simulation (LES), the large-scale field greater than the grid-scale (GS) is directly calculated while the small-scale field called the subgrid-scale (SGS) is modeled with the pioneering Smagorinsky model (Smagorinsky, 1963), dynamic Smagorinsky model (DSM; Germano et al., 1991), dynamic mixed model (DMM; Zang et al. 1993) or dynamic two-parameter mixed model (DTM; Salvetti and Banerjee, 1995). The present study

utilized the DTM, in which the SGS stress τ_{ij} is assumed to be proportional to the modified Leonard stress $L_{ij}^{m} = \overline{v_i v_j} - \overline{v}_i \overline{v}_j$ and the strain rate tensor D_{ij} as follows (Morinishi and Vasilyev, 2001);

$$\tau_{ij}^{a} = C_L L_{ij}^{ma} - C_S |D| D_{ij} \tag{2.12}$$

$$C_L = \frac{\mathcal{L}_{ij}^{a}\mathcal{H}_{ij}^{a}\mathcal{M}_{kl}\mathcal{M}_{kl} - \mathcal{L}_{ij}^{a}\mathcal{M}_{ij}\mathcal{H}_{kl}^{a}\mathcal{M}_{kl}}{\mathcal{H}_{ij}^{a}\mathcal{H}_{ij}^{a}\mathcal{M}_{kl}\mathcal{M}_{kl} - \mathcal{H}_{ij}^{a}\mathcal{M}_{ij}\mathcal{H}_{kl}^{a}\mathcal{M}_{kl}} \tag{2.13}$$

$$C_S = \frac{\mathcal{L}_{ij}^{a}\mathcal{M}_{ij}\mathcal{H}_{kl}^{a}\mathcal{H}_{kl}^{a} - \mathcal{L}_{ij}^{a}\mathcal{H}_{ij}^{a}\mathcal{H}_{kl}^{a}\mathcal{M}_{kl}}{\mathcal{H}_{ij}^{a}\mathcal{H}_{ij}^{a}\mathcal{M}_{kl}\mathcal{M}_{kl} - \mathcal{H}_{ij}^{a}\mathcal{M}_{ij}\mathcal{H}_{kl}^{a}\mathcal{M}_{kl}} \tag{2.14}$$

where $|D|$ is the absolute value of the strain tensor D_{ij}; $\mathcal{L}_{ij} = \widetilde{v_i}\widetilde{v_j} - \widetilde{v_i}\widetilde{v_j}$ is the Germano identity; $\mathcal{H}_{ij} = \widetilde{\overline{v_i}\overline{v_j}} - \widetilde{\overline{v}_i}\widetilde{\overline{v}_j}$; $\mathcal{M}_{ij} = \alpha^2\widetilde{|\overline{D}|\overline{D}_{ij}} - \widetilde{|\overline{D}|\overline{D}_{ij}}$; $\alpha = \tilde{\Delta}/\Delta$, in which Δ and $\tilde{\Delta}$ are the filter widths of the grid and test scales, respectively; the superscript ^{a} represents the anisotropic part of a tensor, e.g., $\tau_{ij}^{a} = \tau_{ij} - \delta_{ij}\tau_{kk}/3$; and the subscripts i, j, k and l are governed by the Einstein summation convention. As indicated in Eqs. (2.13) and (2.14), the coefficients C_L and C_s can be dynamically computed with resolved GS velocities v_i. The input parameter in the DTM is only α, and $\alpha = 2.0$ is adopted after Germano et al. (1991).

2.7 Simulation of Tsunami Interaction with a Rigid Structure

Three-dimensional numerical model developed by Lee et al. (2010) was used for the numerical analysis which is further discussed in Chapter 4. In the model, liquid and gas phases are considered to be immiscible and continuity (Eq. 2.16) and modified Navior-Stokes (Eq. 2.17) equations are used as governing equations, while free surface is determined by advection equation (Eq. 2.18) which incorporates VOF method.

$$\nabla \cdot (\theta V) = \tilde{q} \tag{2.16}$$

$$\frac{\partial V}{\partial t} + (V \cdot \nabla)V = -\frac{\nabla p}{\rho_w} + \nabla \cdot (2v_w E - \tau) - \frac{2}{3}\nabla\{v_w(\nabla V)\} + F_b - \gamma V \tag{2.17}$$

$$\frac{\partial F}{\partial t} + \nabla V \cdot F = F\tilde{q} \tag{2.18}$$

where, V is the velocity vector; $\tilde{q} = q/\Delta x_s$ source term required to generate wave; q is the flux density at wave source position($x = x_s$); t is the time; p is the pressure, ρ_w is the fluid density; υ_w is the kinematic viscosity coefficient; E is the strain rate tensor; τ is the sub-grid stress vector; F_b is the body force such as gravity and surface tension; γ is the wave dissipation factor which equals to zero except in the added dissipation zone.

2.8 Summary

The Arbitrary Lagrangian Eulerian (ALE) description (Hallquist, 2006) was employed in finite element modeling code LS-DYNA to simulate the tsunami-structure interaction. In order to release the heavy computational load, the whole domain is considered as two coupled components. The three-dimensional nonlinear fluid model (Nakamura & Yim, 2011) was employed for the simulation of tsunami generation and propagation up to close distance to the structure. The FSI computational domain defined in LS-DYNA with the ALE description was used in the impact and interaction analysis.

Three dimensional numerical model developed by Lee et al. (2010) was used in the numerical simulation of tsunami interaction with a rigid structure, which discussed in Chapter 4 in detail.

Chapter 3

TSUNAMI INTERACTION WITH MULTI-STORY BUILDING

3.1 General

As discussed earlier in the Chapter 1, the existing design equations for the tsunami force estimation on coastal buildings require further investigations to incorporate different aspects of structural arrangement and configurations of the building. Lukkunaprasit et al. (2009) conducted 1:100 scale modeling experiments to understand the effect of openings and the resulting tsunami force on vertical tsunami evacuation shelters. The study highlighted the reduction of tsunami force with the presence of openings in the building. However further studies are needed to incorporate the effect of openings in to the design tsunami force estimation equations in order to proceed for an effective design guideline for coastal buildings like evacuation shelters, against tsunami. Three-dimensional hydraulic experiments were conducted with the aim of assessing the effect of spatial configurations of the building in the estimation of tsunami force. Characteristics of tsunami run-up and the interaction of tsunami with on-land building which observed through experiment study are discussed in this chapter.

3.2 Experimental setup

Experiments were carried out in a hydraulic flume (30 m in length, 0.7 m in width and 0.9 m in height) of Department of Civil Engineering, Nagoya University. Experimental set-up was prepared according to the Froude similitude law with a scale of 1:50 as shown in Fig. 3.1. Tsunami was generated with piston type wave generator and the inclination of impermeable bed was kept as 1/10 as shown in the figure, while rest of the bed area was maintained to be horizontal. Tsunami wave height was

measured using ten wave gauges which were installed at the positions indicated in the figure. The whole experiment procedure was recorded using a digital video camera placed in aligned with the centerline of the flume just off the shoreline and above free water surface.

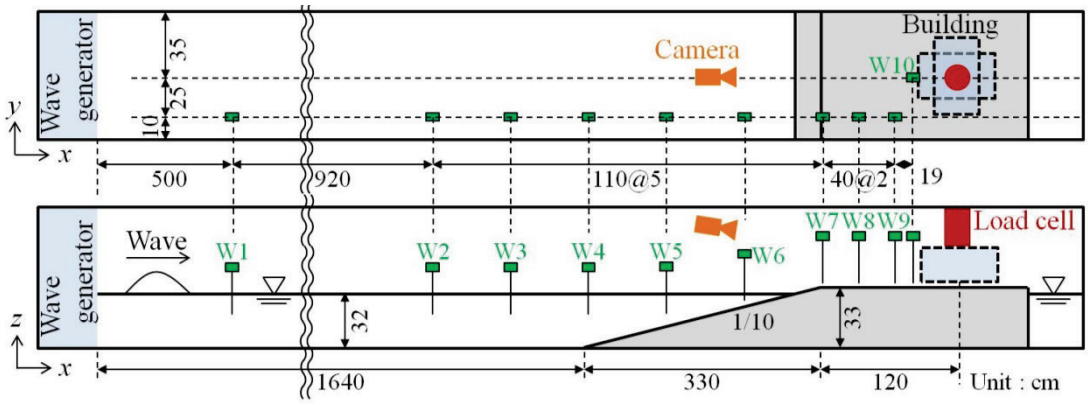

Fig. 3.1. Schematic figure of the experimental set-up and measuring points; top view (above) & side view (below)

Table 3.1. Incident wave conditions

Wave condition	Wave type	Wave period (s)	Wave height (cm)	Tsunami flow type
Wave1	Long period wave	20	3	Bore a
Wave2			4	Bore a
Wave3		15	3	Bore a
Wave4			4	Bore a
Wave5			5.5	Bore b
Wave6		10	3	Bore a
Wave7			5.5	Bore b
Wave8			8	Bore b
Wave9	Half of sinusoidal wave		7	Breaking wave
Wave10			12	Breaking wave
Wave11			17	Breaking wave

The maximum stroke of 1.5 m of the wave generator was employed in generating long period waves while half of sinusoidal waves were also yielded in producing different tsunami conditions of the on-land flow. Three main conditions were considered depending upon the wave profile and the inundation speed of the tsunami as shown in the Table 3.1. The 'Bore a' type represents the situation where the tsunami overflow with slow speed, while the 'Bore b' represents the tsunami overflows with relatively higher speed. The third type of 'Breaking wave' case was used to re-produce the condition where tsunami wave break in front of the structure.

In case of the structure model for tsunami evacuation building, three types of configurations were considered depending upon the special arrangement of the structural elements within the building. The general outer dimensions of the building model which constructed with 10 mm thick acrylic plates, was 400 mm × 320 mm × 270 mm. The model with no openings on either side was considered as building type 'A' (Fig. 3.2). The structure was modeled in the height of three story and the remaining two types of building frames were with the similar dimensions as building 'A' but varied with the openings and the spatial arrangement of the structural elements inside the main frame. Building type 'B' (Fig. 3.3) was considered as a structure with only windows in either side of each story and building type 'C' (Fig. 3.4) consisted of array of pillars in the 1st story (ground level) and the windows on either side of the building for remaining two stories. These particular types were selected for the study depending upon the variety of general building types available in the coastal zone and suggestions and recommendations from previous studies.

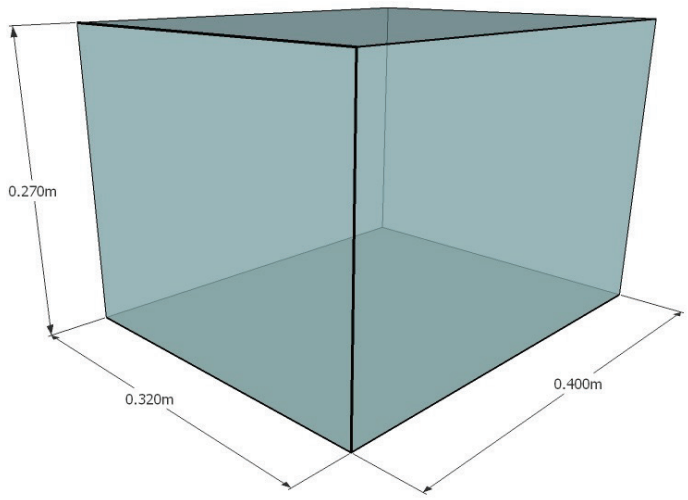

Fig. 3.2. Three-dimensional view of building type 'A' with outer dimensions

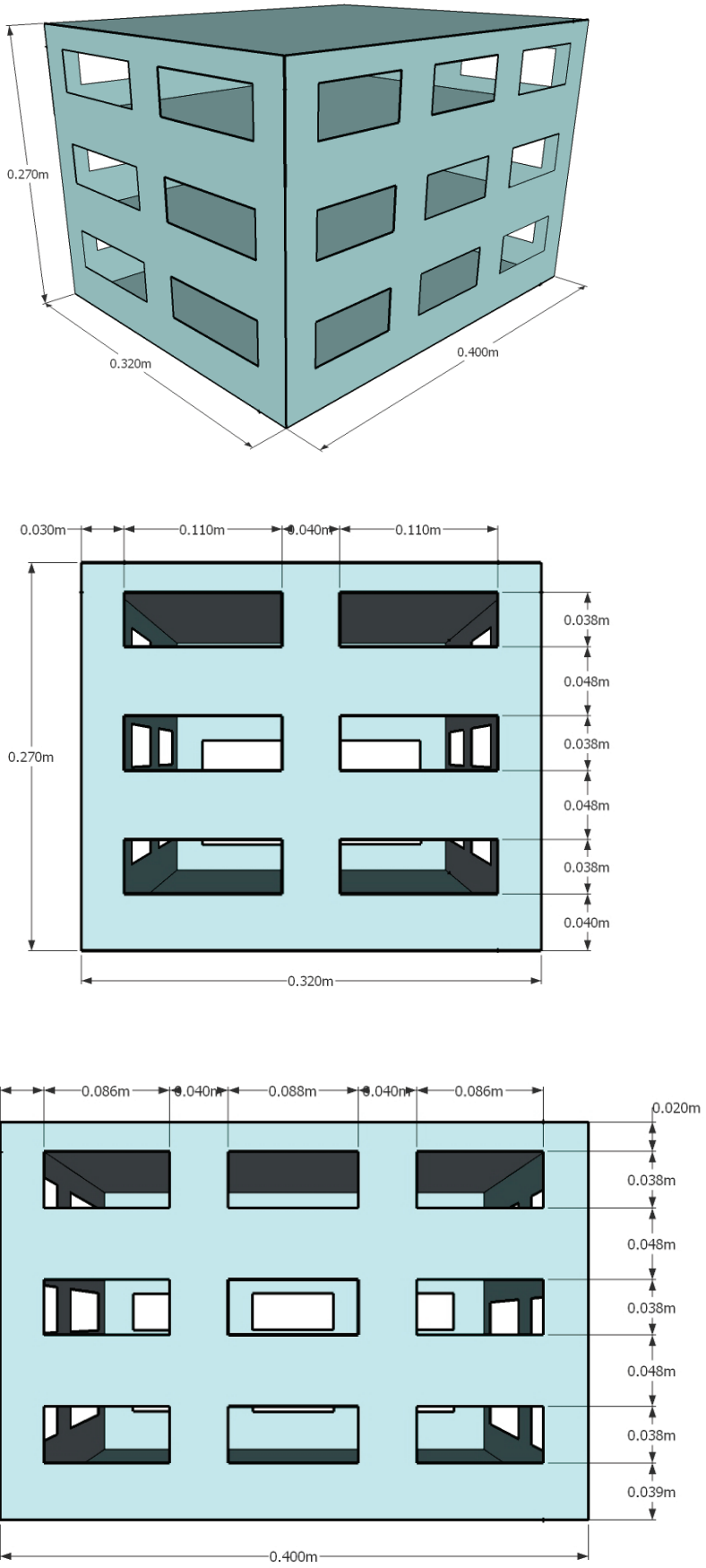

Fig. 3.3. Schematic arrangement of building type 'B'; 3D view (above), front view (middle) and side view (below)

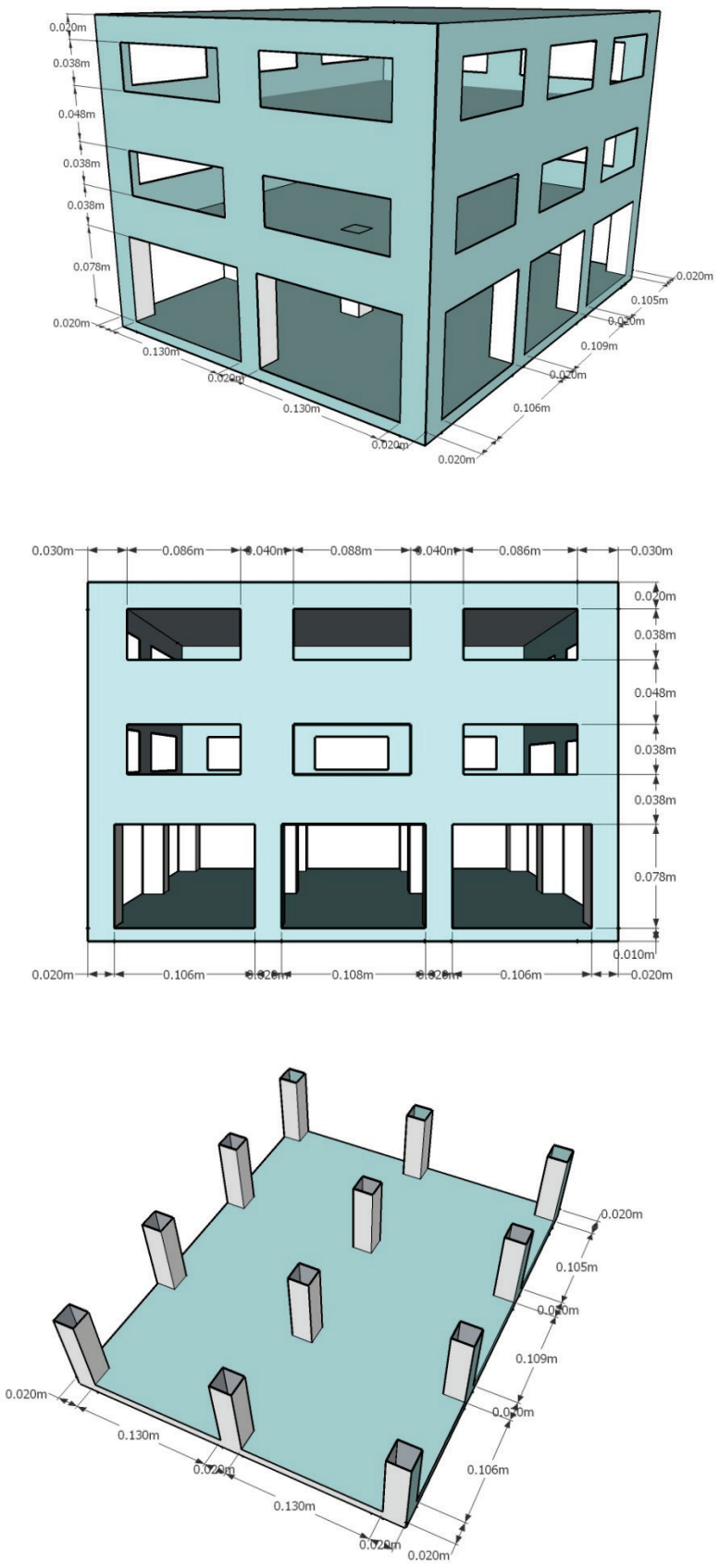

Fig. 3.4. Schematic arrangement of the building 'C'; 3D view (above), side view (middle) and pillar arrangement as a horizontal cross section at the ground level (below)

Two arrangements for the each building model at the installed location were considered in the experiment as width side (shorter dimension) of the building facing tsunami and the length side of the building facing tsunami [Fig. 3.1(above)]. For the building ‘B’ and building ‘C’ additional two configurations were allocated taking the service requirements into account. Accordingly, a living compartment in the 1st floor was created by adding a wall segment in the direction perpendicular to the tsunami flow. Two types of living compartment arrangements were introduced and the positioning of the wall segment for the building ‘B’ is shown in the Fig. 3.5 below. Also, similar positions were selected for the wall in the building ‘C’.

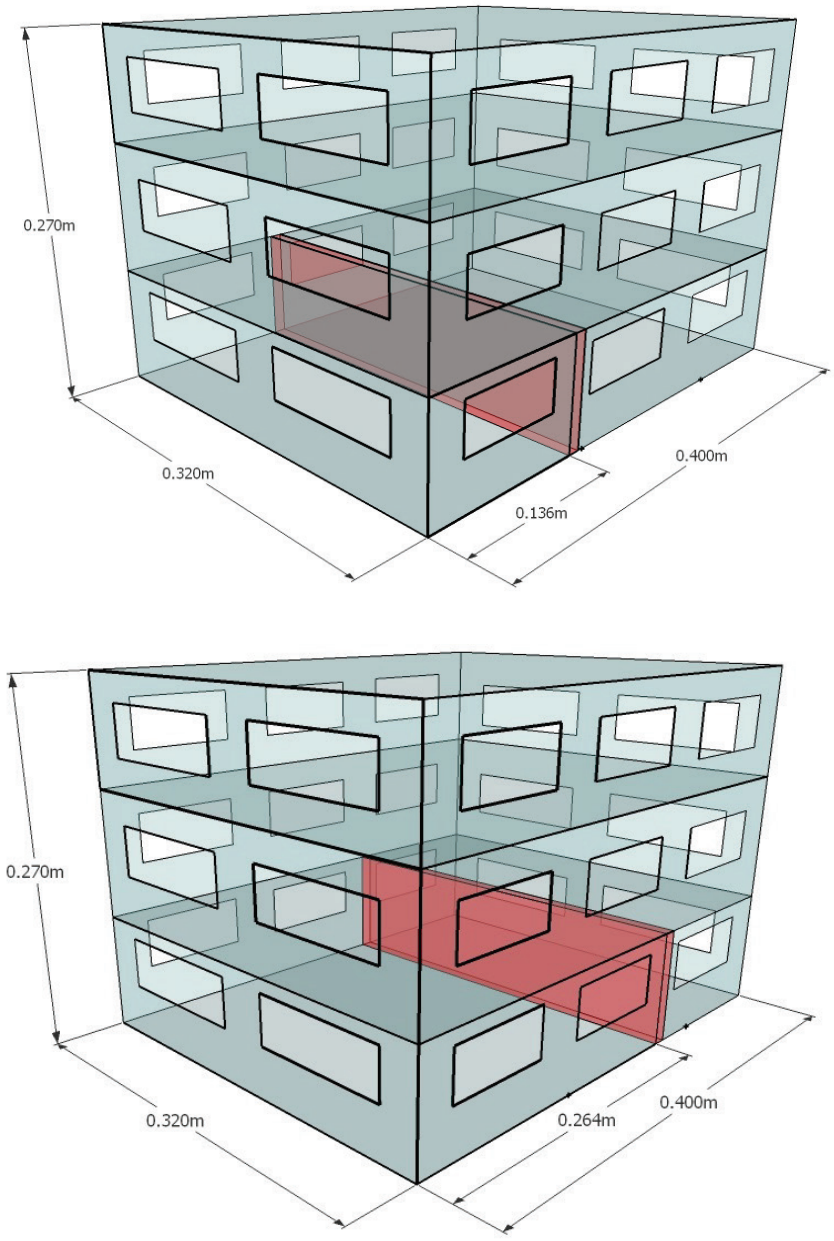

Fig. 3.5. Allocation of wall segment for building 'B'

Additionally, a service location for an elevator shaft also allocated in the building models ‘B’ and ‘C’. The arrangement of service configurations and the notations used in the experiment for each case are shown in Fig. 3.6.

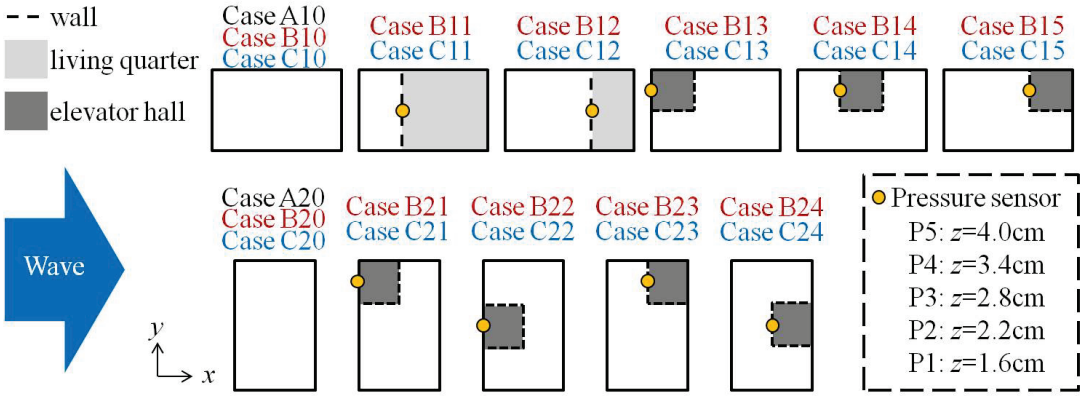

Fig. 3.6. Arrangement of service compartments and the pressure gauge locations for each case considered

Fig. 3.7. Arrangement of pressure sensors in the experiment

(a) Building type ‘A’

(b) Building type ‘B’

(c) Building type ‘C’

Fig. 3.8. Models of each building type used in the experiment. Left to right: Building A, Building B & Building C

Pressure on each type of building models (Fig. 3.8) exerted by tsunami impingement was measured using five pressure sensors placed in line in the vertical direction (Fig. 3.7) at distance of 0.6 cm each and the location of the pressure sensor arrangement for each case is shown by the yellow dot in Fig. 3.6. The signals from the pressure sensors were treated with a low pass filter of 1 kHz sampling frequency to reduce the noise prior to the analysis. At the same time, the measurements for a particular condition were taken three times in order to avoid any sort of variation due to an associated error.

Force transducer for the measurement of the total force acting on the building due to tsunami impact, was installed on top of the structure by supporting from the top and measurements were taken only for the exerted force on the tsunami flow direction (x-direction).

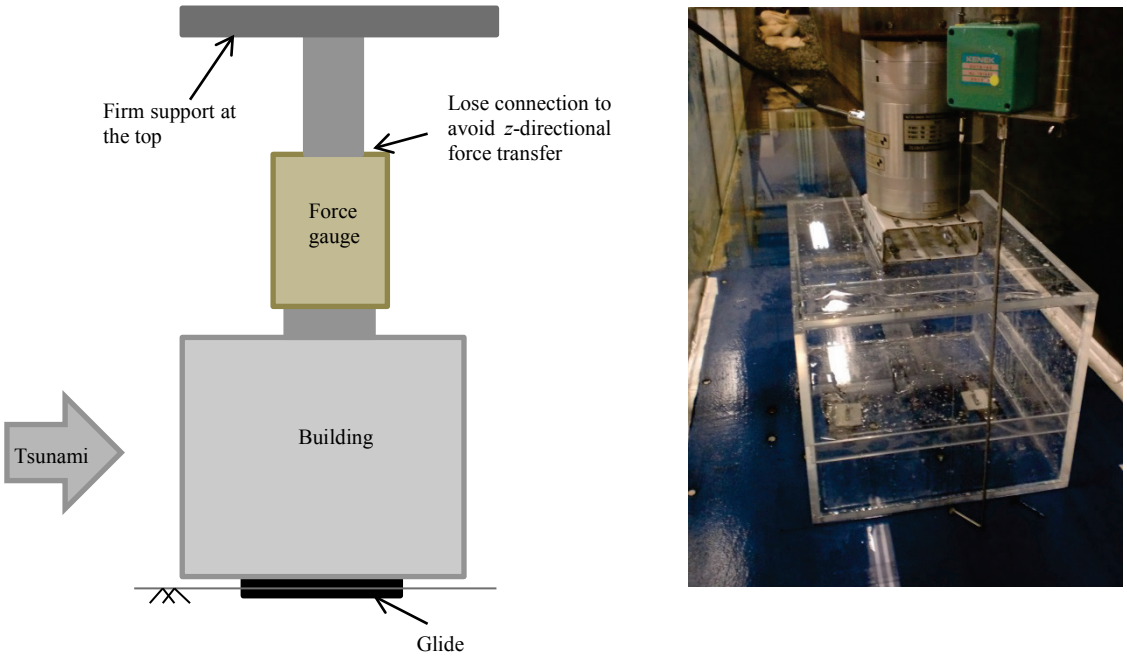

Fig. 3.9. Force gauge arrangement

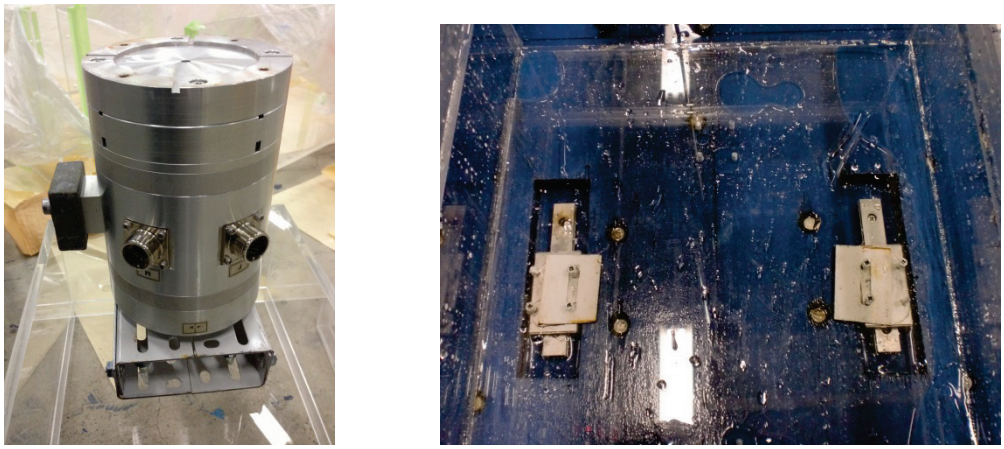

Fig. 3.10. Closer view of force gauge (left) and glider arrangement at the bottom of the structure (right)

Fig. 3.9 shows the schematic arrangement of the force gauge placement (left) and the installed force gauge at the experiment (right). As it is mentioned in the figure, even though the force gauge is supported from the top, an specific connection was maintained between top support and the gauge in order to restrict the force transfer in

the upward direction (z-direction). Additionally, pair of gliders were installed underneath the structure [Fig. 3.10 (right)] allowing the building to move in x-direction under the tsunami impingement, while restraining any movement in any other directions. The resultant force required to stop the *x*-directional movement was detected by the force gauge and taken as the acting external force on the structure. The original output from the force gauge was passed through a low-pass filter in order to reduce the amount of noise associated with the measurement. Cut-off pressure value of 10 Hz was used in the filter and Fig. 3.11 shows the variation of the output signal for different values of cut-off frequency. It can be observed from the figure that the selected cut-off frequency has no significant effect on the maximum tsunami force acting on the building.

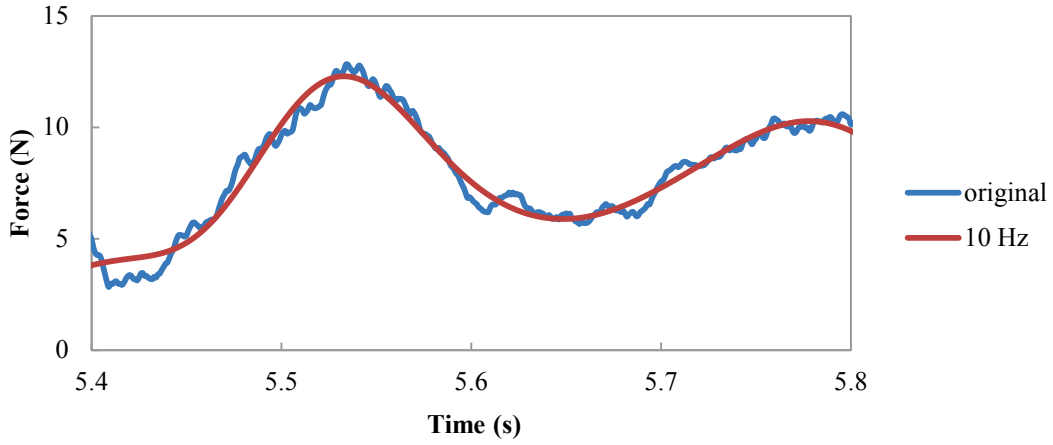

(a) cut-off frequency of 10 Hz

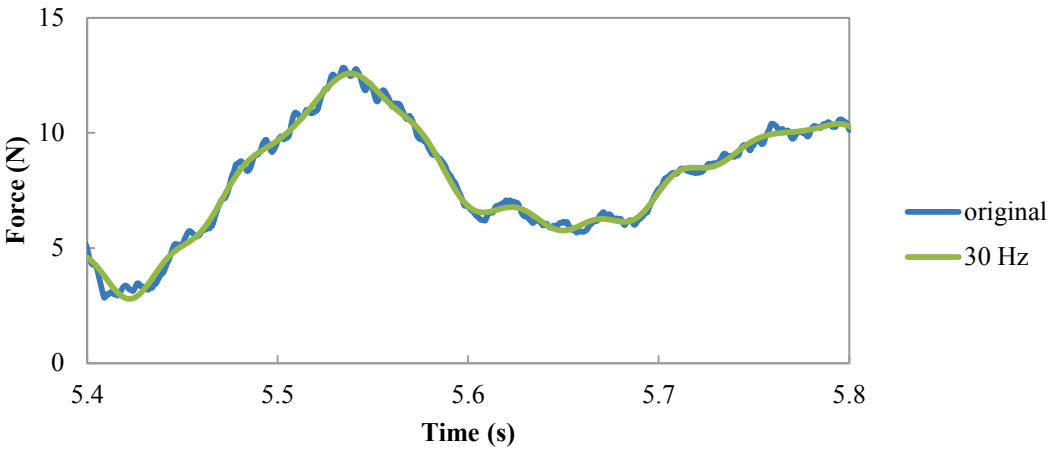

(b) cut-off frequency of 30 Hz

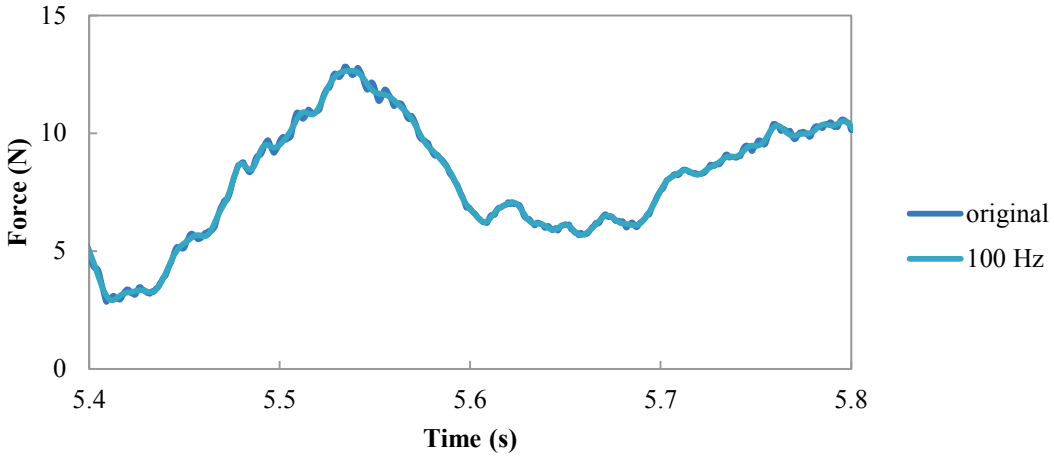

(c) cut-off frequency of 100 Hz

Fig. 3.11. Variation of original force output with the change in cut-off frequency

3.3 Experiment Results

3.3.1 Tsunami run-up characteristics

Fig. 3.12 shows the temporal variation of tsunami profile at the location of the W10 for all wave conditions with no structure installed. According to the figure it can be observed that a clear variation in the water surface profile at the location of the structure depending upon the incident wave type.

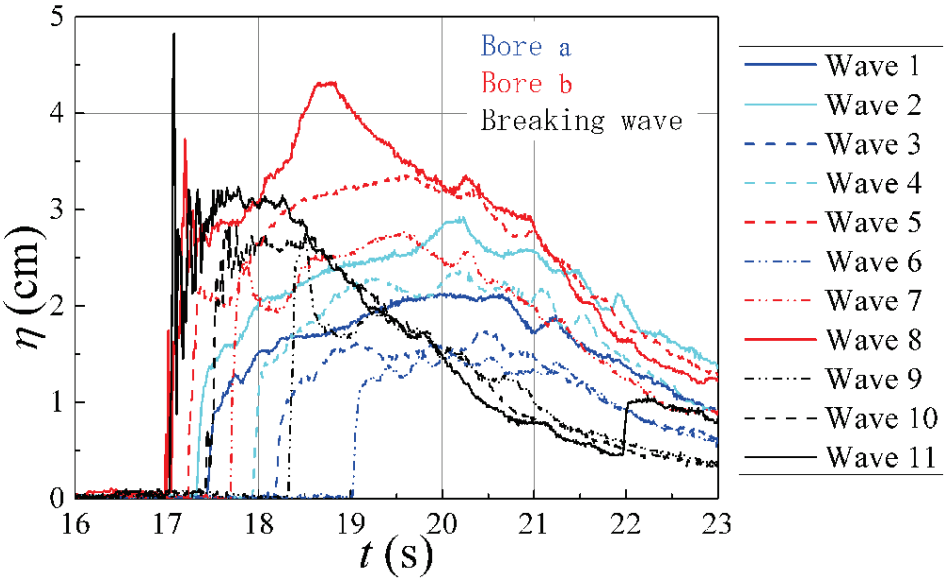

Fig. 3.12. Temporal variation of water surface profile at the wave gauge W10 for each wave case (without the structure)

In case of ‘bore a’ water surface initially increases without a sudden impulse and then reach a maximum and gradually decreases with the time. However, when it goes from ‘bore a’ to ‘breaking wave’ it can clearly observe that maximum wave height occurred at the very initial stage of the arrival of the wave. At the same time, rest of the behavioral pattern of the profile also changes causing higher wave depth at the initial stage. Therefore it is evident that the maximum water depth in front of the structure at the time of impact is getting higher when it is going from long period waves to solitary wave. This kind of behavior occurs mainly due to the addition of additional water volume to the wave front as a result of wave breaking just in front of the structure location.

3.3.2 Effect of the openings on acting tsunami force

Fig. 3.13 and Fig. 3.14 show the maximum tsunami force (F_{max}) against the maximum wave height observed at the location of the structure in Fig. 3.12 (η_h), for the cases where width side of the structure facing tsunami and the length side of the structure facing tsunami, respectively. Here, the cases with inner wall or elevator are not considered. By looking at the figures it can be clearly noticed that F_{max} is higher for the breaking wave type compare to the bore types ‘a’ and ‘b’. In that case there is a significant increment in F_{max} which can be caused due to the high flow depth at the impact and the higher flow volume and velocity due to the breaking of wave.

Further, it is visible that the acting maximum tsunami force decreases with the type of the building in the order of ‘Building A’, ‘Building B’ and ‘Building C’, which supports the statement that present of openings reduces the maximum tsunami force acting on buildings. Additionally, there is a significant drop in F_{max} in case of ‘Building C’ when compare to the ‘Building B’ which is supposedly due to the increase of opening ratio compared to the previous.

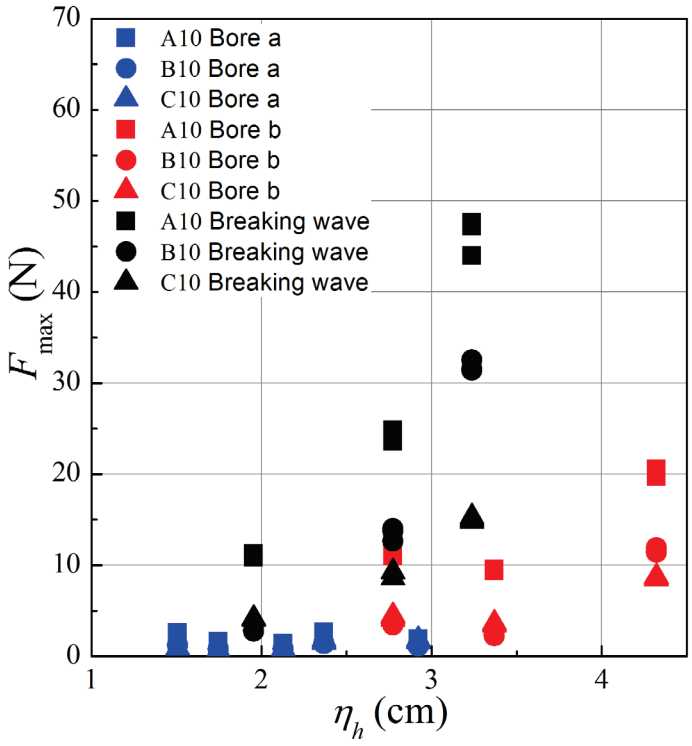

Fig. 3.13. Maximum wave force against maximum wave height for the case that width side of the building facing tsunami

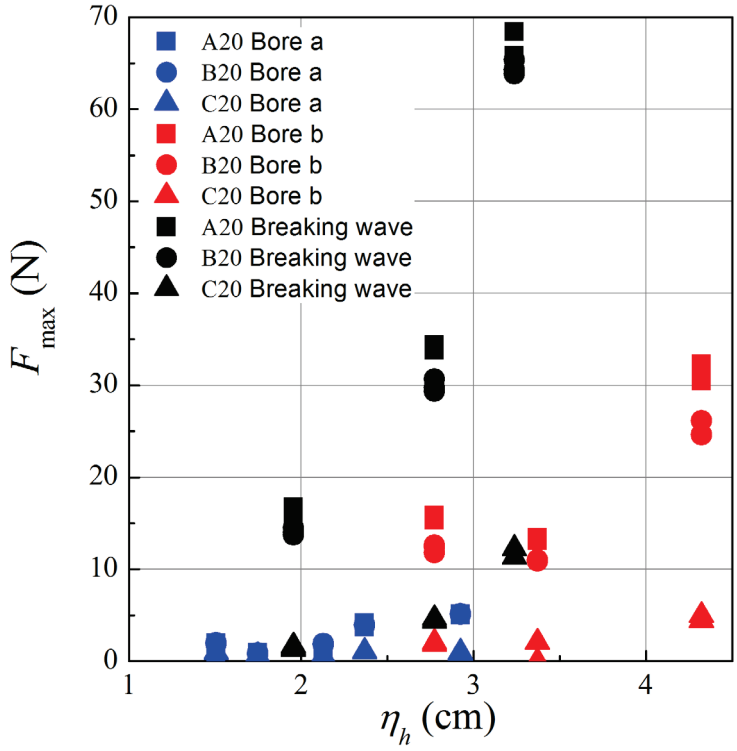

Fig. 3.14. Maximum wave force against maximum wave height for the case that length side of the building facing tsunami

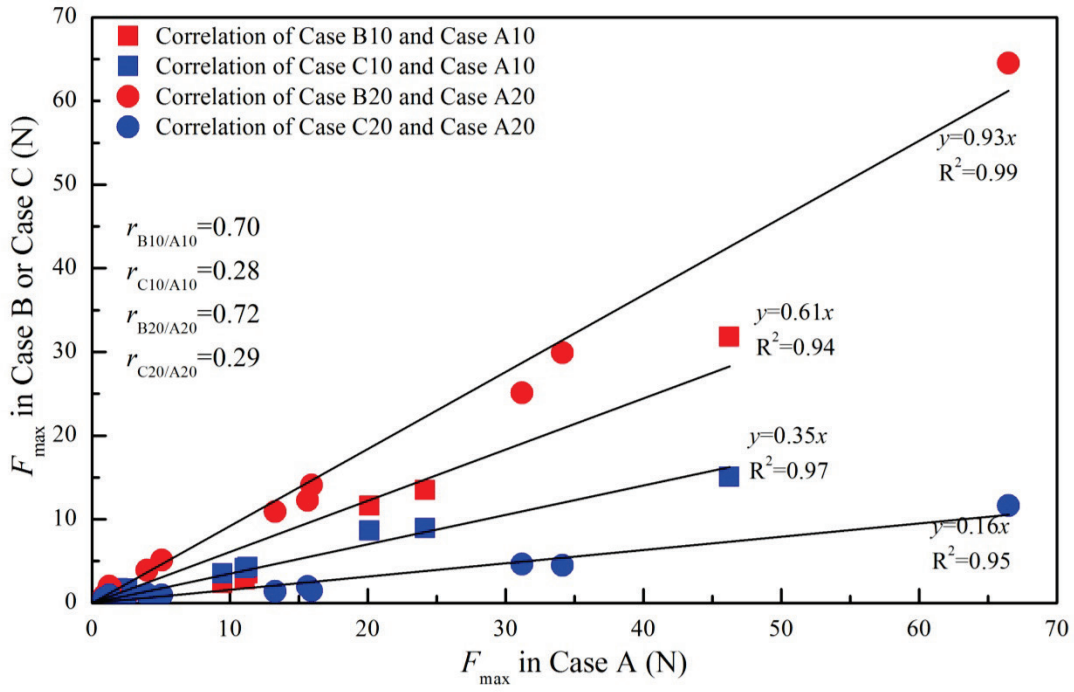

Fig. 3.15. Maximum tsunami force for the Case 'B' and Case 'C' against that of Case 'A'

Fig. 3.14 was prepared in order to quantitatively evaluate the effect of opening ratio on the acting force; which shows F_{max} for the 'Case B' and 'Case C' against that of 'Case A'. The approximate relationship for the each combination is indicated in the straight lines with the equation for the relationship by its side. At the same time, the opening ratio *r* for the front face of the 1st floor of the building is also indicated in the figure. Here, *r* is calculated as the ratio of total wall area which faces the tsunami and hence, lowers the value of *r,* higher the openings in the wall will be. It can be understood from the figure that the rate of reduction of wave force acting on the structure is almost constant regardless of the wave condition. Therefore the opening ratio *r* can be identified as an important physical parameter in estimating the tsunami force acting on a building with openings facing to seaward. At the same time, it can be noticed that the acting tsunami force varies with orientation of the building. In 'Case C' the orientation which the length side of the building facing tsunami is more effective than width side facing tsunami, in the reduction of total tsunami force, while for 'Case B' it is vice versa. But, in actual scenario, one should not ignore the effect of the inner walls of the building in the estimation of the force. Because the water volume which penetrated into the building can exert some force on the structure while increasing the total force.

3.3.3 Effect of internal arrangement of the building on tsunami force

As it was mentioned earlier in the chapter, two main structural components were considered in the study for the internal arrangement of the building, as separation wall and an elevator. Each case employed, depending upon the position of the structural component was shown in Fig. 3.6. Fig. 3.16 below shows the variation of total force acting on the structure plot against that of for the case with no internal arrangement of the building. Fig. 3.16 (a) for the 'Case B' for each orientation separately and Fig. 3.16 (b) shows the same for 'Case C'.

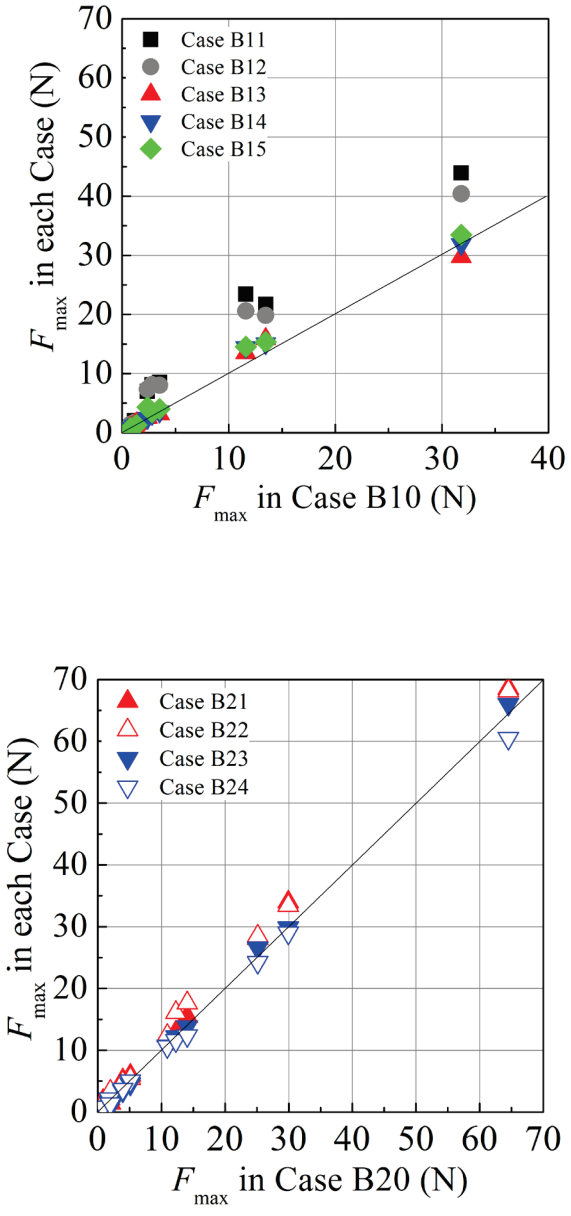

(a) for Case B; orientation 1 (above) and orientation 2 (below)

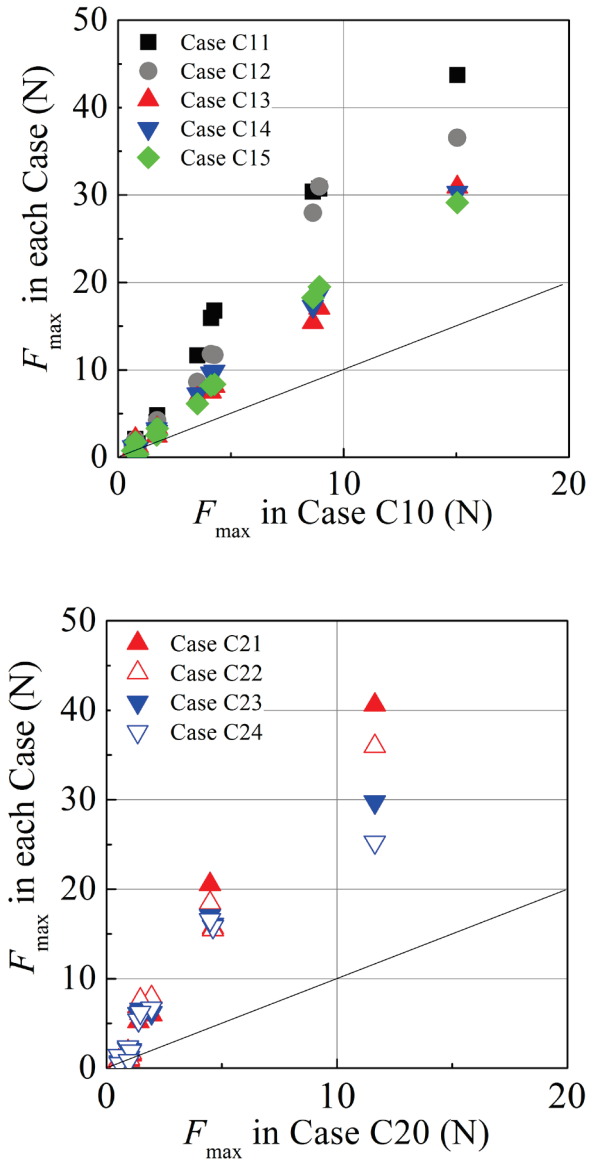

(b) for Case C; orientation 1 (above) and orientation 2 (below)

Fig. 3.16. Variation of total tsunami force depending on the internal arrangement of the building

For the 'Case B' it is visible from the figure that, there is no significant increment in the tsunami force with the introduction of elevator shaft or even for its position. This kind of behavior might occur because of the fact that there is still enough space inside the building to make way for the water volume entered. However, in case of internal separation wall, a significant increase in the force can be observed compared to the case with no internal arrangement (Case B11 & Case B12). Understandably, this increment occurred due to the total blockage of penetrated water volume of tsunami due to the presence of the internal separation wall.

For ‘Case C’ it can be noticed from the figure that the effect of internal arrangement (both elevator shaft and separation wall) is relatively higher than that for ‘Case B’. This indicates that the internal structural arrangements which block the tsunami flow become more influential in estimating the tsunami force, when the openings of the building in the sea side face get larger. In addition, for the cases with internal separation wall shows much higher increments than the cases with elevator shaft. Further, it is evident that the positioning of the separation wall in the seaward side increases the total tsunami force than that it places in the landward side. Therefore, it is important to have a closer look at the acting pressure distribution on the inner separation wall and elevator shaft to understand this kind of behavior.

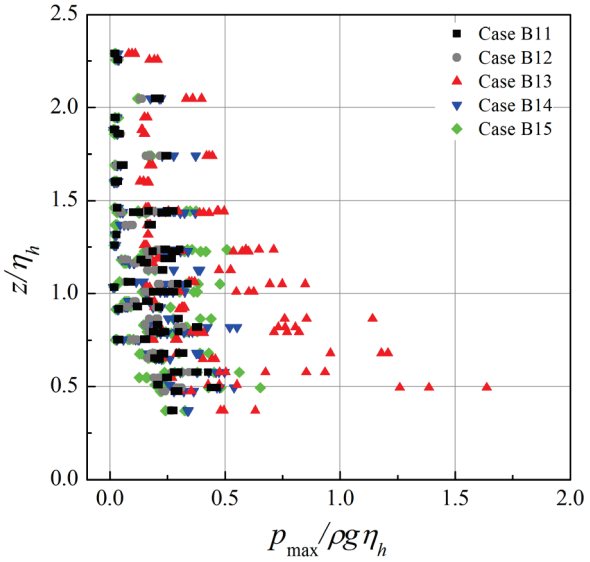

(a)

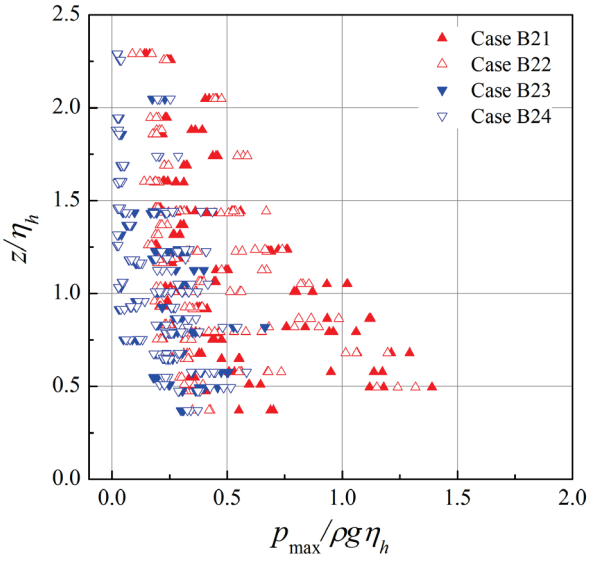

(b)

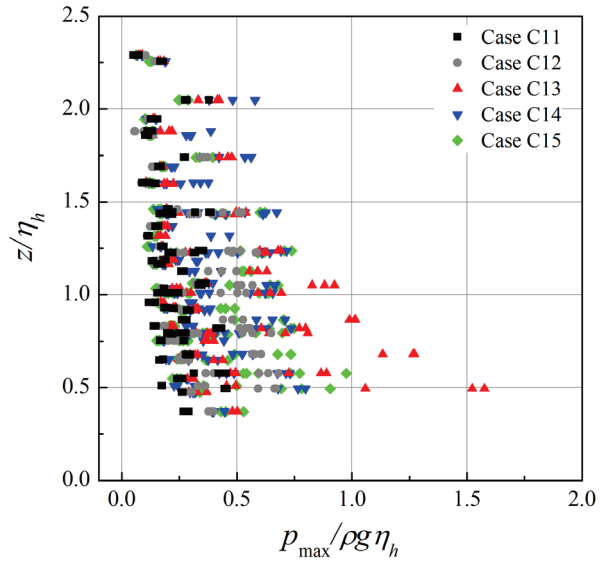

(c)

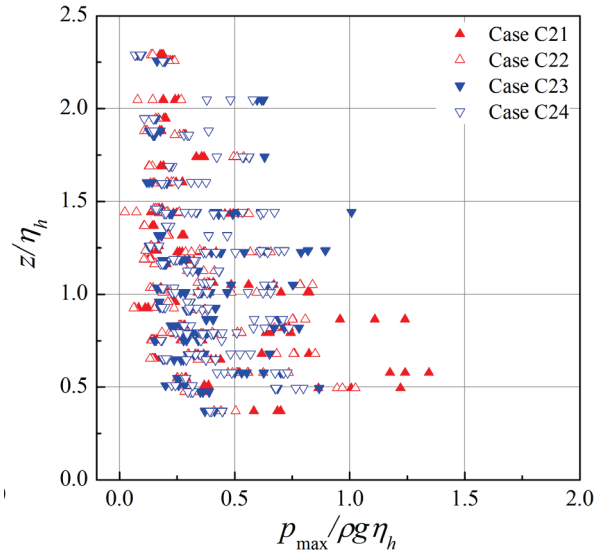

(d)

Fig. 3.17. Vertical distribution of dimensionless maximum wave pressure on the inner wall

Fig. 3.17 shows the vertical distribution of non-dimensional maximum pressure distribution on the inner wall and the elevator shaft for each case. The maximum pressure value was normalized by dividing with $\rho g \eta_h$ and the dimensionless vertical height was obtained by, the installation height of the pressure gauge divided by the relevant $\eta_h$value for the case. The distribution is shown separately for the Cases 'B' and 'C' depending upon its orientation. It can be seen from the figure that for the cases which internal structural component (wall or elevator shaft) placed in the seaward side (Cases 13, 12, 22) of the building shows higher pressure value irrespective of the opening ratio of the building (for both structure 'B' and 'C'). At the

same time, a triangular distribution of pressure distribution can be observed in those cases. The lower pressure values for the cases which the structural component positioned in the landward side of the structure can be occurred due to the energy dissipation of the tsunami flow when contact with windows and pillars, prior to reach the separation wall or elevator shaft. Additionally, it is also evident that the pressure values for the structure 'C' are generally higher than that of structure 'B' for the similar cases. It can be explained by the larger openings in the structure 'C' allowed more water volume to penetrate into the structure which eventually increase the acting pressure. The analysis was continued further to estimate the total force acting on the inner wall (both separation wall and elevator shaft).

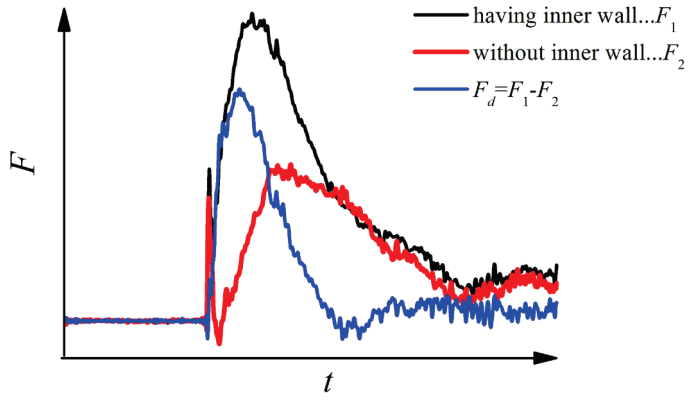

Fig. 3.18. Estimation of the total acting force on the inner wall

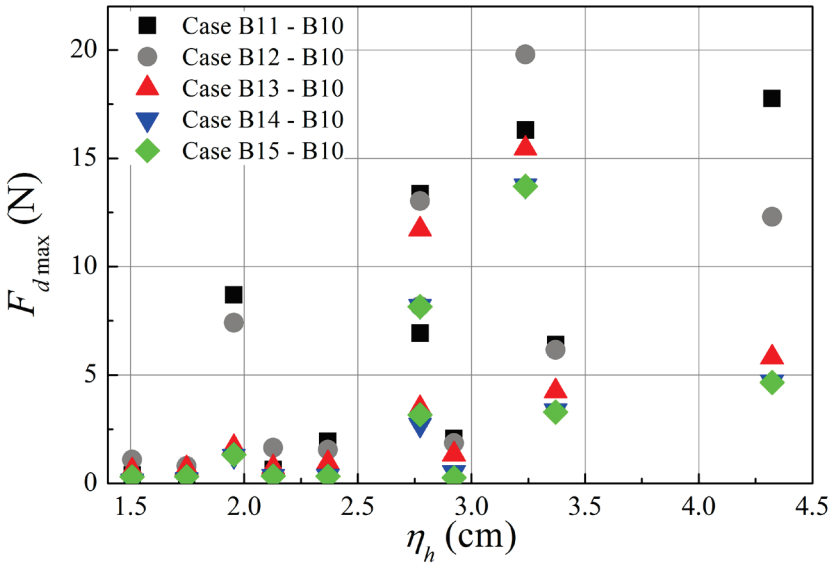

(a)

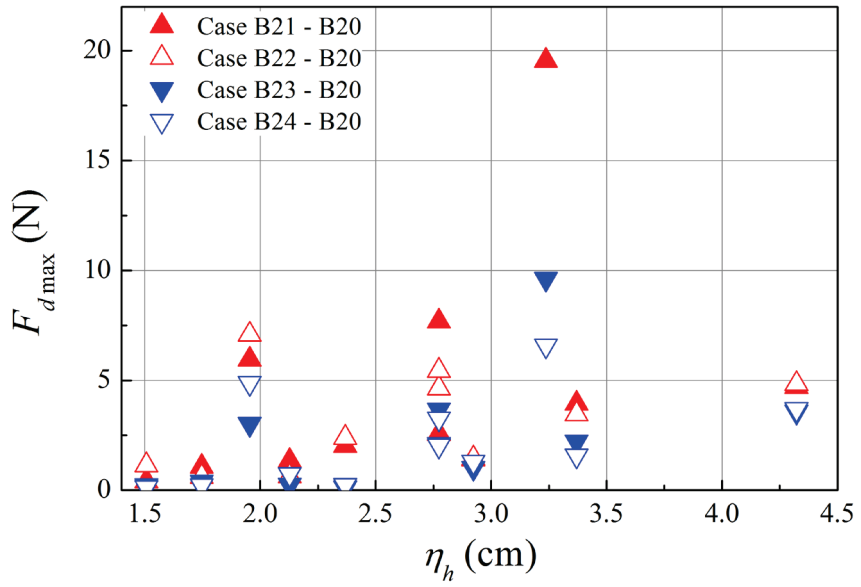
Case B21 - B20
Case B22 - B20
Case B23 - B20
Case B24 - B20
$F_{d\max}$ (N)
η_h (cm)

(b)

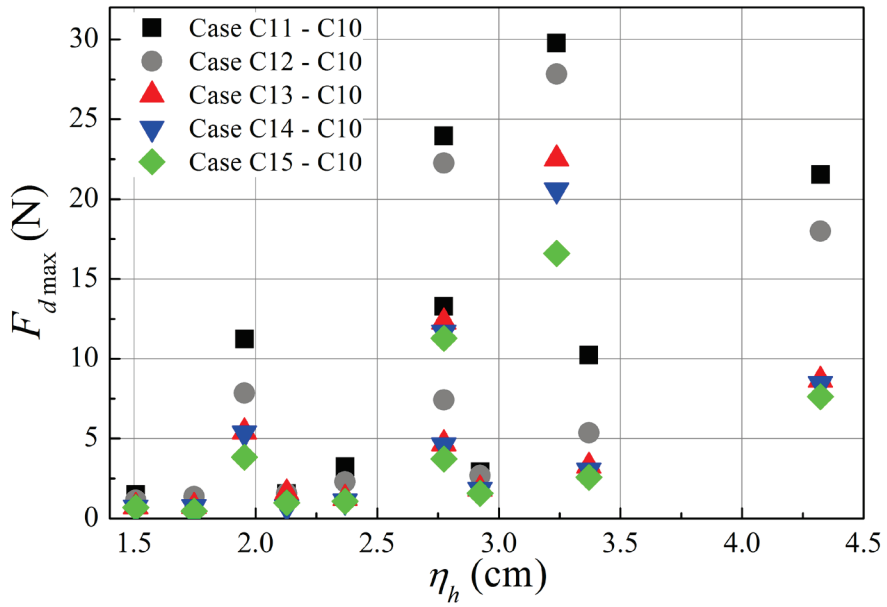
Case C11 - C10
Case C12 - C10
Case C13 - C10
Case C14 - C10
Case C15 - C10
$F_{d\max}$ (N)
η_h (cm)

(c)

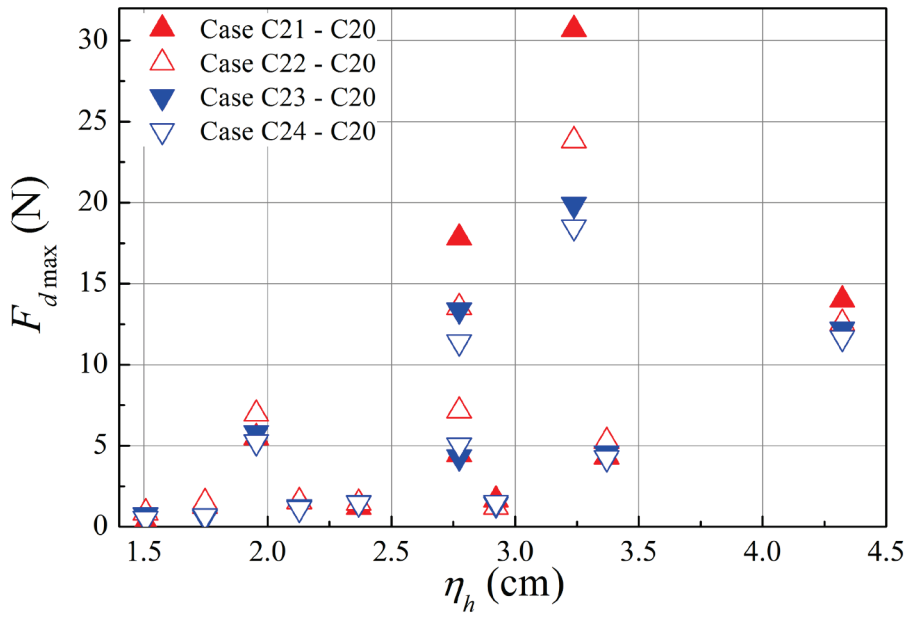

(d)

Fig. 3.19. Maximum force on the inner wall for different cases

The maximum force acting on the inner wall was estimated by deducting the maximum force acting on the building without inner wall from the maximum force acting on the building with the inner wall, as it is graphically explained in Fig. 3.18. The estimated values for each case are plotted against η_h in Fig. 3.19 which are categorized depending upon the structure type and its orientation. In the figure it was confirmed from the experiment that generally the higher values for $F_{d\,max}$ were observed from the breaking type waves. At the same time it can be noticed that, $F_{d\,max}$ is increasing with the increase of η_h. Further, higher $F_{d\,max}$ for inner separation wall case when compared with the elevator shaft case is observed and that can be occurred due to the larger resistance area of the separation wall. It is also evident that $F_{d\,max}$ is higher when inner wall positioned in the seaward side when compared with the cases where it is placed in the landward side. Therefore, to minimize the total horizontal force acting on the structure it is recommended that the inner walls to be placed more landward within the structure, rather than place it toward seaward side.

3.4 Tsunami force estimation for a building with openings

In the estimation of the total force acting on the building it was assumed pressure distribution to be triangular in the vertical direction (Fig. 3.20).

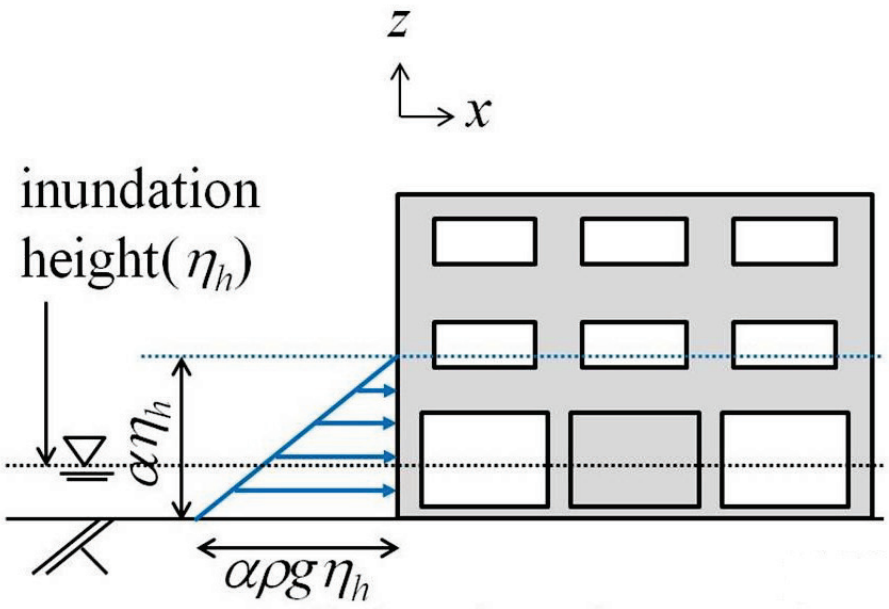

Fig. 3.20. Triangular pressure distribution on the structure

The effective height for the pressure action was taken as $\alpha\eta_h$, where η_h is the inundation depth and the α is to be estimated from the experiment. For the force calculation two approaches were considered according to the recommendations by the Japanese cabinet office (2012). One approach is to estimate the force excluding the pressure action on the areas where openings are present (Fig. 3.21) while the other approach is to take the integration of wave pressure without considering the presence of the openings (Fig. 3.22).

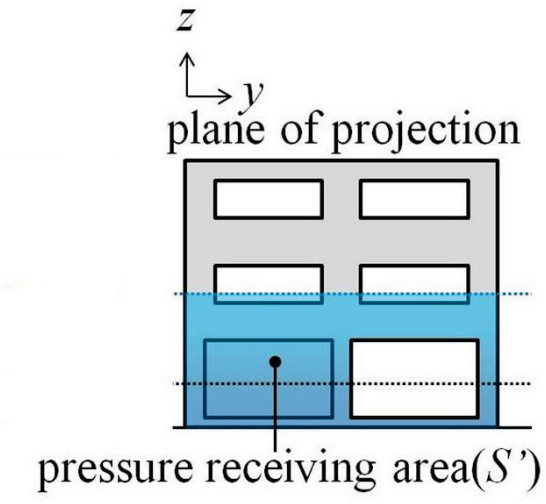

Fig. 3.21. Effective area for the force calculation excluding the openings

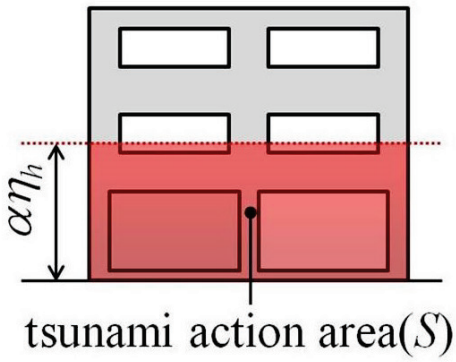

Fig. 3.22. Effective area for the force calculation neglecting the presence of openings

According to the explanation the estimated force from the each approach can be expressed as follows;

acting force, considering the presence of openings,

$$F_i = \int_{S'} \rho g(\alpha\eta_h - z)ds \tag{3.1}$$

acting force, neglecting the presence of openings,

$$F_r = \frac{S'}{S}\int_S \rho g(\alpha\eta_h - z)ds \tag{3.2}$$

In the estimation of *Fr* (Eq. 3.2), the pressure calculation is multiplied by the ratio of actual pressure receiving area (S') to the tsunami acting area (*S*). Further, the opening area is calculated as the projected area in the plane perpendicular to the tsunami propagation. The estimated tsunami force from the each estimation method is plotted against the F_{max} observed in the experiment for relevant cases are shown in Fig. 3.23 and Fig. 3.24. In the calculation the value of α which is the multiplication factor for the effective water depth, was assumed as 3 as it is the general recommendation. By referring to the figures it can be observed that, difference between the force estimation from each method is insignificant. Further, for the bore type '*a*' and '*b*' the estimations lies within the safe side regardless of the spatial arrangement of the building, while some of the cases for the bore '*b*' are marginally unsafe.

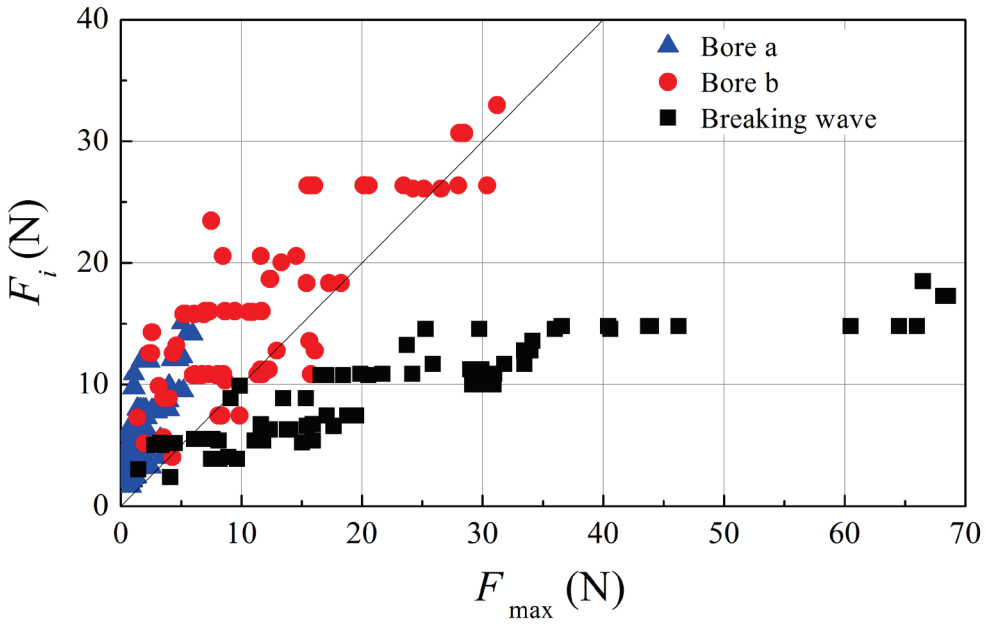

Fig. 3.23. Estimated tsunami force from the integration, considering actual pressure acting area

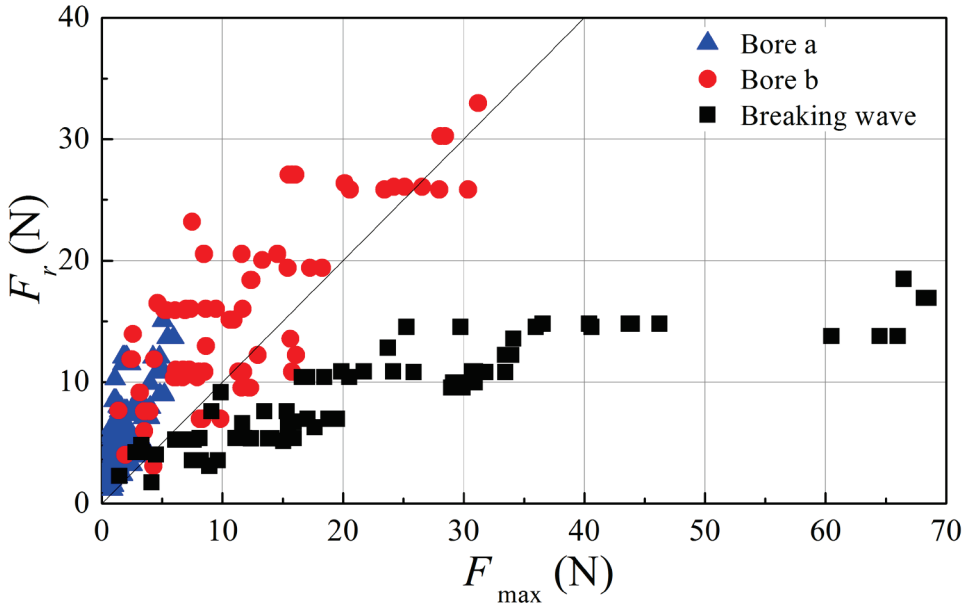

Fig. 3.24. Estimated tsunami force considering the opening ratio

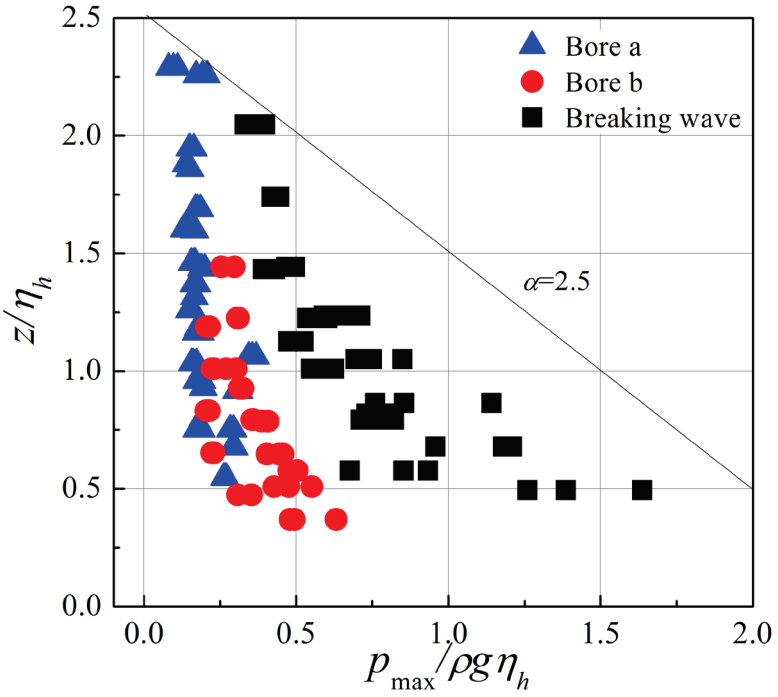

Fig. 3.25. Non-dimensional wave pressure distribution for Case B13

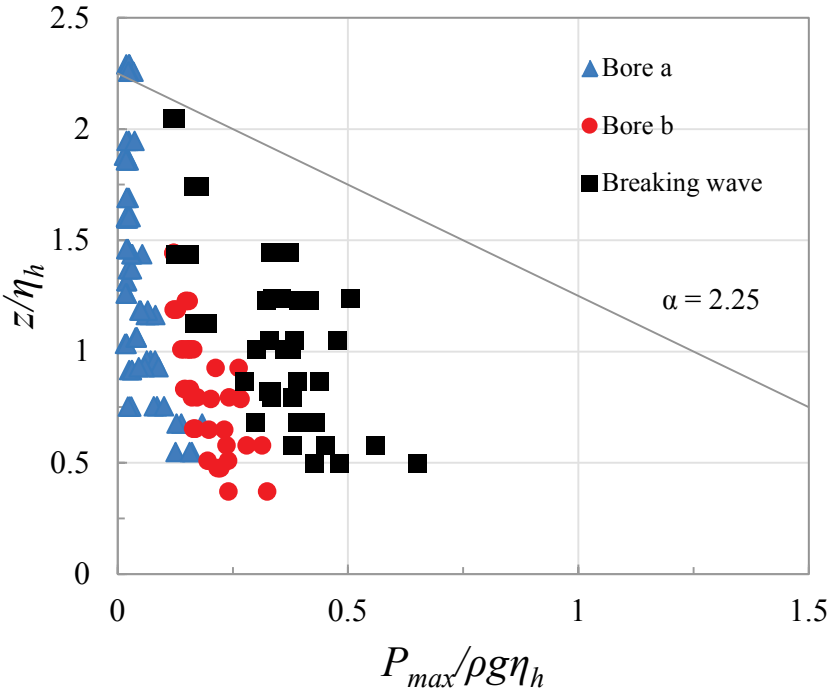

Fig. 3.26. Non-dimensional pressure distribution for Case C24

Further, in Fig. 3.23 indicates that $\alpha = 3$ is not an effective assumption for the estimation of tsunami force in the case of breaking waves. Therefore, special attention should be paid in deciding the value of α, which can be crucial under certain tsunami conditions. Fig. 3.25 shows the non-dimensional wave pressure distribution for the 'Case B13'. It is clearly visible that non-dimensional pressure distribution varies with the incident wave type (i.e, bore *a*, bore *b* and breaking wave). Moreover, the nonlinear pressure distribution and the estimation of α for Case C24 demonstrated in Fig. 3.26. As indicated in the figures the value of α for the estimation of tsunami force can be selected in a way that it envelopes the whole distribution. The estimated α values for each case are tabulated in Table 3.2.

Table 3.2. Estimated value for α for each case

Case	α	Case	α
B11	2.0	C11	2.25
B12	2.0	C12	2.25
B13	2.25	C13	2.25
B14	2.0	C14	2.25
B15	2.0	C15	2.25
B21	2.25	C21	2.25
B22	2.25	C22	2.25
B23	2	C23	2.25
B24	2	C24	2.25

In this way, it is possible to estimate an appropriate value for α to use in the tsunami force estimation. Results shows that in general, the value of α reduces for the building with openings, compare to the general recommendation $\alpha = 3$ (Asakura et al., 2000). At the same time, the value of α shows almost no variation with respect to the internal spatial configuration of the building, as far as one particular type of building

is concerned. However, α for type 'B' building is slightly lower than the type 'C' building which has larger openings. This can be resulted due to the more water volume interact directly on the inner wall in type 'C' building, compare to the case with less openings which is case 'B'. However, it should be noted that the location of the pressure gauges can affects to the final estimation, mainly because the flow pattern inside the building can be varied upon the spatial arrangement of the building.

3.5 Summary

In this chapter, the effect of the structural configuration of building toward the acting tsunami force was assessed through an experiment study and the possibility of the estimation of design tsunami force under such circumstances was examined. The variation of the tsunami force on the whole structure as well as inner wall component alone was discussed. From the results it was noticed that the tsunami force on the building varies with the incident wave type at the location of the structure as well as the internal configuration of the structure. Significant reduction of the acting force was observed with the increase of the openings in the building. Further, it was found that the tsunami force on the structure can be minimized by positioning the inner walls of the structure in the landward side. However it should mention that the acting vertical force on the structure can be varied on the placement of the inner wall, which is not discussed in the current study.

Additionally, two tsunami force estimation approaches were discussed for the buildings with openings and it was found that the difference of the force from both estimation methods is insignificant. Moreover, importance of selecting appropriate value for the coefficient of the effective depth (α) in pressure distribution, is highlighted and the estimation method for α is suggested. The value of α for one particular type of structure shows an almost uniform value irrespective of the internal arrangement of the inner wall. Value of α reduces for the building with openings, compare to the general recommendation $\alpha = 3$ (Asakura et al., 2000).

Chapter 4

TSUNAMI FORCE ON THREE-DIMENSIONAL STRUCTURES

4.1 General

As it is discussed in Chapter 1, in high populated coastal plain areas, time needed for the complete evacuation under tsunami threat becomes a critical factor, especially when tsunami source is close to the coast. Therefore, it is essential to apply artificial evacuation structures like evacuation buildings and towers (Yasuda et al., 2007) in those areas. According to the existing tsunami evacuation building design guideline (Cabinet Office, 2005), in the estimation of the tsunami force acting on building, current practice is to use hydrostatic pressure distribution considering three times the height of tsunami inundation depth at the location of the building without the existence of the building. The validity of this estimation method was confirmed by the experimental study by Asakura et al. (2000) and by following studies (Fauzie et al., 2009). Meantime several other studies (Arikawa et al., 2005; Ikeya et al., 2005) have suggested that the above method underestimates the actual force, which demands further analysis on tsunami force estimation. Furthermore, a study of Asakura et al. (2000) assumes infinite width for the structure, and result could have been different for a three-dimensional structure due to the variations in tsunami flow mechanism around the structure. There is a lack of studies in evaluation of the applicability of above mentioned tsunami force estimation method for such cases. This section of the study was conducted with the aim of assessing the applicability of this existing approach to estimate the tsunami force acting on a three-dimensional building and discuss the differences in tsunami acting mechanism for two-dimensional and three-dimensional cases.

4.2 Numerical Study

Three-dimensional numerical model developed by Lee et al. (2010) was used for the numerical analysis. In the model, liquid and gas phases are considered to be immiscible and continuity (Eq. 4.1) and modified Navior-Stokes (Eq. 4.2) equations are used as governing equations, while free surface is determined by advection equation (Eq. 4.3) which incorporates VOF method.

$$\nabla \cdot (\theta V) = \tilde{q} \tag{4.1}$$

$$\frac{\partial V}{\partial t} + (V \cdot \nabla)V = -\frac{\nabla p}{\rho_w} + \nabla \cdot (2v_w E - \tau) - \frac{2}{3}\nabla\{v_w(\nabla V)\} + F_b - \gamma V \tag{4.2}$$

$$\frac{\partial F}{\partial t} + \nabla V \cdot F = F\tilde{q} \tag{4.3}$$

where V is the velocity vector; $\tilde{q} = q/\Delta x_s$ is the source term required to generate wave; q is the flux density at wave source position$(x = x_s)$; t is the time; p is the pressure; ρ_w is the fluid density; v_w is the kinematic viscosity coefficient; E is the strain rate tensor; τ is the sub-grid stress vector; F_b is the body force such as gravity and surface tension; and γ is the wave dissipation factor which equals to zero except in the added dissipation zone.

Fig. 4.1 shows the calculation domain for the study. Considering its symmetry, only half of the domain was considered in the calculation and computational grid sizes were selected as Δx=1~2cm, Δy=1~2cm, Δz=1~2cm while allowing finer grid around the structure. Tsunami was generated using dam break scenario with the variation of offshore water depth H_1 and nearshore water depth H_2 as shown in Table 4.1, for six wave conditions. At the same time five cases of blockage ratio (*B/W)* were considered (Table 4.2) while *B* and *W* represent width of the structure and width of the channel respectively.

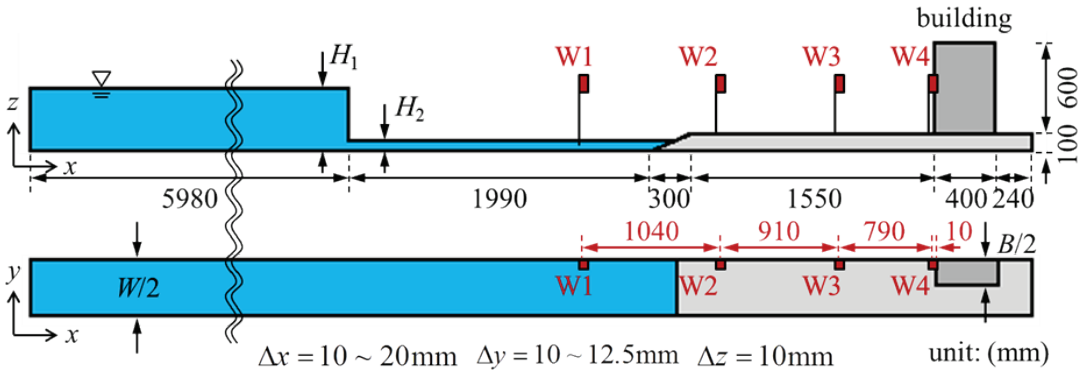

Fig. 4.1. Arrangement of computational domain; top: side view, bottom: top view

Table 4.1. Water level at source

	H_1 (cm)	H_2 (cm)
Wave1	20	5
Wave2	20	10
Wave3	40	5
Wave4	40	10
Wave5	60	5
Wave6	60	10

4.2.1 Model verification

The results of the two-dimensional experimental study conducted by Ikeno et al., 2003 (similar with Case2) were used to verify the re-producibility of the employed numerical model. Fig. 4.2 shows the comparison of experimental and calculated results for wave heights at W1~W4 wave gauge locations (Fig. 4.1), for Wave 3 condition. From the figure it can be observed that numerical model re-produces the offshore wave heights at W1 and W2 accurately. Meanwhile, comparing the results at the W3 and W4 it can be observed that the numerical model shows a slight deviation at the time of impact, but shows good agreement for the rest. In the current study

major attention was paid upon the estimation of maximum tsunami force acting on the building, which is appeared to occur after a significant time of the initial impact. Therefore, it minimizes the effect of possible under estimation of impact force.

Table 4.2. Blockage ratio for different channel & structure width

	Channel width W (cm)	Structure width B (cm)	B/W
Case1	10	0	0.00
Case2	10	10	1.00
Case3	35	8	0.23
Case4	35	16	0.46
Case5	35	24	0.69

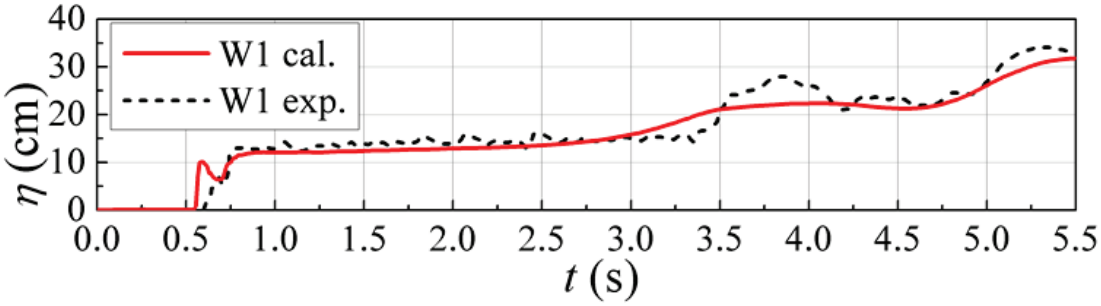

(a)

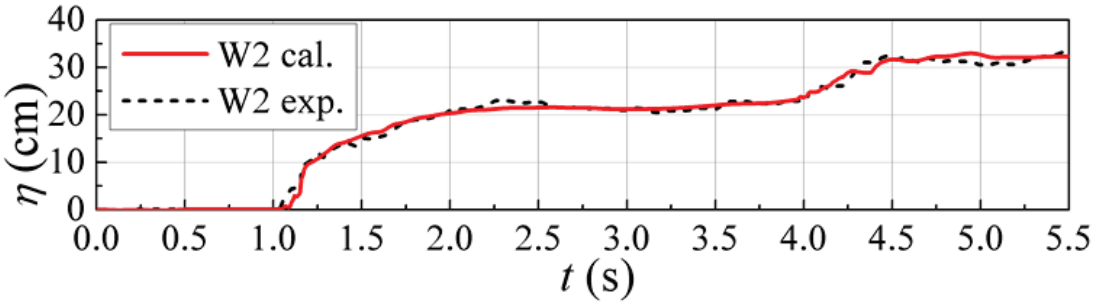

(b)

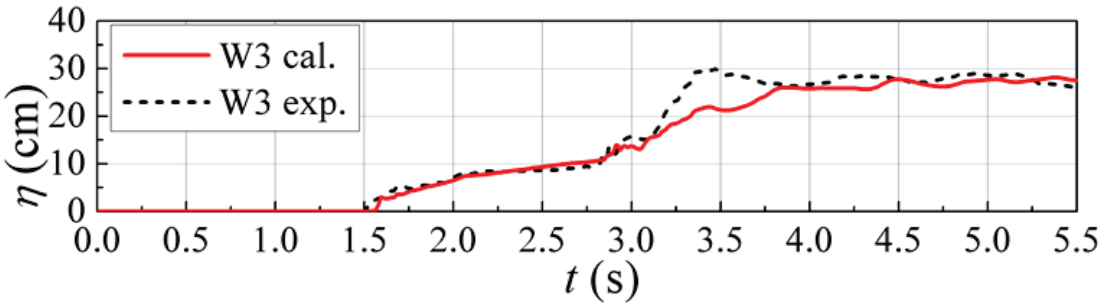

(c)

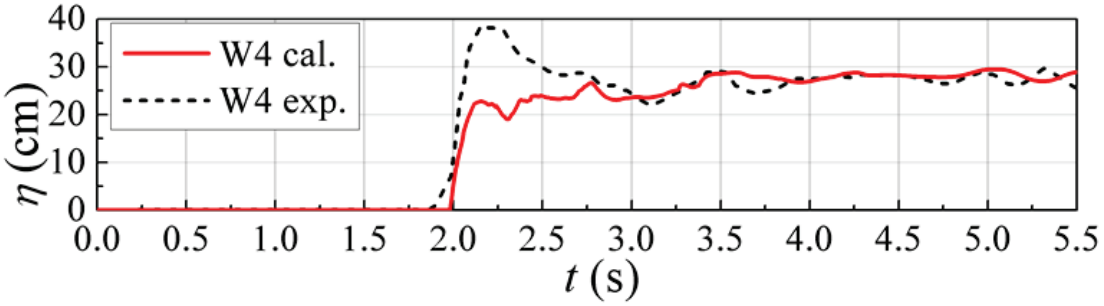

(d)

Fig. 4.2. Comparison of experiment and calculated flow profiles at each gauge location

4.2.2 Wave run-up characteristics

This section discusses the results based on Case1, in which the structure is not installed. Fig. 4.3 shows the flow velocity (u) in x-direction which measured at z = 1cm under different wave conditions, and temporal variation of flow profile, at the location of $W4$. A smooth variation can be observed from the figure. Further, flow characteristics show no variation with respect to the value of H_2 for the same value of H_1, while the arrival time of tsunami decreases with the increase of H_1. At the same time, high values of flow velocity at the tsunami front, appears to be decreased with time. It is also evident that the arriving velocities at the impact location are significantly affected by the variation of H_1, and increase for the smaller values of H_2. In order to estimate the Froude number (Eq. 4.4) for each time step, $\sqrt{g\eta}$ was calculated and plotted against the velocity u as shown in Fig. 4.4. In the figure the gradient of the each straight line starts from the origin gives the Froude number for the particular points on the line.

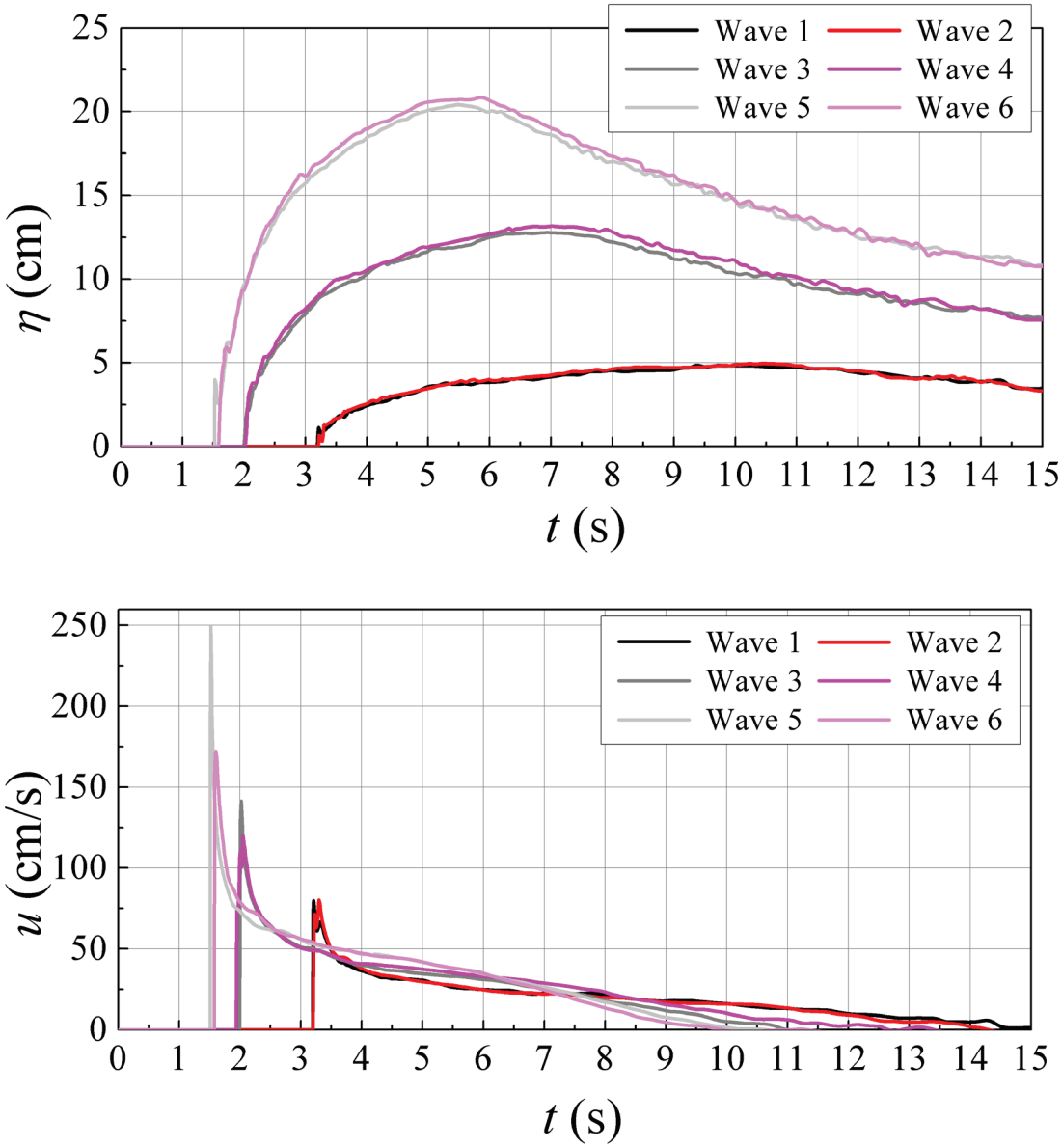

Fig. 4.3. Temporal variation of flow characteristics for Case1 (Above : Water surface Below : Flow velocity)

$$Fr = \frac{u}{\sqrt{g\eta}} \tag{4.3}$$

From the figure, at the time of initial impact, high Froude number values can be observed due to lower flow depth and higher velocities, which decrease over time as flow velocity drops and flow depth increases. Value of the Froude number continues to decrease further as flow depth and velocity drop down with time. It is also evident

from the figure that, even though the effect of H_2 is insignificant in the subcritical condition of the flow, it has a significant influence in the supercritical region of the flow.

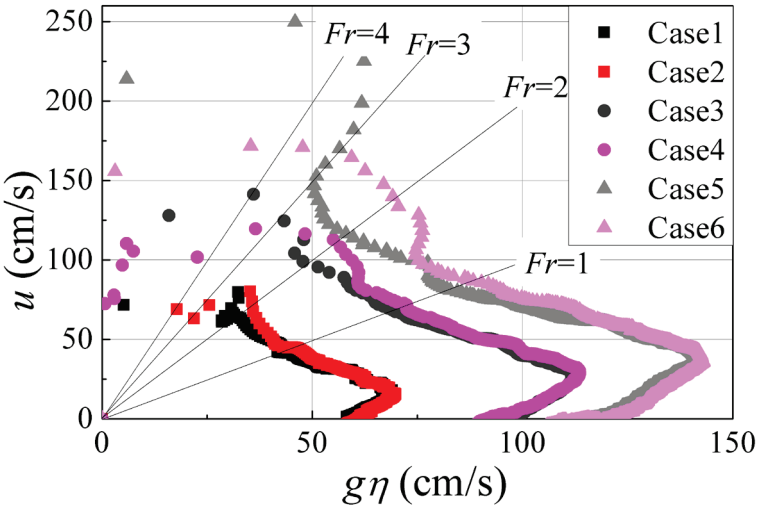

Fig. 4.4. Estimation of Froude number

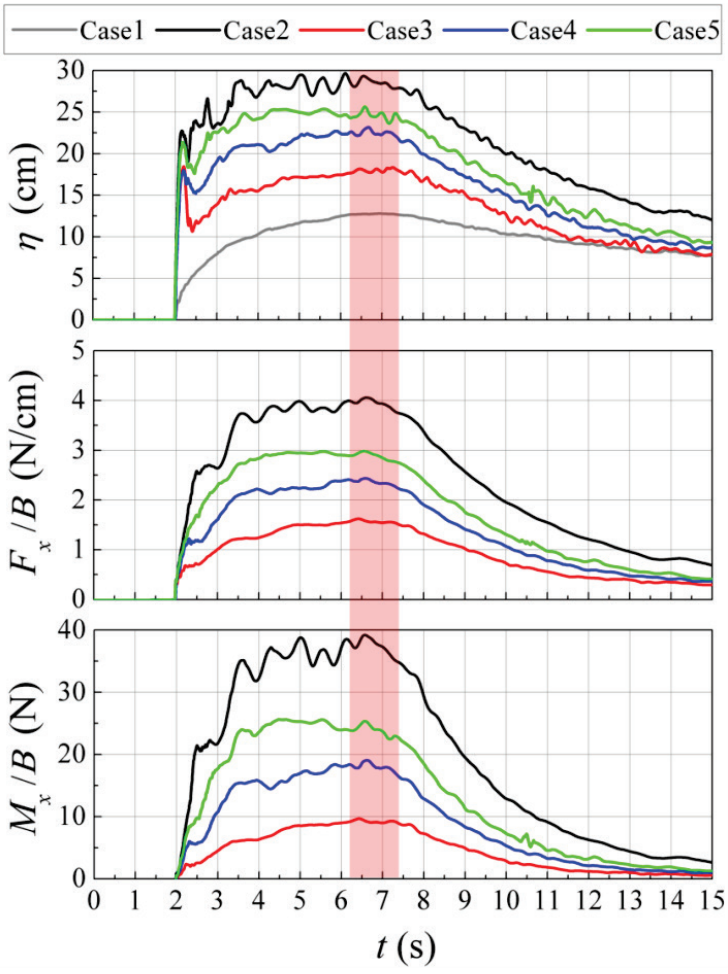

Fig. 4.5. Temporal variation of (from above) water surface, tsunami force and overturning moment for Wave3

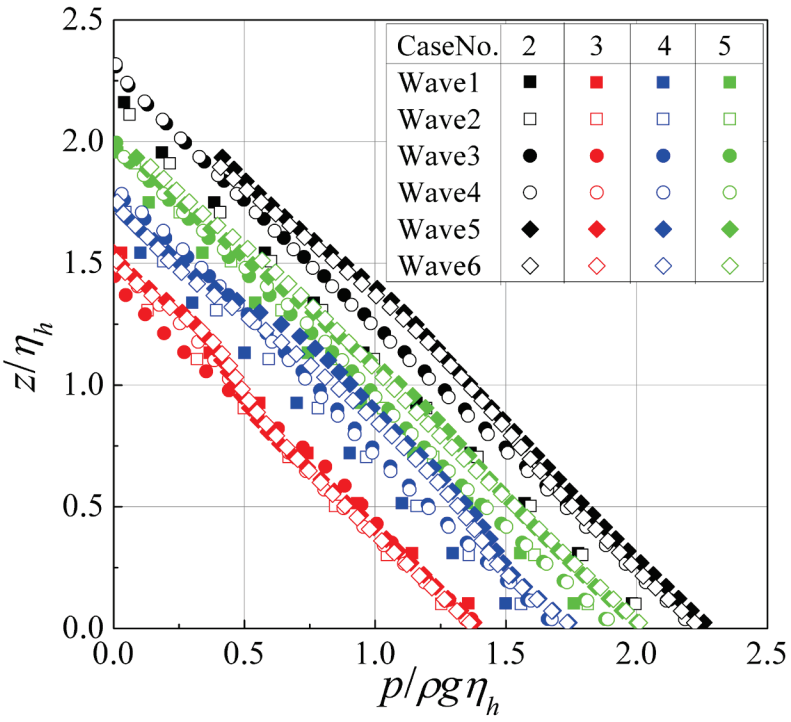

Fig. 4.6. Dimensionless wave pressure distribution in vertical direction

4.2.3 Effect of the blockage ratio on the flow mechanism

Fig. 4.5 shows the temporal variation of water profile, acting external force and moment on the structure, for Wave 3 condition. Water surface profile is measured in front of the structure and the external force and moment are measured along the vertical centerline of the structure considering a unit width, while considering the tsunami pushing in *x*-direction around horizontal axis at the ground level as positive in moment calculation. It is observed from Fig. 4.5 that each hydraulic characteristic increases its value with the increment in blockage ratio. Further, when water level in front of the structure reaches its maximum (except the splash at the initial impact), it can be seen that acting external force and overturning moment also reach to their maximum values (region of red strip in the figure). In addition, since a similar trend is observed when compare Case2 results with the results for Case3~5, the tsunami acting mechanism in two-dimensional simulation appeared to be without significant change from the three-dimensional simulation. With these observations it can be confirmed that, regardless of the condition whether the tsunami flow is allowed to pass by the structure or not, the maximum force on the structure occurred at the time of flow depth in front of the structure reaches its maximum. Even though, the results

discussed here are curtailed to Wave 3 condition due to space limitation, it should be mentioned that similar trend was observed in results for rest of the cases.

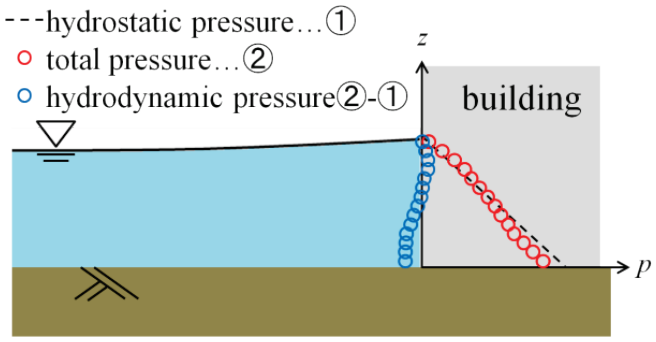

Fig. 4.7. Derivation of hydrodynamic pressure

4.2.4 Wave pressure distribution analysis

The vertical distribution of the dimensionless wave pressure distribution at the occurrence of maximum wave force is shown in Fig. 4.6. Here, the vertical axis represents the dimensionless height, which the height of pressure action (z) divided by the maximum inundation depth in front of the structure (η_h) obtained from Case 1. Meanwhile, horizontal axis represents the dimensionless wave pressure, which the wave pressure acting on structure measured along the centerline, divided by $\rho g \eta_h$. It can be observed from the figure that the dimensionless pressure distribution has a similarity with hydrostatic triangular pressure distribution. In addition, it shows no variation with respect to the initial wave condition and especially to the change in nearshore water depth H_2. At the same time, dimensionless pressure appeared to be increased when blockage ratio increases. This behavior can be explained as a result of limiting the ability of incoming tsunami to pass the structure by its sides with increasing the blockage ratio, which enhance the flow action on the front face of the structure.

As it is shown in Fig. 4.7, the hydrodynamic pressure acting on the structure is calculated by taking the difference of, total pressure acting on the structure at the occurrence of maximum wave force and the hydrostatic pressure with respect to the flow depth at the particular moment.

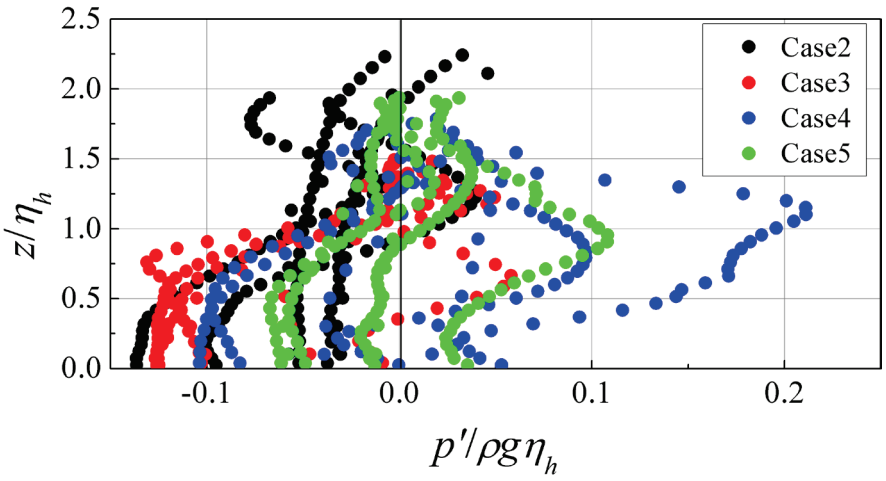

Fig. 4.8. Distribution of dimensionless hydrodynamic pressure

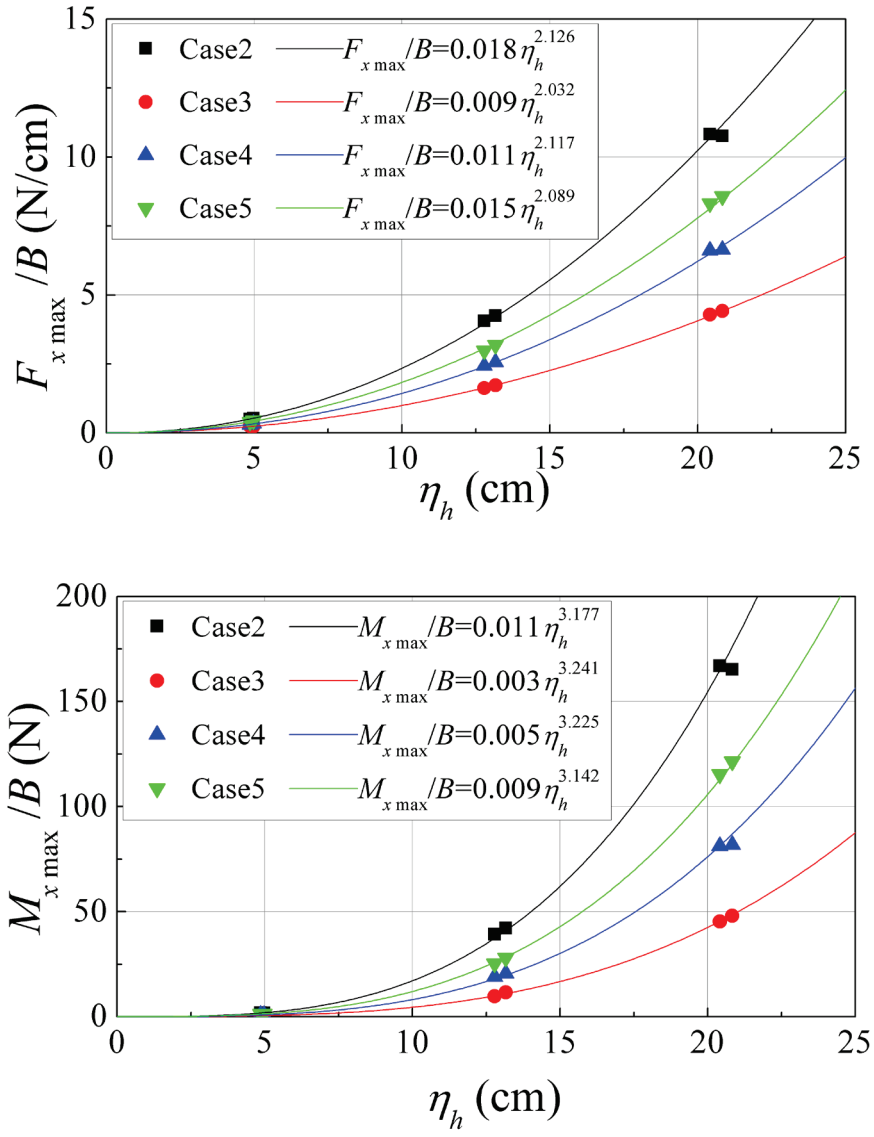

Fig. 4.9. Relationship of tsunami force (above) and overturning moment with maximum inundation depth for Case1

Fig. 4.8 shows the variation of non-dimensional hydrodynamic pressure against the non-dimensional flow depth, where p' denotes the hydrodynamic pressure. The total pressure value for Case2 appeared to be slightly lower than the hydrostatic component, because of the negative value of hydrodynamic pressure, in the figure. Further, since the absolute value of $p'/\rho g\eta_h$ close to 0.2 is comparatively smaller than the related value for the dimensionless wave pressure in Fig. 4.6, it can be understand that the hydrostatic pressure component is dominant compared to the hydrodynamic component, at the time of maximum wave force acting on the structure.

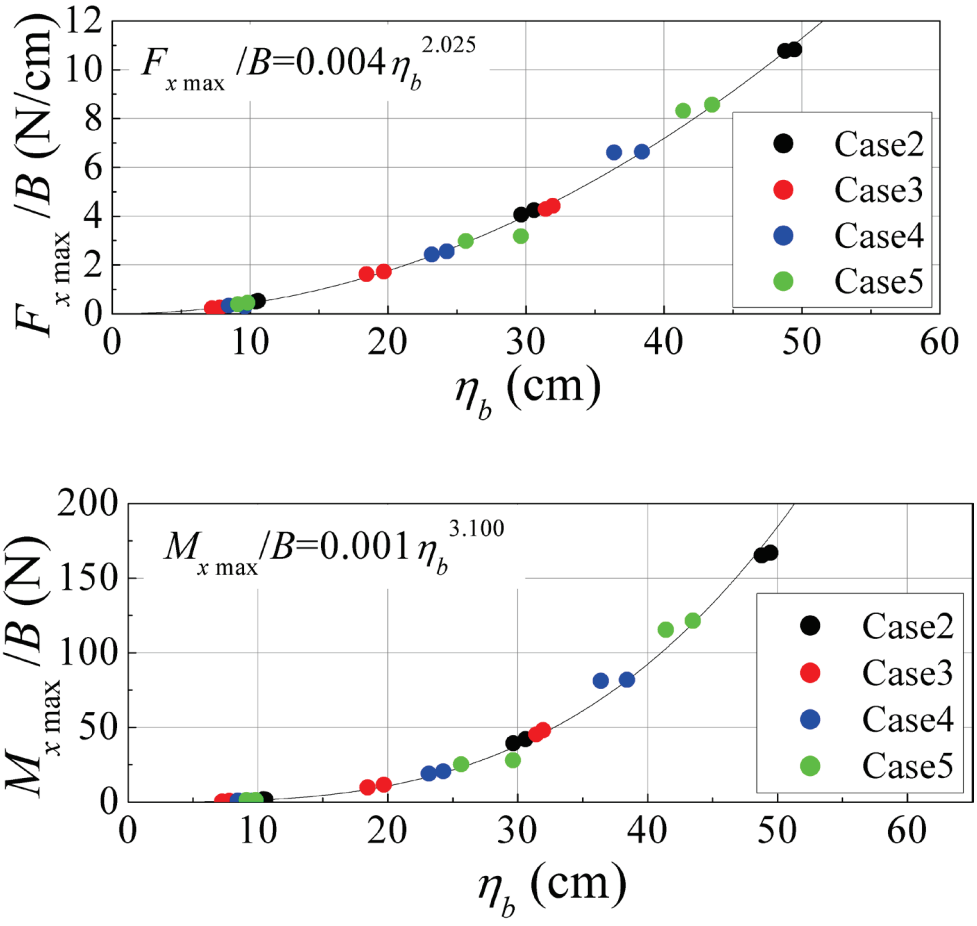

Fig. 4.10. Relationship of force (above) and moment (below) with water depth in front of the structure

4.2.5 Relationship between blockage ratio and maximum tsunami force

Fig. 4.9 shows the relationship between tsunami force and the maximum inundation depth of the tsunami run-up (from Case 1). An approximation curve is plotted for each blockage ratio, as it is described in the figure. The increase of the tsunami force acting on the structure with the increase in blockage ratio can be

confirmed from the figure. Also, for all the blockage ratios, rise in wave force can be observed with the increase of maximum inundation depth. It is noticed that the acting force is approximately proportional to the η_h^2 while it is η_h^3 for the overturning moment. Further, Fig. 4.10 shows the relationship between tsunami force and the maximum inundation depth for each case of η_b measured in front of the structure. An approximate relationship for the whole distribution is derived and shown in the figure. It can be noticed that the relationship is independent from the blockage ratio and the tsunami force acting on the structure increases with the increase of flow depth in front of the structure. Further, acting force is approximately proportional to the η_b^2while it is η_b^3 for the overturning moment. With use of this relationship, the acting tsunami force on the structure can be directly estimated for a known value of inundation depth in front of the structure. Here, the increase of wave force with the increase of blockage ratio which discussed in the previous section is included as a factor of fluctuation of water level in front of the structure.

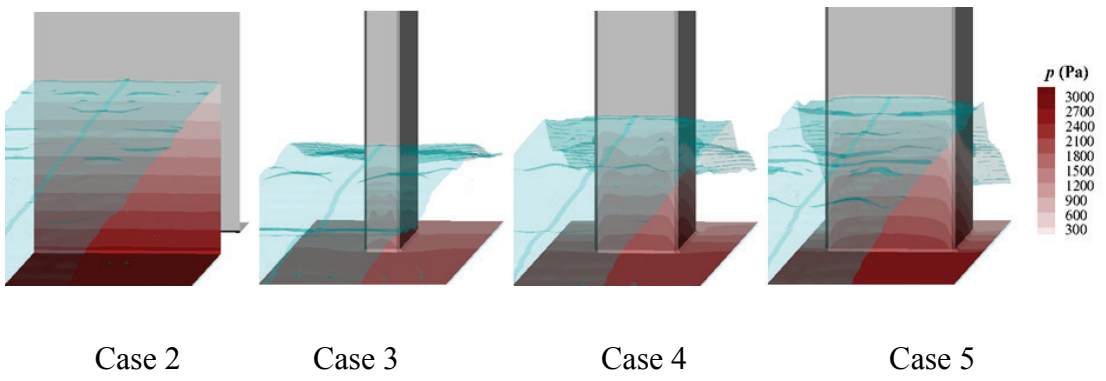

Fig. 4.11. Water surface profile and distribution of pressure acting on the structure for each case (Wave3)

The wave pressure distribution for each blockage ratio is shown in Fig. 4.11, for the time of maximum wave force acting on the structure. From the figure it can be seen that the pressure distribution is uniform in horizontal direction for the Case 2. Even though a slight decrease in pressure is observed at the edge of the structure for other cases, overall it is safe to state that the pressure distribution is uniform in horizontal direction. Further, it can be seen that the flow depth which causes the maximum wave force, is increasing with the increased blockage ratio.

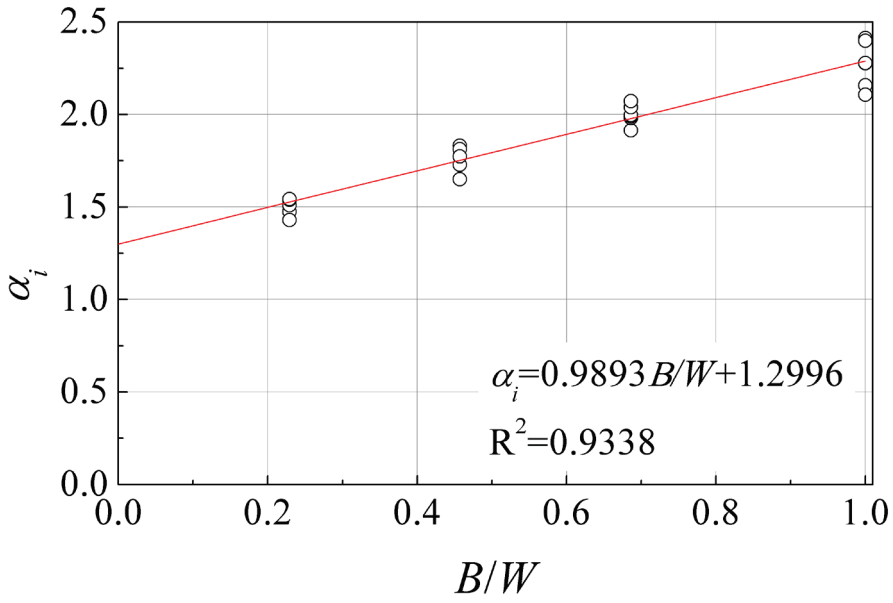

Fig. 4.12. Relationship between horizontal wave pressure index and blockage ratio

4.2.6 Modified equations

As described in the previous sections, since the contribution of hydrodynamic pressure to the total pressure is small regardless of the blockage ratio, the wave pressure distribution on the structure becomes closely similar to the hydrostatic pressure distribution. Therefore, once the horizontal wave pressure index for each blockage ratio α_i (the intercept values of the each case shown in Fig. 4.6) and the maximum inundation depth without the structure is known, it can estimate the tsunami force acting on the structure. The relationship between α_i, which obtained in numerical study and blockage ratio B/W is shown in Fig. 4.12. Assuming a linear variation of α_i against B/W, a relationship as shown in the figure was obtained. Further, considering the value of α_i in the two-dimensional (B/W=1) case α as basis, a relationship between blockage ratio and $\alpha_i$was obtained as shown in Eq. 4.4.

$$\left.\begin{aligned} \alpha_i &= \alpha\beta \\ \beta &= 0.4322\frac{B}{W} + 0.5678 \end{aligned}\right\} \tag{4.4}$$

Here, β is the correction factor for wave pressure reduction due to blockage ratio. This relationship was applied to the formula derived by Asakura et al. (2000) in order to obtain the tsunami force applied in a three-dimensional case, which is shown as in Eq. 4.5.

$$\left.\begin{aligned} Fx' &= \frac{1}{2}\rho g B(\alpha\beta\eta_h)^2 \\ Mx' &= Fx \times \frac{1}{3}(\alpha\beta\eta_h) \end{aligned}\right\} \tag{4.5}$$

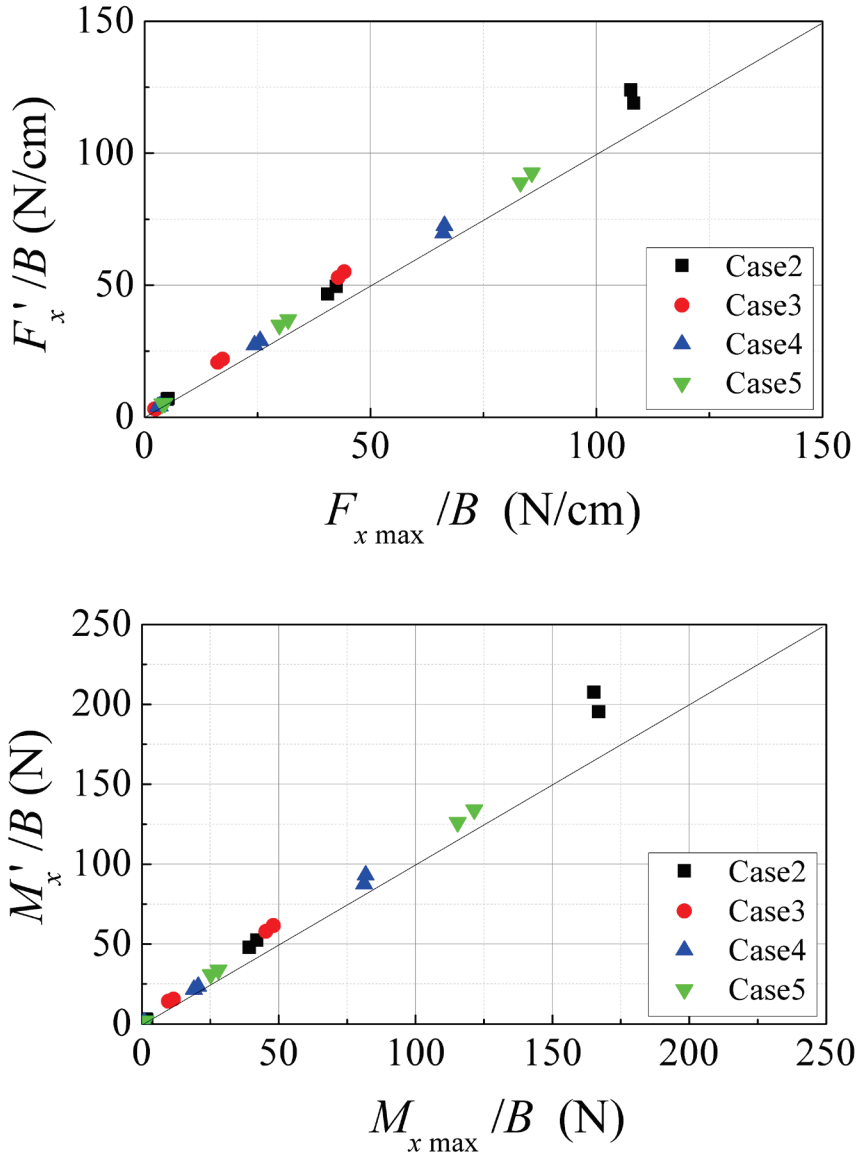

Fig. 4.13. Tsunami Force (above) and overturning moment (below) per unit width of the structure

It should be noted that in the derivation of Eq. 4.5, the wave pressure distribution in the horizontal direction was assumed to be uniform. The comparison of the tsunami force estimated from the above modified equation, and the maximum tsunami force measured in the experiment is shown in the Fig. 4.13. Even though, both tsunami force and overturning moment appeared to be slightly overestimated from derived method, they lie on the safe side and hence prove their applicability in practice. The slight deviation between practical and estimated values occurs due to the ignorance of the effect of hydrodynamic pressure component in the estimation of α for two-dimensional case (from Fig. 4.6), which can leads to a slightly larger wave pressure value than in practice.

4.3 Summary

Tsunami force acting on the structure increases with the blockage ratio, which is caused due to the rise of water level in front of the structure with the increase of blockage ratio.

Vertical wave pressure distribution for both two-dimensional and three-dimensional cases is closer to triangular distribution profile. Through the estimation of hydrodynamic pressure component, it was confirmed that the effect of flow velocity is minimum in the estimation of maximum wave force.

The acting wave pressure distribution in the horizontal direction is confirmed to be closely uniform even in the three-dimensional case. However slight drop of pressure was observed close to the edge of the structure.

To estimate the maximum tsunami force acting on the structure, blockage ratio and horizontal pressure index were introduced. Tsunami force estimation formula was suggested which inclusive of blockage ratio, and its practical applicability and effectiveness was discussed.

Chapter 5

FAILURE OF CONCRETE STRUCTURE UNDER TSUNAMI LOADING

5.1 General

As it was highlighted in Chapter 1, Aftermath field studies (Imamura & Anawat, 2012; Nakano, 2008) of tsunami events also revealed the fact that the destruction of coastal buildings adds vast amount of floating debris to the on-going tsunami flow, which increase the damage to the surrounding properties. Properly constructed coastline buildings not only would helpful in minimizing the damage but also have an added advantage of using as tsunami evacuation buildings. Japanese Cabinet Office has published a design guideline (2005) for such tsunami shelters primarily based on two-dimensional laboratory experiments conducted by Asakura et al. (2000). Further, Nakano (2008) conducted post-tsunami studies to compare design load estimated by the design formula from the guideline with the observed damage in Sri Lanka and Thailand following 2004 Indian Ocean Tsunami and study highlights the variation in failure pattern of coastal structures under tsunami loading, depending on different structural shapes and construction techniques. Meanwhile, Nishiyama (2011) classified damage to the reinforced concrete buildings by 2011 Tohoku earthquake and tsunami into six categories as, collapse of first floor, overturning, movement and wash away, tilting by scouring, fracture of the wall and debris impact based on post-tsunami survey. Therefore, it is important to distinctly understand the behavior of acting load and mechanism of failure of coastal building under tsunami wave, in order to develop a comprehensive guideline to support the coastline building design procedures in the future. Significant amount of studies have being carried out in the

past in ambition of estimating the tsunami force acting on buildings and its damage. Shuto (1993) estimated the damage to individual house in terms of tsunami height and type of house, from the collection of past post-tsunami data. Iizuka and Matsutomi (2000) have been tried to measure the degree of damage to buildings by estimating fluid force acting on structure which obtained from fore and rear inundation heights. Even though these damage estimation criteria generally cover several types of buildings, it still has to be developed in order to capture the detail damage to concrete structures. Further, the failure of coastal buildings under recent tsunami events has highlighted the inadequacies in those estimation methods in the practical applications.

5.2 Material Modeling in LS-DYNA

5.2.1 Equation of State

Equation of state is used in the aim of linking three inter dependent thermodynamic quantities, pressure, density and internal energy. The Gruneisen EOS (Eq. 5.1) is used in the simulation of pressure variation in the water (Hallquist, 2006).

$$p = \frac{\rho_0 C^2 \mu \left[1 + \left(1 - \frac{\gamma_0}{2}\right)\mu - \frac{a}{2}\mu^2\right]}{\left[1 - (S_1 - 1)\mu - S_2 \frac{\mu^2}{\mu + 1} - S_3 \frac{\mu^3}{(\mu + 1)^2}\right]^2} + (\gamma_0 + a\mu)E \tag{5.1}$$

where E is the internal energy per initial volume; C is the speed of sound in water; S_1, S_2 and S_3 are the coefficients of the slope of the $u_s - u_p$ curve; γ_0 is the Gruneisen gamma; a is the first order volume correction to γ_0; u_s and u_p are the shock wave velocity and the particle velocity respectively. The compression is defined in terms of the initial density ρ_0 and the current density ρ as;

$$\mu = \frac{\rho}{\rho_0} - 1 \tag{5.2}$$

The parameters for the EOS, used in the study are shown in Table 5.1.

Table 5.1. Material properties for the water

Property	Value
Initial density ρ_0	997 kg/m^3
Speed of sound in water C	1484 m/s
Gruneisen S_1	1.97
Gruneisen γ_0	0.11

5.2.2 Concrete Material Model

The Karagozian & Case (K&C) concrete model (release III) (Malvar et al., 2000; Schwer & Malvar, 2005) was employed due to its relative simplicity compared to the other constitutive models used for the concrete like material modeling, and the numerically robustness. Even though the effectiveness of the model in impact analysis has been confirmed by several past studies (Markovich et al., 2011; Abu-Odeh, 2008; Magallanes, 2008), the applicability of such constitutive model in fluid-structure interaction analysis is yet to be assessed.

In this particular plasticity concrete model, there are three independent fixed surfaces to define the behavior of concrete; initial yield surface $\Delta\sigma_y$ (Eq. 5.3), maximum failure surface $\Delta\sigma_m$ (Eq. 5.4) and residual failure surface $\Delta\sigma_r$ (Eq. 5.5).

$$\Delta\sigma_y = a_{0y} + \frac{p}{a_{1y} + a_{2y}p} \tag{5.3}$$

$$\Delta\sigma_m = a_0 + \frac{p}{a_1 + a_2 p} \tag{5.4}$$

$$\Delta\sigma_r = \frac{p}{a_{1f} + a_{2f}p} \tag{5.5}$$

where $\Delta\sigma$ is the difference in the principal stresses; p is the compressive/tensile pressure; a_{0y}, a_{1y}, a_{2y}, a_0, a_1, a_2, a_{1f} and a_{2f} are the parameters which have to be defined by the user through experimental study. The automatic parameter generation capability available with the LS-DYNA finite element code was used in deciding those parameters for the current study. Once the failure surfaces are known during the simulation, the stress after yield is determined from linear interpolation (Fig. 5.1) as,

$$\Delta\sigma = \eta\Delta\sigma_m + (1-\eta)\Delta\sigma_y \tag{5.6}$$

Similarly the stress related to post failure surface is determined by the linear interpolation between maximum failure surface and the residual surface,

$$\Delta\sigma = \eta\Delta\sigma_m + (1-\eta)\Delta\sigma_r \tag{5.7}$$

where the parameter η is the yield scale factor which can be estimated from damage function λ. Damage function is distinctively defined for compression and tension as,

$$\lambda = \begin{cases} \int_0^{\bar{\varepsilon}_p} \dfrac{d\bar{\varepsilon}_p}{\left[1+\left({}^{p}/_{f_t}\right)\right]^{b_1}} & (p \geq 0) \\ \int_0^{\bar{\varepsilon}_p} \dfrac{d\bar{\varepsilon}_p}{\left[1+\left({}^{p}/_{f_t}\right)\right]^{b_2}} & (p < 0) \end{cases} \tag{5.8}$$

where $d\bar{\varepsilon}_p$ is the effective plastic strain increment which is expressed as,

$$d\bar{\varepsilon}_p = \sqrt{\left({}^{2}/_{3}\, d\varepsilon_{ij}^{p} d\varepsilon_{ij}^{p}\right)} \tag{5.9}$$

where f_t is the quasi-static concrete tensile strength, b_1 & b_2 are damage scaling parameters for uniaxial compression and tension respectively, and $d\varepsilon_{ij}^{p}$ is the plastic strain increment tensor.

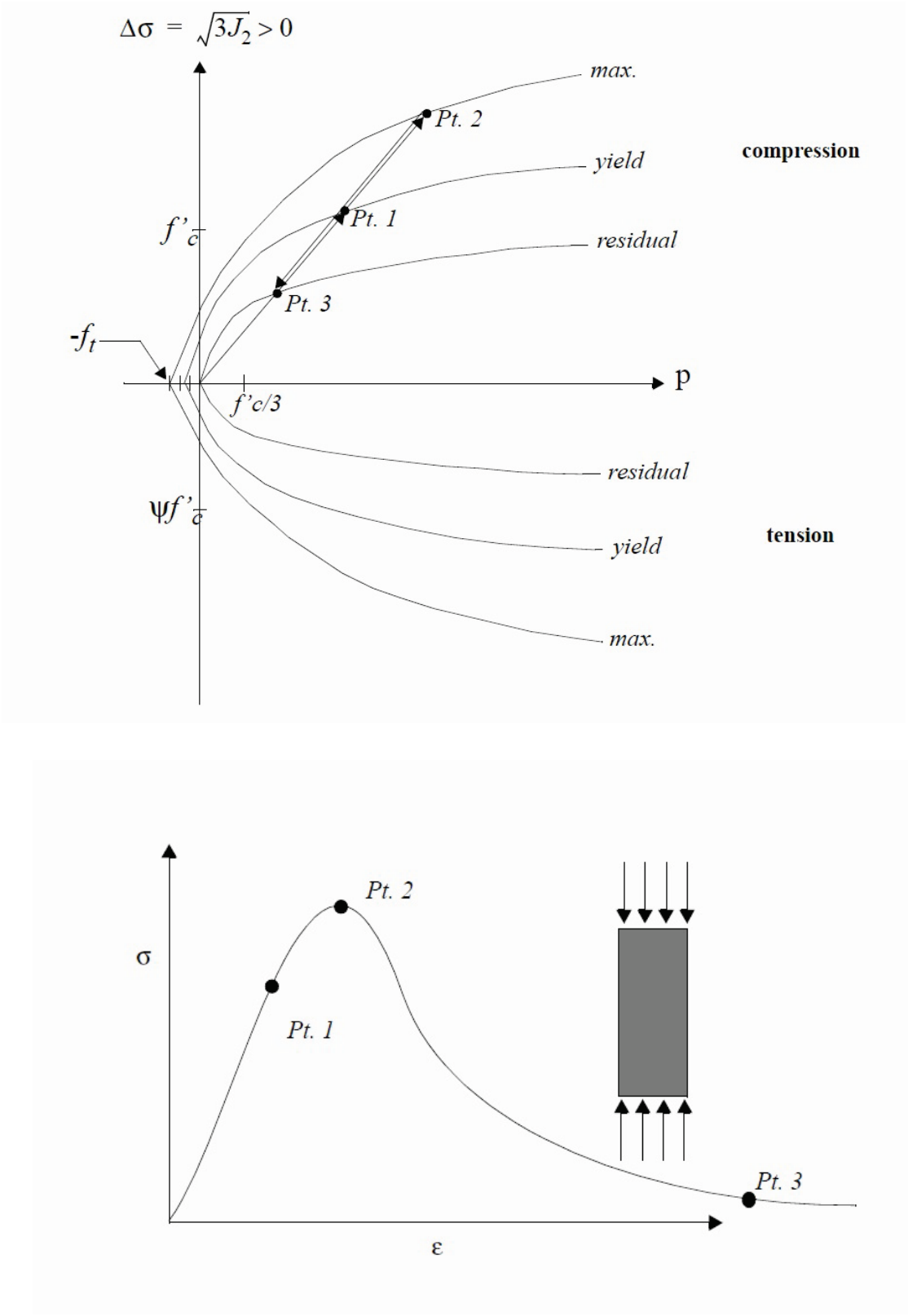

Fig. 5.1. Three failure surfaces (above) and uni axial stress strain responce (below) for the first revision of K & C concrete model

Table 5.2. Material properties used

Property	Value
Density of concrete	2400 kg/m^3
Poisson's ratio of concrete	0.2
Compressive strength of concrete	21 N/mm^2
Density of steel	7800 kg/m^3
Modulus of elasticity of steel	200,000 MPa
Poisson's ratio of steel	0.3
Yield stress of steel	250 MPa
Failure strain of steel	0.2

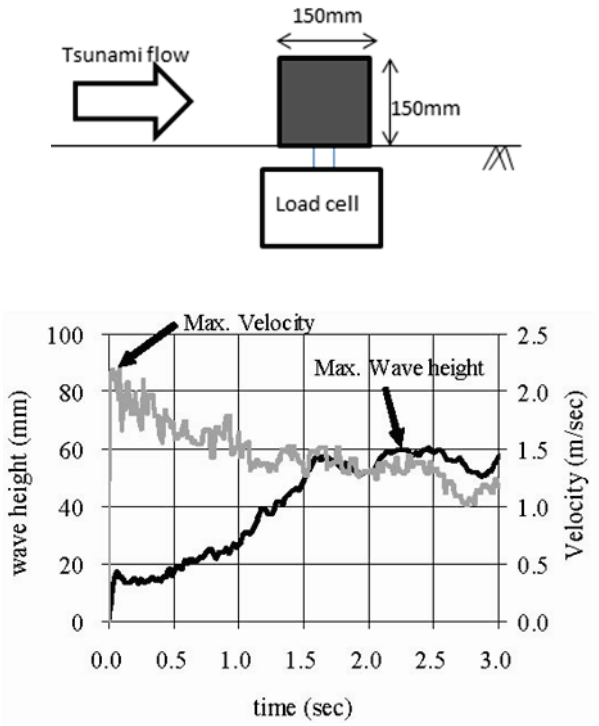

Fig. 5.2.Top: Basic arrangement of the building model (side view), Bottom: Typical time history records of wave height and velocity at location considered (without structure) (Lukkunaprasit et al., 2009)

Table 5.2 shows the material properties used in the study for reinforced concrete.

5.3 Tsunami Force on a Rigid Body

The experimental study conducted by Lukkunaprasit et al. (2009) to evaluate the tsunami force acting on a building, was simulated for a building without openings. In the experiment, tsunami had been generated by breaking of a solitary wave and the cubic model dimensions for the building were 150 mm × 150 mm × 150 mm. Fig. 5.2 shows the basic arrangement of the structure and the measured wave height and the flow velocity at the location of the structure (without structure) from the experimental study. When constructing the computational domain, the measured flow depth and velocity were used as the inflow conditions at the boundary.

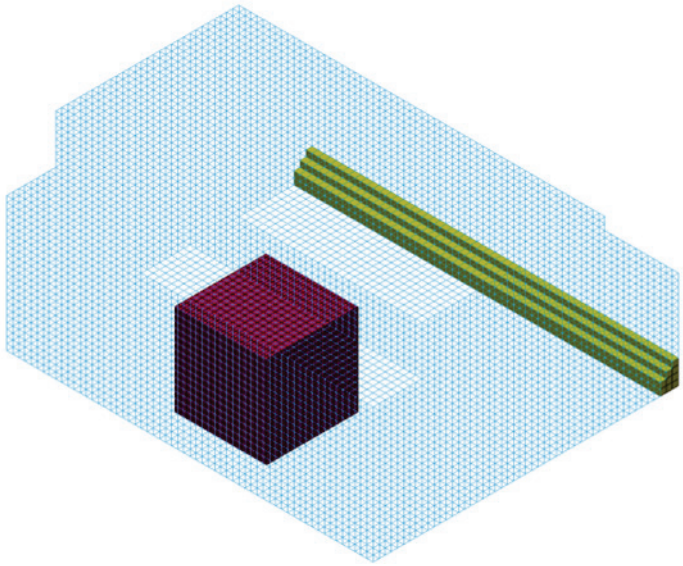

Fig. 5.3. Computational domain

Numerical computational domain (Fig. 5.3) consisted of 10mm × 10 mm × 10 mm numerical cells which are allowed to contain both water and air materials and the tsunami inflow was considered as a source at the boundary. A flow pattern similar to the experimental study (Fig. 5.4 top) was observed during the simulation (Fig. 5.4 bottom) and the Lagrangian and ALE mesh showed no penetration during the interaction. The observed temporal variation for the total tsunami force acting on the building for the experiment and the numerical simulation are shown in Fig. 5.5. It is evident that the both numerical and experimental results eventually settle for same steady force value around 15 N (~1 s after initial collision). The maximum acting force (~18 N) on the structure was observed around 0.7 s after the initial impact in the

experiment which well reproduced by the numerical model. Therefore, numerical model accurately predicts the acting tsunami force on the building.

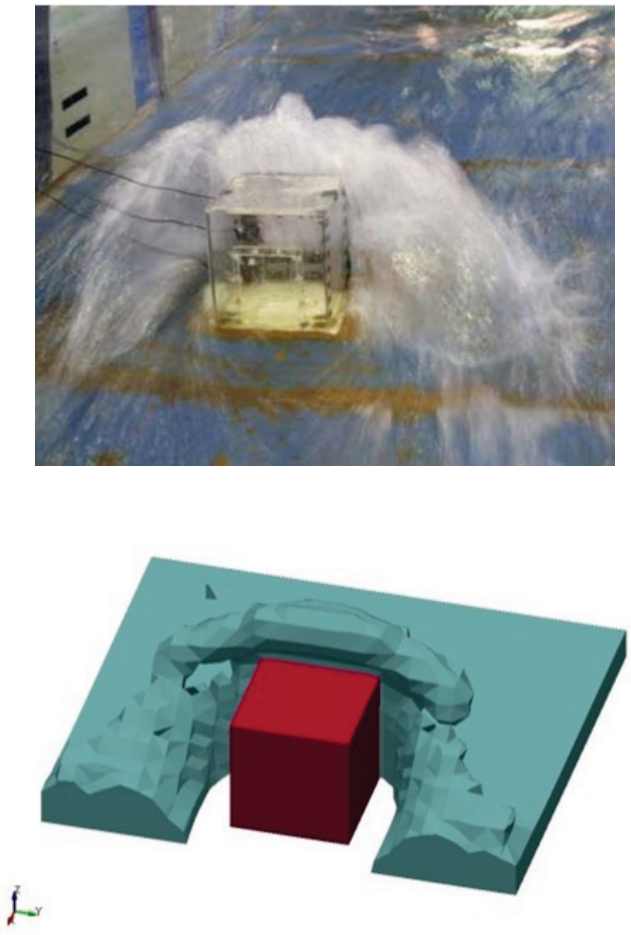

Fig. 5.4. Flow around the building during the experiment (Lukkunaprasit et al., 2009), Bottom: Deformed ALE mesh in Numerical study

5.4 Failure of reinforced concrete wall under tsunami loading

The failure mechanism of a concrete wall under tsunami loading was assessed in order to understand the failure process which has a significant importance in aspect of design. Majority of the coastal structures are constructed using concrete material and its ability to absorb large amount of incoming energy prior to the failure, has a significant advantage in the shielding against tsunami.

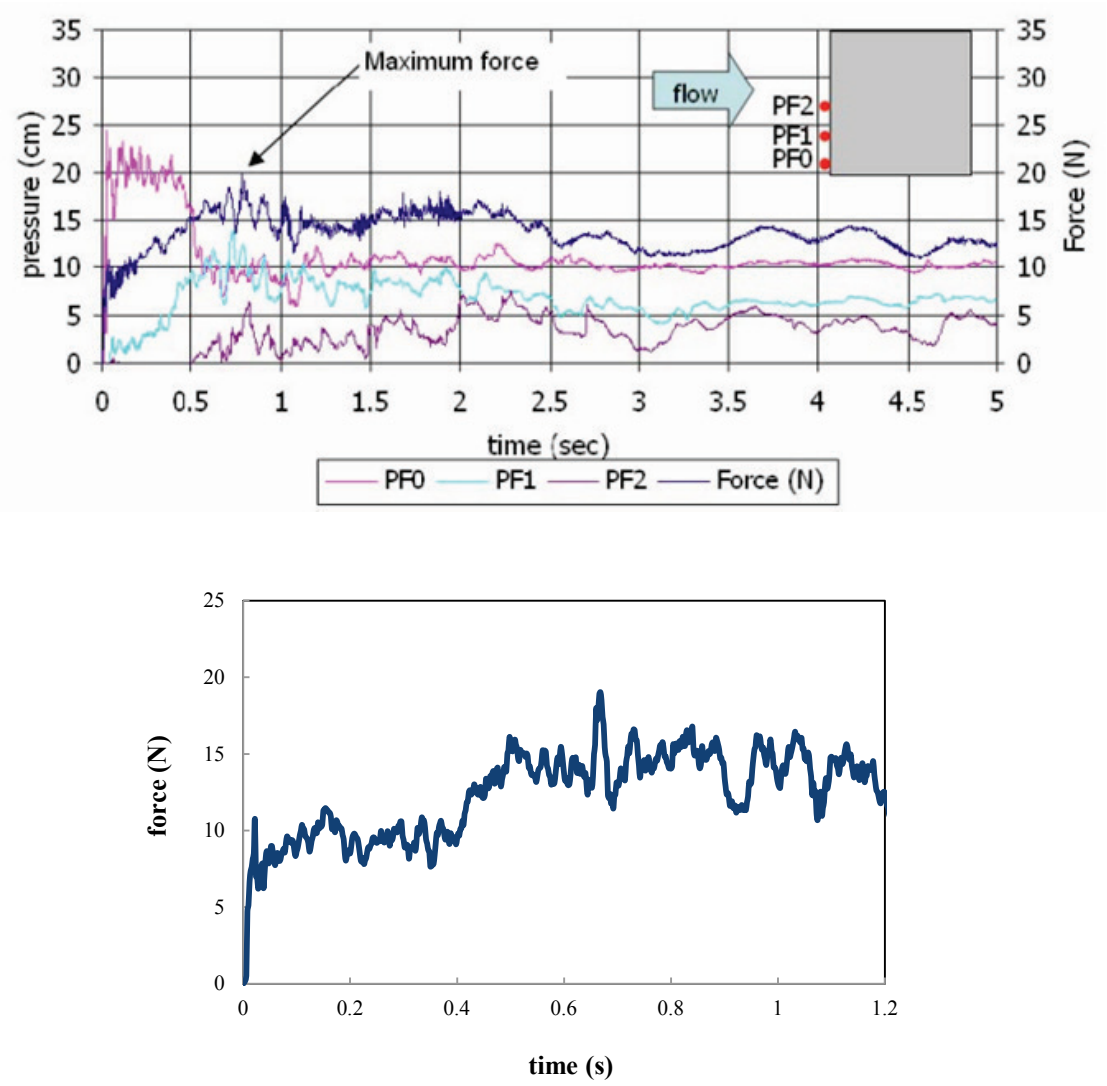

Fig. 5.5. The temporal variation of the acting tsunami force on the building for the experiment (Top, black) (Lukkunaprasit et al., 2009) and numerical simulation

5.4.1 Experiment study

Arikawa (2009) conducted real scale laboratory experiments in a large flume at the Port and Airport Research Institute, Japan, which was considered for the numerical simulation in the current study. In the experiment, tsunami impingement on a reinforced concrete wall was examined and the schematic arrangement of the flume and reinforced wall were considered as in Fig. 5.6. Tsunami has been generated using a wave paddle and the measured wave profile at 30 m offshore is shown in Fig. 5.7.

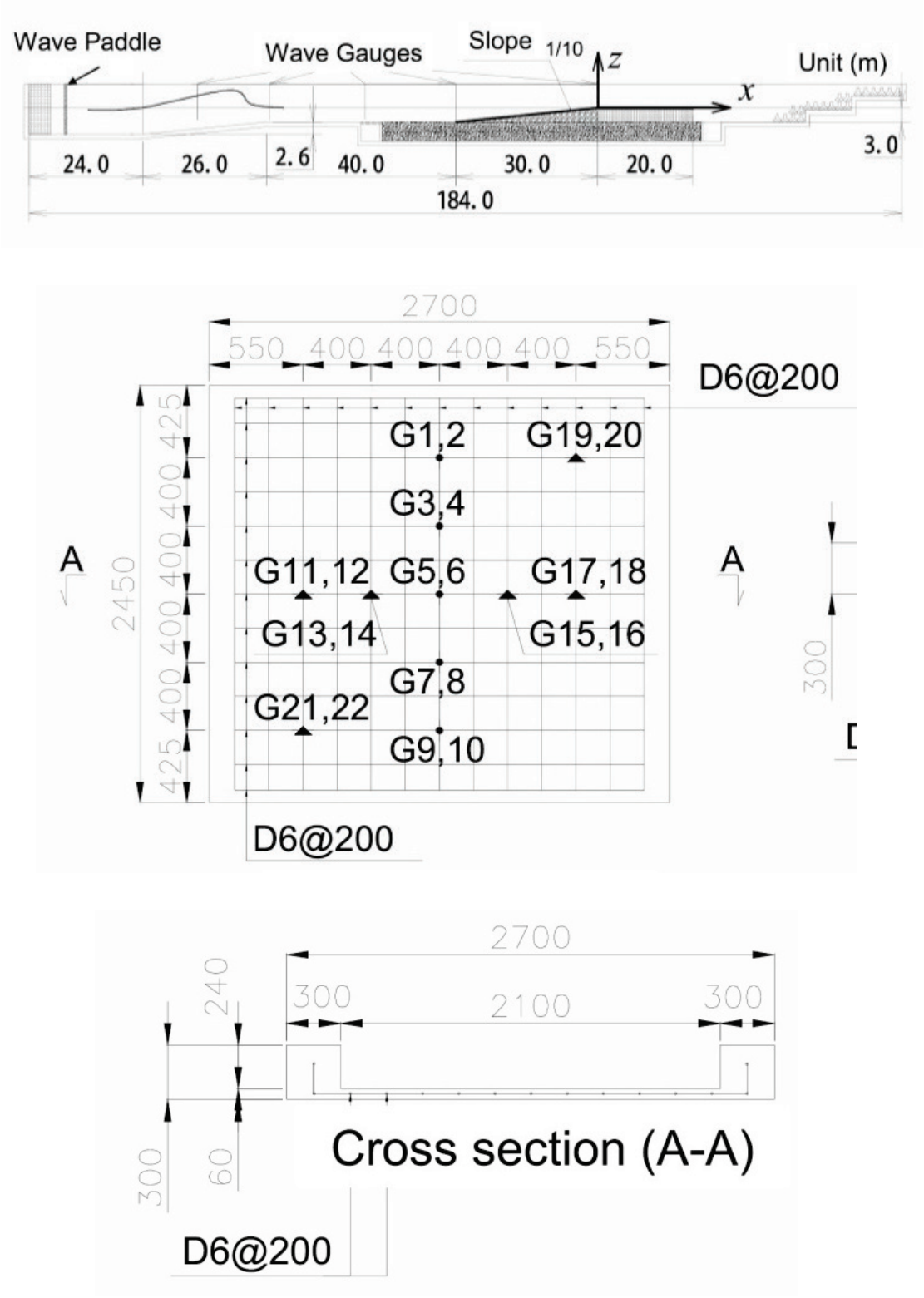

Fig. 5.6. Schematic side section of the flume (top); side view dimensions of the concrete wall and the reinforcement arrangement (middle); detailed cross section of the wall (bottom) (Arikawa, 2009)

5.4.2 Numerical study

Three-dimensional fluid model developed by Nakamura and Yim (2011) was used for the tsunami generation and propagation, and the generated wave profile at 30 m was compared with the wave profile observed in the experiment in Fig. 5.7. Good agreement was reflected in the comparison and the observed wave parameters 0.35 m prior to the structure location from the numerical result were used as the input parameters for the wave source in the Fluid-Structure Interaction (FSI) computational domain (Fig. 5.9). Selection of the source location with respect to the structure was determined by referring to Yeom (2010), where Yeom et al. (2009) successfully simulated the drifting of a container by run-up tsunami using drift collision coupled model. The reinforced concrete wall was modeled in the real scale with 20 mm × 20 mm × 20 mm solid elements and the outer domain consists of 50 mm × 50 mm × 50 mm numerical cells.

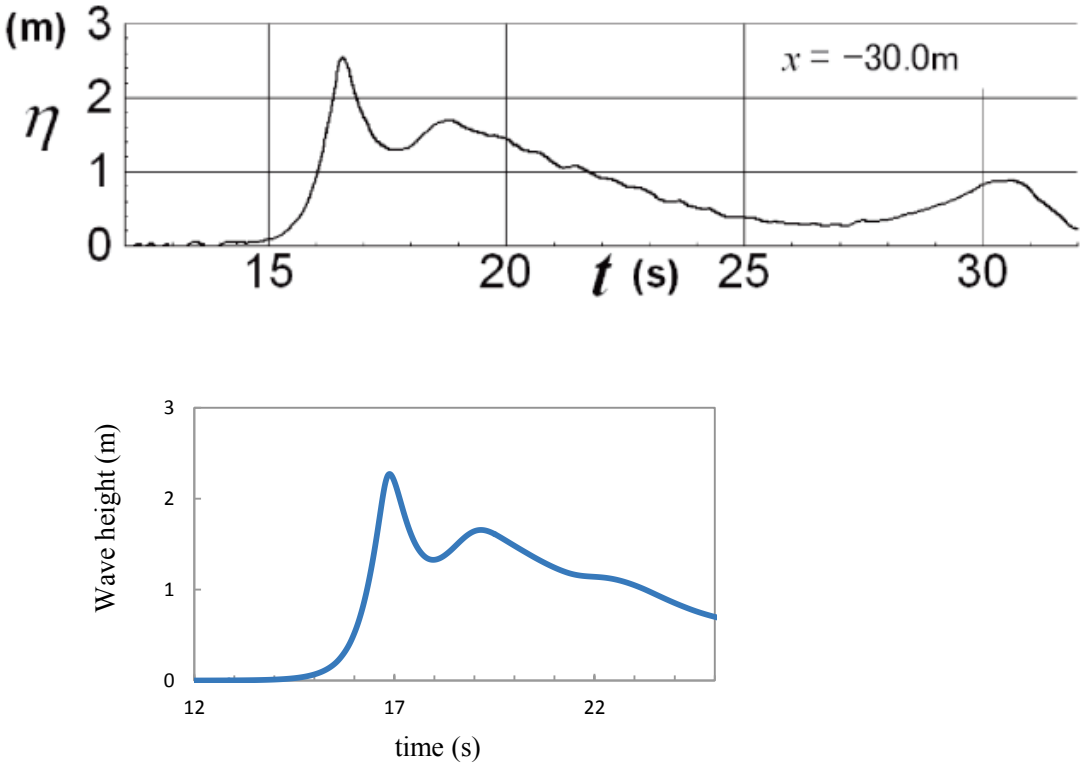

Fig. 5.7. Measured 30 m offshore wave height in the experiment (top) (Arikawa, 2009) and numerical (bottom) study

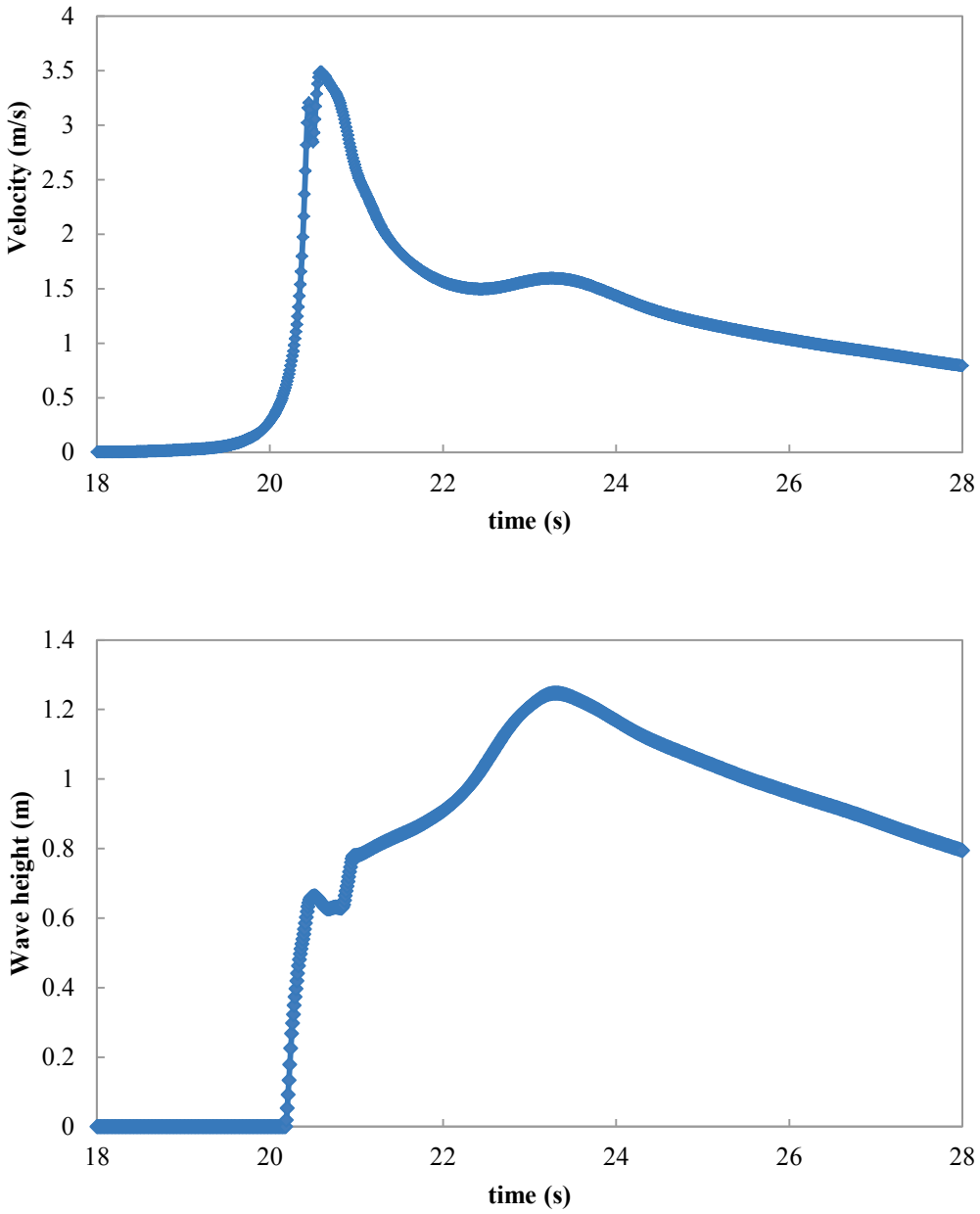

Fig. 5.8. Time variation of velocity measured at 20 cm above bed level (above) and wave height (below), measured at the location of the source for the FSI model, from the three-dimensional fluid model.

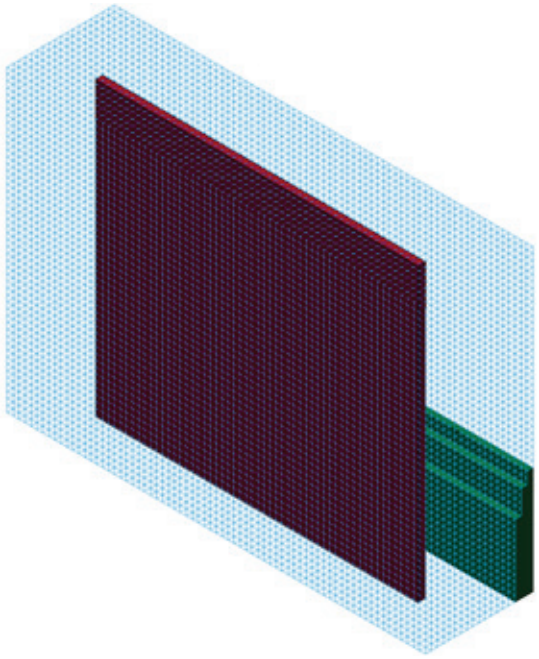

Fig. 5.9. Computational domain for numerical study

Two cases from the experiment study were considered in the numerical study, which are 60 mm and 80 mm thickness walls. The compressive strength of the concrete for each case is 21 N/mm^2 and 32.7 N/mm^2 respectively.

5.4.3 Results and discussion

The deformed ALE mesh at different time steps during the simulation is demonstrated in Fig. 5.10. In the study an erosion criterion for concrete is added for a principal tensile strain of 0.002, to start the crack generation. The criterion is helpful in visualizing the separation of the failed parts of the concrete wall due to the impact. It is clearly visible that the failure of the concrete wall occurs following the impact of tsunami and the damage is severe in the bottom of the wall.

Fig. 5.11 demonstrates the damage distribution for the 60 mm thick wall in the numerical simulation and compared it with the graphical result from the experiment. In the numerical simulation result of Fig. 5.11, the damage to the concrete is visualized as a function of effective plastic strain ε_p. The output value of ε_p varies between 0 and 2 and the value increase with the damage. Generally, primary damage is subjected to $\varepsilon_p > 1.95$, while $1.95 > \varepsilon_p > 1.85$ is considered to be as secondary damage (Malvar et al., 1997; Malvar et al., 2000). Numerical model accurately simulates the damage pattern from the experiment with identical damage pattern. Initial cracking starts from the bottom of the wall and then propagates completely

dissembling the bottom portion of the wall making a hole in rough shape of an arc. Cracking continues to propagate upward in the sides of the wall due to the bending failure at the supports, which is clearly visible in the numerical simulation results. At the same time, experimental observations indicate some damage in the top half of the wall and similar observations can be made from the numerical modeling results.

The failure pattern for the 80 mm thick wall slightly varies from the 60 mm wall. As shown in the Fig. 5.12 the failure starts at the bottom center part of the wall with the initial impact of the tsunami and spread out. But the damage area doesn't spread till the vertical supports as in the case of 60 mm wall. Moreover it can be observed that a failure line is forming along the vertical centerline of the wall which is caused due to the bending failure of the wall. Fig. 5.13 further compares the numerical simulation result for the damage with the failure pattern observed in the experiment. From the figure it can be seen that the numerical result closely agrees with the result observed at the real scale experiment.

Overall the numerical model accurately simulates the damage to the concrete wall by tsunami impact.

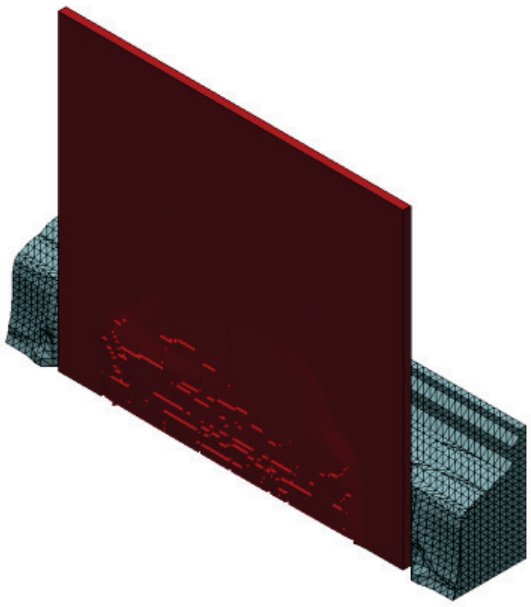

(a) $t = 0.18$ s

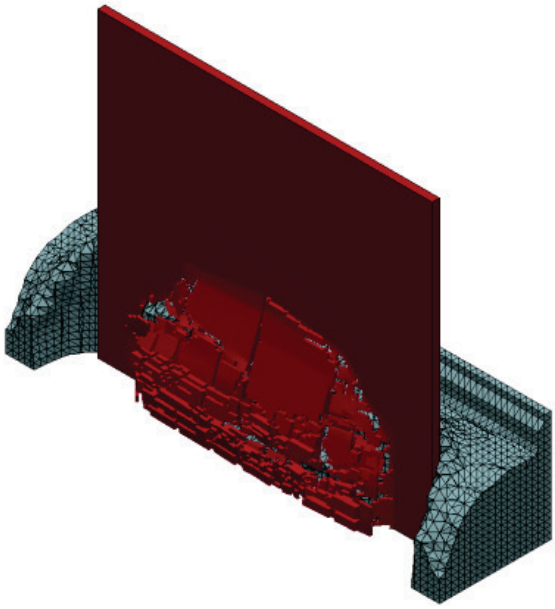

(b) $t = 0.24$ s

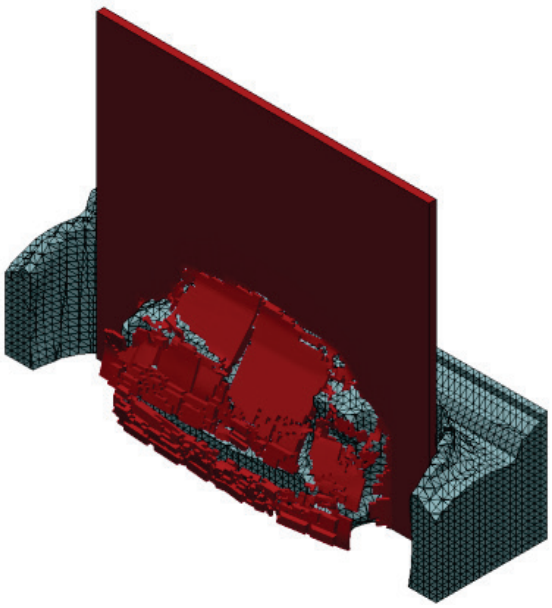

(c) $t = 0.28$ s

Fig. 5.10. Deformed ALE fluid mesh and the failure of concrete wall (60 mm thick) following the tsunami impact at different time steps

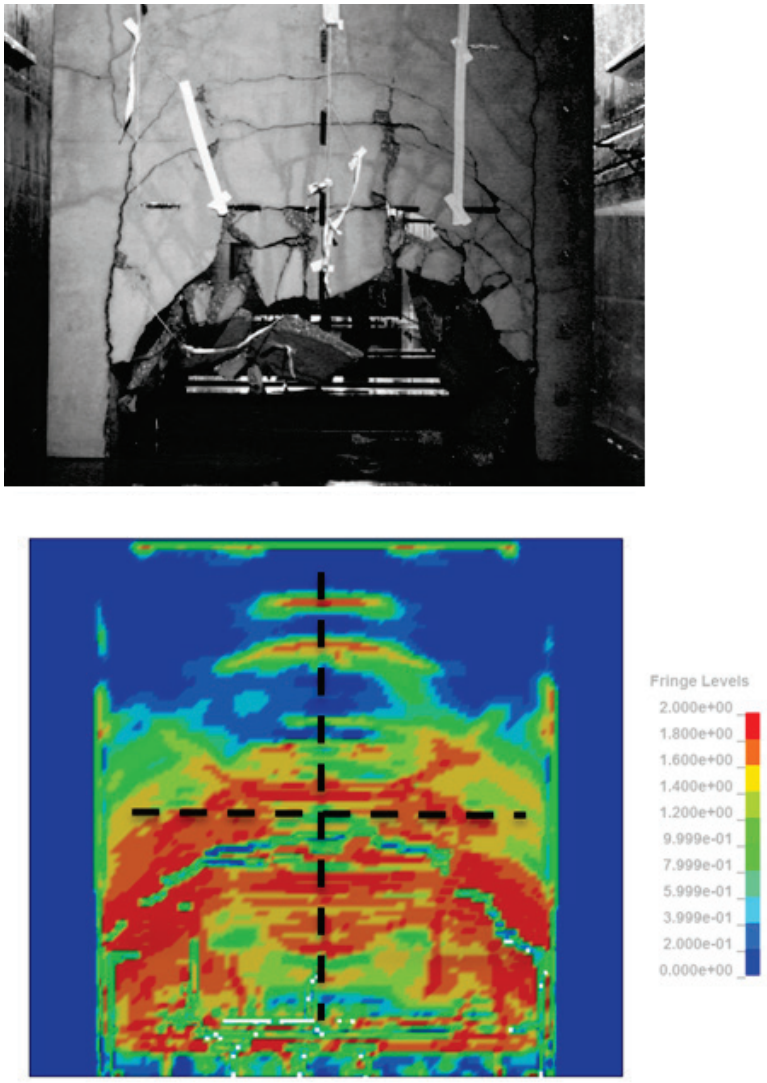

Fig. 5.11. Damage to the 60 mm thick concrete wall in the experiment (top) (Arikawa, 2009) and in numerical simulation (bottom)

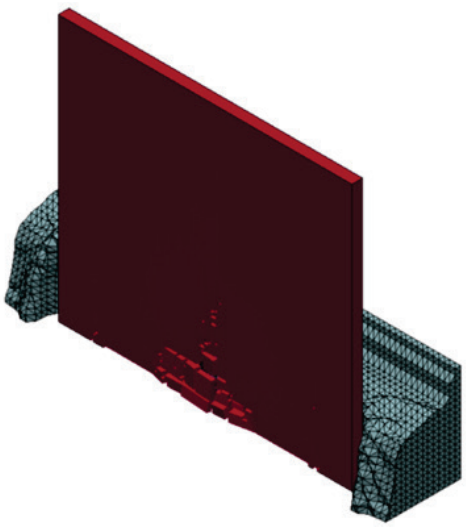

(a) $t = 0.14$

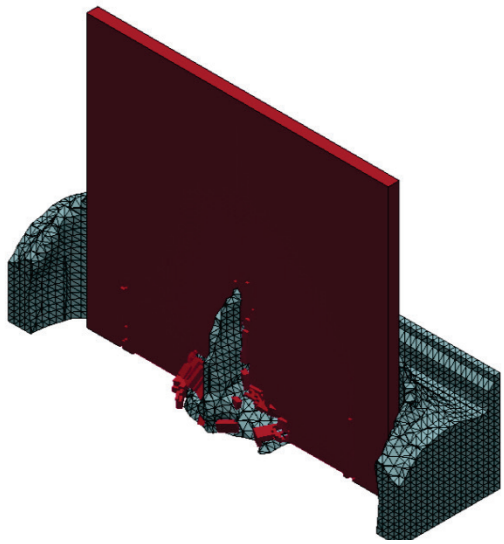

(b) $t = 0.20$

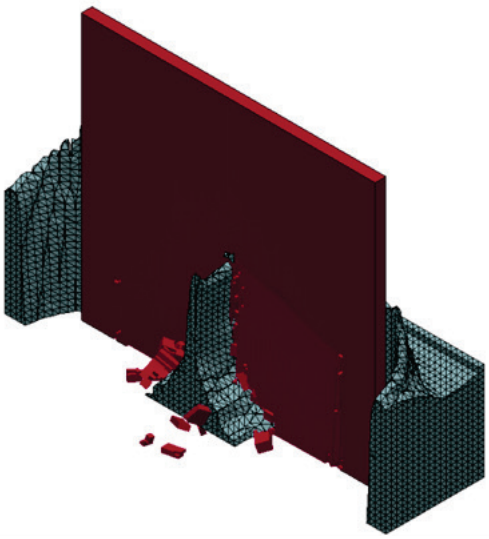

(c) $t = 0.28$

Fig. 5.12. Deformed ALE fluid mesh and the failure of concrete wall (80 mm thick) following the tsunami impact at different time steps

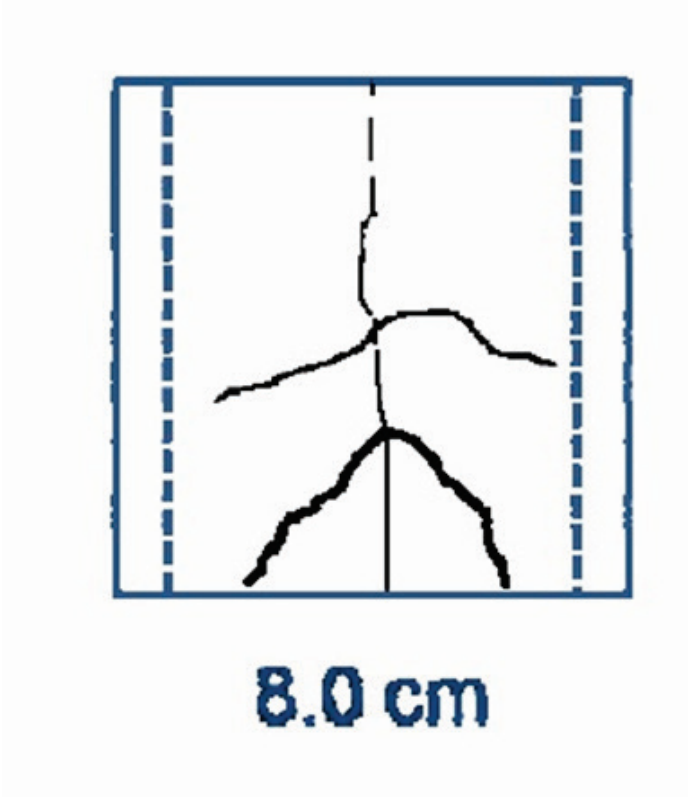

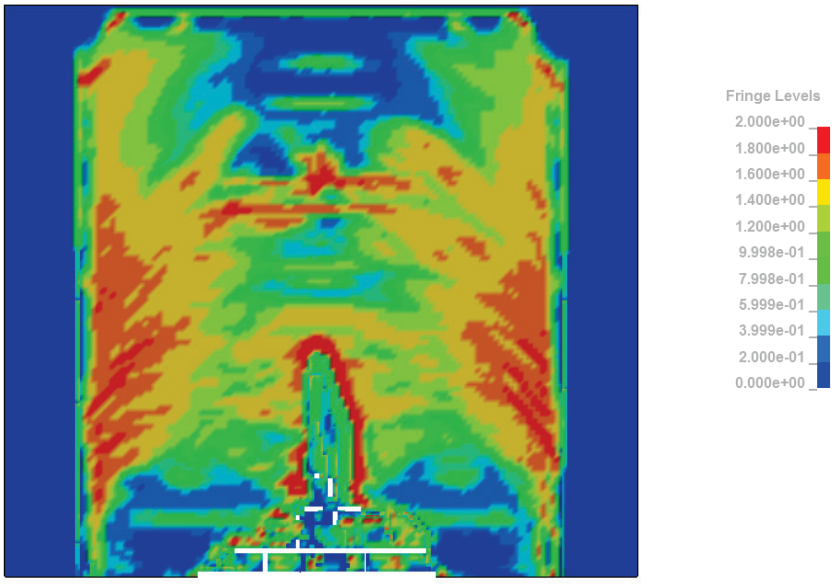

Fig. 5.13. Rough damage pattern to the 80 mm thick concrete wall in the experimemnt (top) (Arikawa, 2009) and damage observed in numerical simulation (bottom)

5.5 Tsunami Force on Enclosed Structures

When tsunami strikes into an enclosed structure such as a building with walls on either side of an opening, the impact force will be distributed into the lateral walls as

well. Such situations had been observed at number of occasions in recent tsunami events. Fig. 5.14 shows failure of a reinforced concrete lateral wall, observed in the aftermath of 2011 Tohoku tsunami. A numerical study was conducted to assess the force distribution to the lateral walls under such scenario. Fig. 5.15 shows the basic arrangement of the rigid structure considered in the analysis. The span of the structure (B) varied during the analysis, while the height of the structure (H =1 m) and the length of the side wall (D) keep unchanged. Accordingly, tsunami inflow conditions to the computational domain also kept unchanged for all the cases considered. Combinations of the test runs are shown in Table 5.3.

Fig. 5.14. Failure of a lateral wall in the 2011 Tohoku tsunami event. Location: Rikuzentakata, Iwate prefecture

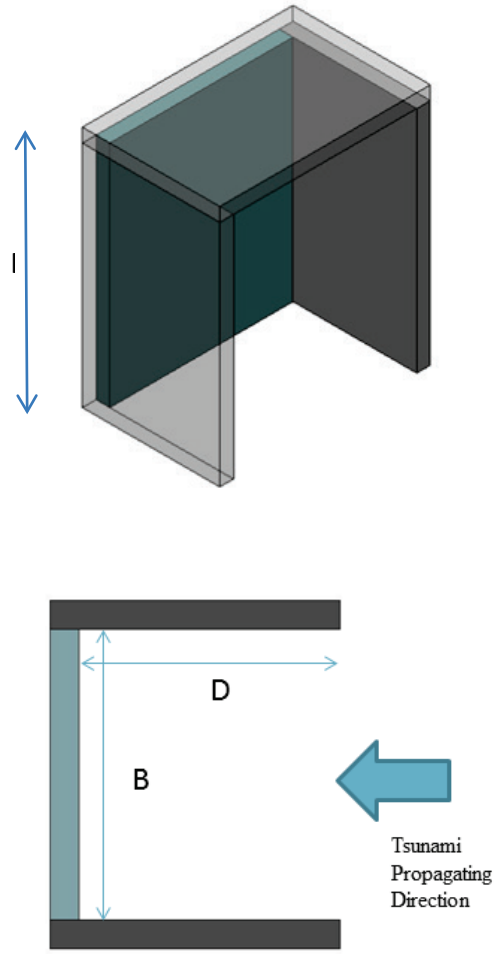

Fig. 5.15. 3D view of the structure arrangement (top); Top view of the arrangement without slab (bottom)

Table 5.3. Test cases

	B (m)	*D* (m)	*H*(m)
Case1	0.6	0.6	1.0
Case2	0.8	0.6	1.0
Case3	1.0	0.6	1.0

In the interaction of the wave with the structure (Fig. 5.14), it was make sure that the wave force acting on the lateral walls are only in the outward direction (minimum interaction of wave from the outside). In that way, the maximum possible force

normal to the wall was assured, which represented the critical condition. Simulations were conducted for both 'with top slab' (w/s) and 'without top slab' (n/s) conditions to assess fully and partially enclosed conditions. Slight convergence of tsunami front towards the center of the enclosed space is observed (Fig. 5.17 a) upon the initial interaction of flow with the front edge of the lateral wall. Following the collision with the main wall (i.e., wall normal to the flow direction) flow diverts in both horizontal and vertical planes, at which it starts to exert force on the lateral walls. Initial splash, which is moving upward along the main wall, is blocked by the top slab and water volume is retained inside the enclosed space. Because of this entrapment of fluid volume, it starts to pile additional force on the lateral walls.

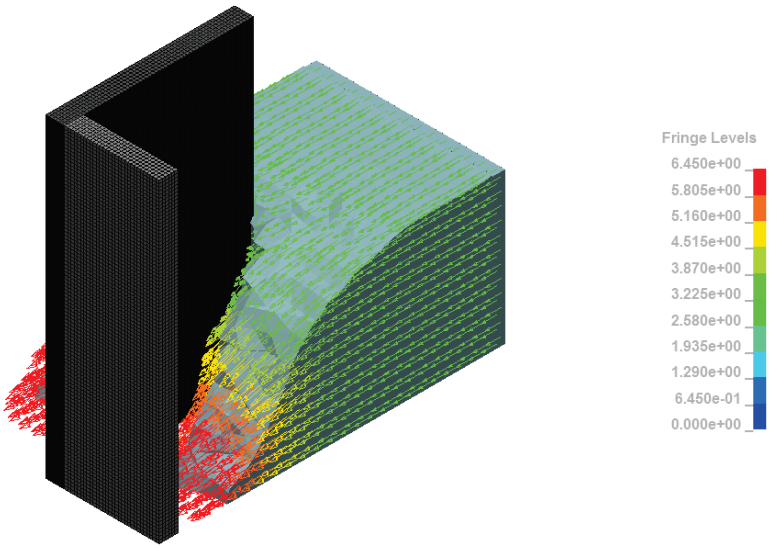

(a) $t = 0.2$ s

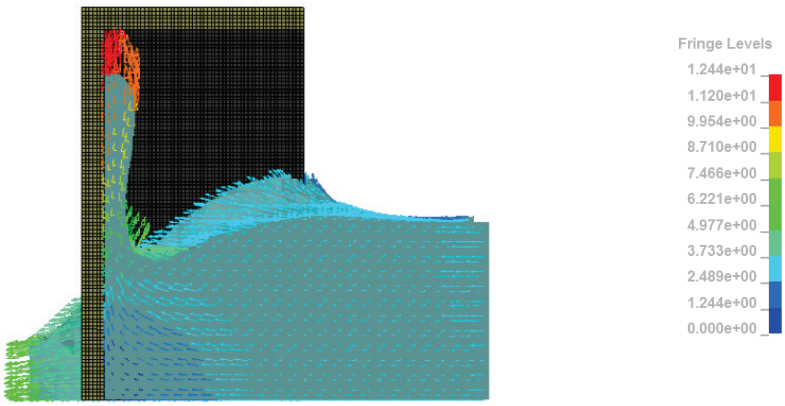

(b) $t = 0.3$ s

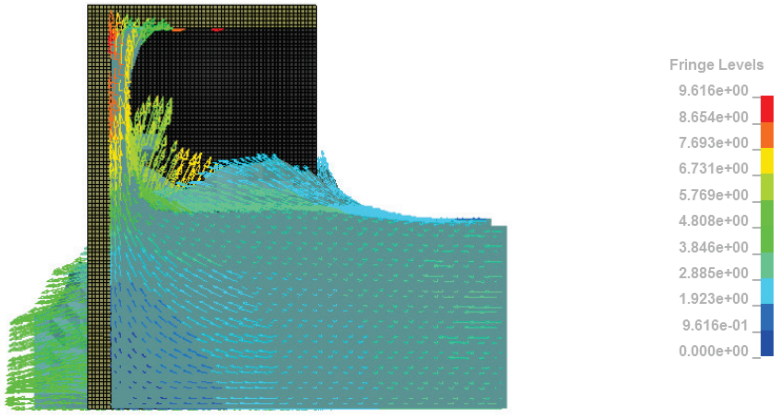

(c) $t = 0.35$ s

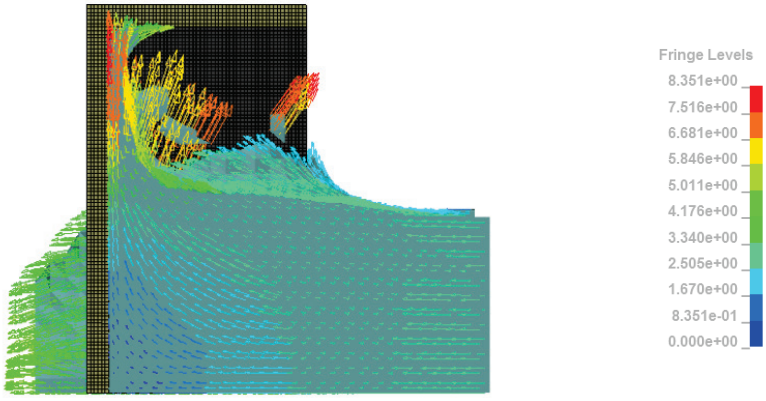

(d) $t = 0.37$ s

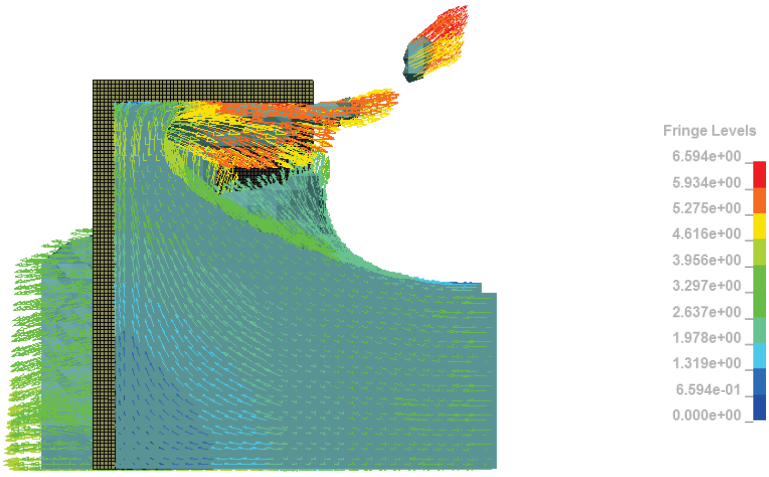

(e) $t = 0.46$ s

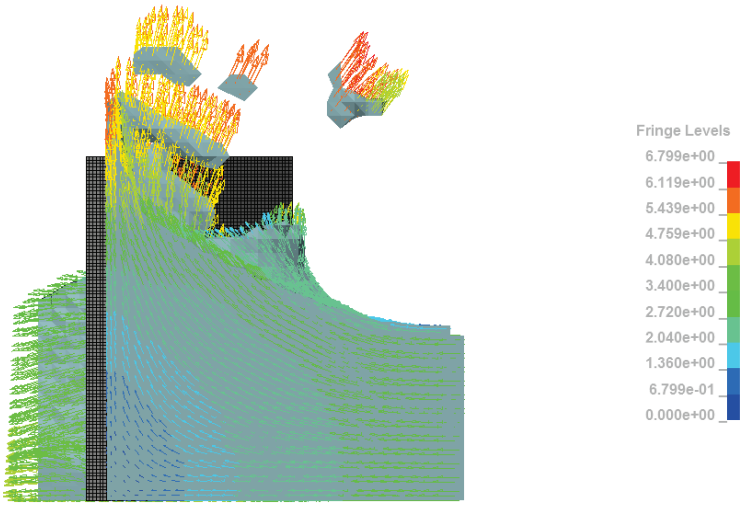

(f) $t = 0.46$ s

Fig. 5.16. Flow behavior with velocity vector plot along the vertical mid plane section for the w/s case (a, b, c, d & e) and for the n/s case (f)

The effect is clearly visible in the Fig. 5.18, which for a similar case, the force acting on the lateral wall drastically increase after around $t = 0.4$ s (time which the splash hits the top slab) for the fully enclosed case comparing to the n/s case. As it is indicated the maximum tsunami force on the lateral wall for the w/s case is almost double the value that of in n/s case. However, similar variation for the force can be observed for both cases for the time period prior to the time that up-going edge of the water profile hit the upper slab. At the same time it can be noticed that the influence of span of the structure (B) is negligible as the force history for the all the cases shows similar behavior in each partially and fully enclosed conditions. During the simulation, the main wall was considered to be rigid and no failure occurred under tsunami impact. The condition was applied in order to make sure the lateral walls went under the maximum possible force from the tsunami impact. In case of a failure of the main wall, the force acting on the lateral walls can be lower than the values observed in the analysis, due to the drop of pressure exerts by the fluid trapped inside the enclosure.

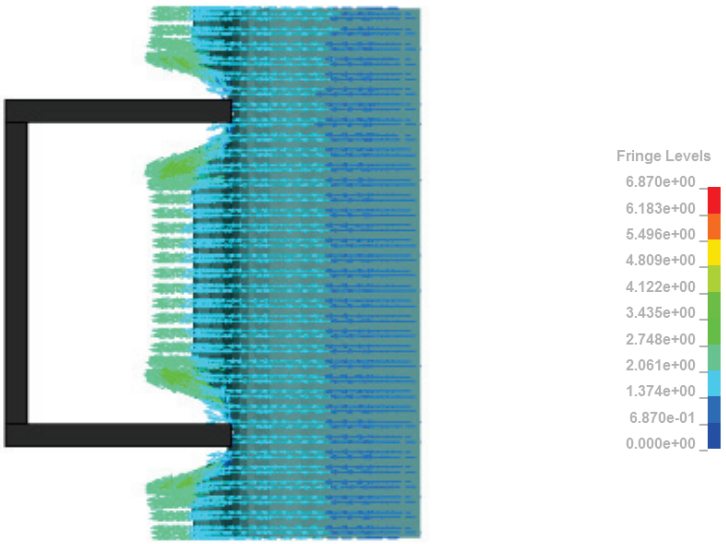

(a) t = 0.15 s

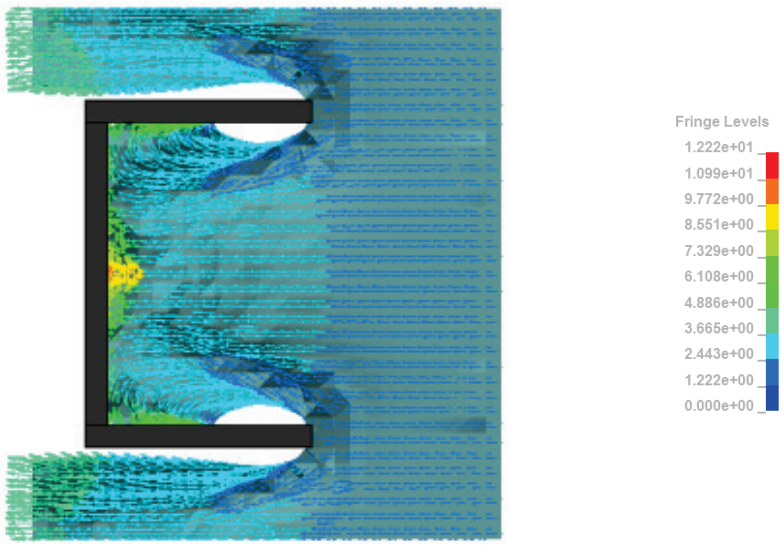

(b) t = 0.3 s

Fig. 5.17. Flow velocity vector plot during the interaction along horizontal cross section

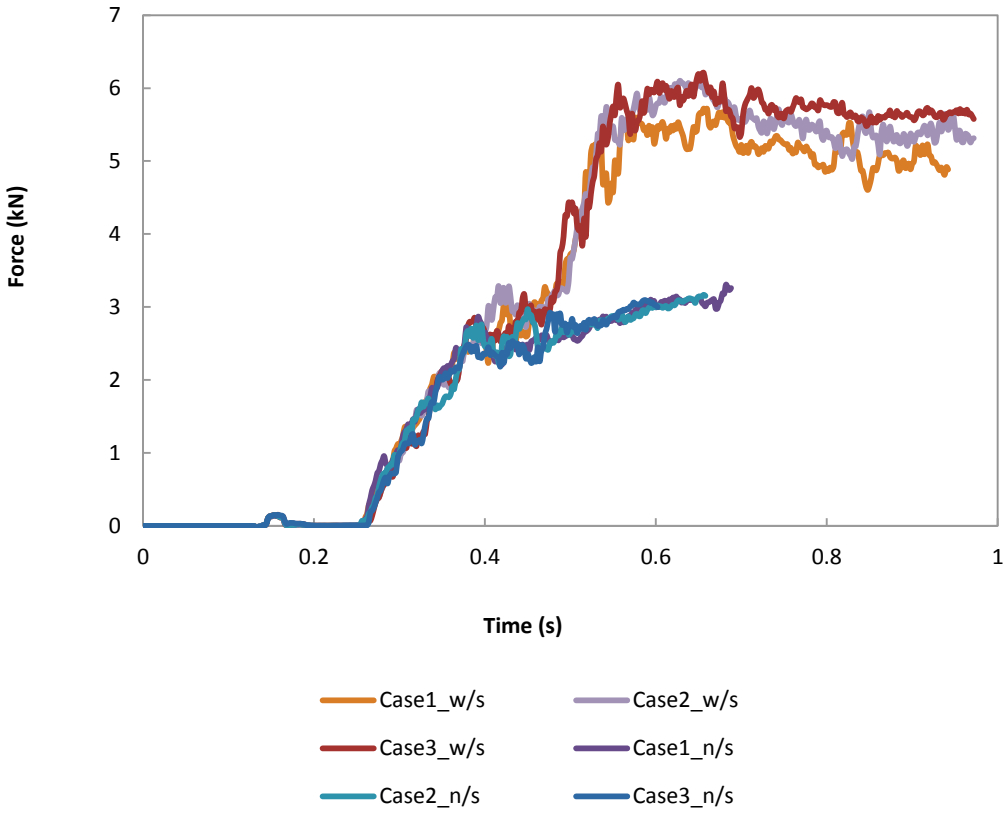

Fig. 5.18. Force acting on the lateral wall in perpendicular direction to the wall

5.6 Summary

The implemented fluid-structure interaction model effectively simulated the failure of a reinforced concrete wall under tsunami loading and the failure pattern was well captured compared to the real scale experiment results. Simulation can be adopted to assess the structural response of coastal structures against tsunami loading, which has high importance in aspect of structural design.

Tsunami force on the lateral walls of the enclosed structure with the top slab was estimated as almost doubled as it was for a case without a top slab.

Meanwhile the span of the enclosed structure had a negligible effect on the force on lateral wall. Further analysis should be carried out to understand the failure of lateral walls which aligned in parallel to the direction of tsunami propagation.

Chapter 6

DISCUSSION AND CONCLUSIONS

The damage to the coastal buildings in case of a tsunami event has been caused numerous problems in the past. Especially with the recent major tsunami events like 2004 Indian Ocean tsunami and the 2011 Tohoku earthquake tsunami, the vulnerability and the instability of the coastal buildings were exposed and the reliability of the existing tsunami force estimation guidelines has put under question mark. Since the different spatial arrangement of buildings had influenced to the failure of the buildings and structural components in different ways, the estimation of tsunami force for such buildings with different spatial arrangements, has to be assessed and still a satisfactory amount of research work has not been carried out in the particular area. The current study focused on the estimation of tsunami force on three-dimensional buildings with different structural configurations and assess the failure of reinforce concrete structures under tsunami loading.

Laboratory experiments were conducted in the hydraulic flume of the Department of Civil Engineering, Nagoya University. Tsunami force on a three-dimensional building model with different structural configurations was examined in the study and the experiment set-up and results are discussed in the Chapter 3. Through the observations it was found that the presence of openings in the building has a significant influence on the acting tsunami force on the building and the force decreases with the increase of opening area. Further, even for the same structural arrangement, tsunami force varied with the incoming tsunami flow condition at the location of the structure. Three flow conditions were created using long period waves and solitary waves generated by the piston type wave generator of the flume and it was found that generally breaking wave type has the highest impact force on the

structure than the bore type flow. At the same time, placing the inner walls of the ground floor of the building in the landward side of the structure was found to be effective in minimizing the total tsunami force acting on the structure. Further, two force estimation methods were assessed which were in the basis of whether or not opening area facing the tsunami propagation direction is considered in the pressure integration and it was found that there is no significant difference in both approaches. However, it was confirmed that it is possible to estimate the tsunami force assuming triangular pressure distribution in front of the structure, together with the opening ratio of the building. Further, in such estimation the height factor α which was used in estimation of effective height of pressure action, found to be varied with the different wave conditions for a safe estimation of tsunami force for the design purpose. Additionally, the general recommendation of $\alpha = 3$ (Asakura et al., 2000) found to be not effective under certain flow condition like breaking wave. Moreover, it was confirmed that the value of α decreases for the buildings with openings, compare to the above recommendation ($\alpha = 3$).

Moreover, numerical study was carried out to assess the effect of three dimensionality of the structure in the estimation of tsunami force on buildings like tsunami evacuation structures as suggested in Japanese Cabinet Office guideline (Cabinet Office, 2005) for the design of tsunami shelters. Since the recommendation of the guideline is based on the two-dimensional laboratory experiment conducted by Asakura et al. (2000), the effectiveness of the existing force estimation equation was examined in the study. The three-dimensional numerical model developed by Lee et al. (2000) was employed in the study and the procedure and results are presented in the Chapter 4. The term of the blockage ratio is introduced to represent the three-dimensional effect of the building and it was found that the tsunami force on the structure increases with the increase of blockage ratio. At the same time a triangular pressure distribution in the vertical direction was observed for both three-dimensional and two-dimensional cases, and hence the effect of flow velocity (hydrodynamic force component) found to be small in the estimation of the maximum tsunami force. Additionally, the pressure variation in the horizontal direction on the structure was closely uniform even though a slight variation was observed close to the edge of the structure. A modified equation for the calculation of maximum tsunami force acting on a rigid structure is proposed which include the effect of blockage ratio through a

correction factor β, and the effectiveness of the suggested formula for practical application was confirmed.

Even though the tsunami force estimations are carried out under the assumption of rigid structures, in practice, coastal buildings tend to show non-rigid behavior especially for the large and impulsive forces in the likes of tsunami. But the study of non-rigid structures and tsunami interaction has been a difficult area mainly because of its complex behavior, which basically limited most of the studies into physical experiments. But with the advancement of computational capabilities number of non-linear computation models has been developed which capable of modeling such complex physical phenomena. In the current study the applicability of three-dimensional non-linear finite element model LS-DYNA was assessed for the simulation of fluid-structure interaction (FSI). The Arbitrary Lagrange Eulerian (ALE) modeling capability available with LS-DYNA was employed in the study and the process and results are presented in Chapter 5. In order to avoid the one of major draw backs of ALE modeling, which is the high computational cost, a three-dimensional non-linear fluid model developed by Nakamura and Yim (2011) was employed to the simulation up to the FSI domain which consists of ALE elements. The wave parameters to the FSI domain input as a wave source and the effectiveness of such input method was also discussed. The applicability of the model in estimating tsunami force was confirmed by comparing with the experiment results.

The failure of a reinforced concrete wall under tsunami impact was assessed and the computational model results showed a good agreement with the real scale experiment results by Arikawa (2009). The Karagozian & Case (K&C) concrete model (release III) (Malvar et al., 2000; Schwer & Malvar, 2005) was employed in simulating the concrete material and the failure is observed through a graphical representation, as well as by in cooperating an erosion criteria on top of the concrete model. The output results from the both approaches showed a good agreement with the experiment results and the applicability of the model was confirmed. Further, the model was applied to estimate the tsunami force acting on a lateral wall of an enclosed building structure. It was found that the presence of top slab in an enclosed structure significantly increase the force on the lateral walls. Further, studies should be carried out to assess the failure conditions of a lateral wall in buildings and to understand the tsunami flow behavior under such circumstances.

As far as future studies are concerned, further investigations should be carried out to understand the failure of a complete building structure under tsunami loading. At the same time, it would be interesting to consider difference construction materials and study their influence to the failure mechanism and the failure pattern of the structure. Moreover, author suggest assessing the effect of having different physical shapes for the seaward side of the coastal building which can be helpful in minimizing the total force acting on the structure. Ultimately the study would target to develop a comprehensive guideline for the design of coastal buildings like tsunami shelters in the vulnerable areas.

REFERENCES

Abu-Odeh, A., 2008. Modelling and simulation of bogie impacts on concrete bridge rails using LS-DYNA. In *10th International LS-DYNA Users Conference*., 2008.

Aoki, S. et al., 2013. Experiment study on tsunami force acting on tsunami evacuation buildings and effect of configurations of building structure. *Journal of Japan Society of Civil Engineers, Series B2 (Coastal Engineering)*, 69(2). (revised) in Japanese.

Aquelet, N., Souli, M., Gabrys, J. & Olovson, L., 2003. A new ALE formulation for sloshing analysis. *Structural Engineering and Mechanics*, 16, pp.423-40.

Arikawa, T., 2009. Structural behavior under impulsive tsunami loading. *Journal of Disaster Research*, 4(6), pp.377-81.

Arikawa, T. et al., 2005. Large model test of tsunami force on a revetment and on a land structure. *Annual Journal of Coastal Engineering*, 52, pp.746-50. in Japanese.

Asakura, R. et al., 2000. An experimental study on wave force acting on on-shore structures due to overflowing tsunamis. In *Coastal Engineering*., 2000. JSCE.

Borvik, T., Hanssen, A.G., Langseth, M. & Olovsson, L., 2009. Responce of structures to planer blast loads - A finite element engineering approach. *Computers and Structures*, pp.507-20.

Cabinet Office, 2005. *The guideline concerning the tsunami evacuation building*. Cabinet office of Japanese Government.

Day, J., 2009. *Guideline for ALE Modeling in LS-DYNA*. Draft. LSTC.

El-Tawil, S., Severino, E. & Fonseca, P., 2005. Vehicle Collision with Bridge Peers. *Journal of Bridge Engineering*, 10(3), pp.345-53.

Fauzie, A., Shigihara, Y., Fujima, K. & Mizutani, N., 2009. A study on estimation of tsunami force acting on structures. *Journal of JSCE*, 65, pp.321-25.

Fujima, K., Achmad, F., Shigihara, Y. & Mizutani, N., 2009. Estimation of tsunamiforce acting on rectangular structure. *Journal of Disaster Research*, 4(6), pp.404-08.

Germano, M., Piomelli, U., Moin, P. & Cabot, W.H., 1991. A dynamic subgrid-scale eddy viscosity model. *Physics and Fluids A*, 3(7), pp.1760-65.

Hallquist, J.O., 1976. UCID-17268 *Preliminary user's manuals for DYNA3D and DYNAP (Nonlinear Dynamic Analysis of solids in three dimension)*. University of California.

Hallquist, J.O., 2006. *LS-DYNA Theory Manual*. Livermore Software Technology Corporation.

Hinrichsen, D., 1999. *The coastal population explosion*. Ocean and Coastal Stakeholders.

Hua, C. & Fang, C., 2011. Simulation of Fluid-Solid Interaction on Water Ditching of an Airplane by ALE Method. *Journal of Hydrodynamics*, pp.637-42.

Huertas-Ortecho, A.C., 2006. *Robust bird-strike modelling using LS-DYNA*. Master Thesis. University of Puerto Rico.

Iizuka, H. & Matsutomi, H., 2000. Estimation of damage due to tsunami current. *Annual Journal of Coastal Engineering*, 47, pp.381-85. in Japanese.

Ikeno, M. & Tanaka, H., 2003. Experimental study on impulse force of drift body and tsunami running upto land. In *Coastal Engineering*., 2003.

Ikeya, T. et al., 2005. Spatio-temporal variation of tsunami wave pressure acting on a land structure. *Journal of Civil Engineering in the Ocean*, 21, pp.121-26. in Japanese.

Imamura, F. & Anawat, S., 2012. Damage due to the 2011 Tohoku earthquake tsunami and its lessons for future mitigation. In *International symposium on Engineering Lessons Learned from the 2011 Great East Japan Earthquake*., 2012.

Lee, K.H., Mizutani, N. & Kang, Y.K., 2010. Applicability of 3D numerical wave tank to silt-type cassion breakwater with complex geometry. *Annual Journal of Civil Engineering in the Ocean*, 26, pp.69-74. in Japanese.

Lin, Y., 2002. Performance evaluation on the ALE formulation in MPP LS-DYNA. In *7th International LS-DYNA Users Conference*. Detroit, 2002.

Lukkunaprasit, P., Ruangrassamee, A. & Thanasisathit, N., 2009. Tsunami loading on building with openings. *Science of Tsunami Hazards*, 28(5), pp.303-10.

Magallanes, J.M., 2008. Importance of concrete material characterization and modelling to predicting the responce of structures to shock and impact loading. *Structures Under Shock and Impact*, 98, pp.241-50.

Malvar, L.J., Crawford, J.E. & Morill, K.B., 2000. *K & C concrete material model release III; Automated generation of material model input*. Karagozian & Case.

Malvar, L.J., Crawford, J.E. & Wesevich, J.W., 1997. A plasticity concrete material model for Dyna3D. *International Journal of Impact Engineering*, 873(19(9-10)), p.847.

Markovich, N., Kochavi, E. & Ben-Dor, G., 2011. An improved calibration of the concrete damage model. *Finite Elements in Analysis and Design*, 47, pp.1280-90.

Morishini, Y. & Vasilyev, O.V., 2001. A recommonded modification to the dynamic two-parametermixed subgrid scale model for large eddy simulation of wall bounded turbulent flow. *Physics and Fluids*, 13(11), pp.3400-10.

Nakamura, T., Kuramitsu, Y. & Mizutani, N., 2008. Tsunami Scour Around a Square Structure. *Coastal Engineering Journal*, 50(2), pp.209-46.

Nakamura, T., Mizutani, N. & Fujima, K., 2010. Three-Dimensional Numerical Analysis on Deformation of Run-up Tsunami and Tsunami Force Acting on Square Structures. In *Coastal Engineering*., 2010.

Nakamura, T., Nakashima, A. & Mizutani, N., 2013. Study on effects of the arrangement of rigid structures along coasts on landward buildings during tsunami. *Journal of Japan Society of Civil Engineers, Series B3 (Ocean Engineering)*, 62(2). in press.

Nakamura, T. & Yim, S.C., 2011. A nonlinear three-dimensional coupled fluid-sediment interaction model for large seabed deformation. *Journal of Offshore Mechanics and Arctic Engineering*, 133(3), pp.031103-1-031103-14.

Nakano, Y., 2008. Design load evaluation for tsunami shelters based on damage observations after Indian Ocean Tsunami. In *14th World Conference on Earthquake Engineering*., 2008.

Nishiyama, I., 2011. Building damage by the 2011 off the pacific coast of Tohoku earthquake and coping activities by NLIM and BRI collaborated with the administration. In *US-Japan Meeting on "Wind and Seismic Effects"*. Tsukuba, 2011.

Noble, C. et al., 2005. *Concrete model descriptions and summary of benchmark studies for blast effects simulations*. Lawrence Livermore National Laboratory, University of California.

Ohmori, M. et al., 2000. Numerical simulation of water level, velocity and wave force of the tsunami which overflow the perpendicular revetment. In *Costal Engineering*., 2000. JSCE. (in Japanese).

PINAC working group 53, 2009. *Mitigation of tsunami disaster in ports*. Draft. PINAC.

Sakakiyama, T., Matsuura, S. & Matsuyama, M., 2009. Tsunami Force Acting on Oil Tanks and Buickling Analysis for Tsunami Pressure. *Journal of Desaster Research*, pp.427-34.

Salvetti, M.V. & Banerjee, S., 1995. Apriori test of a new dynamic subgrid-scale model for finite deference large-eddy simulations. *Physics and Fluids*, 7(11), pp.2831-47.

Schwer, L.E. & Malvar, L.J., 2005. Simplified Concrete Modelling with *MAT_CONCRETE_DAMAGE_REL3. In *LS-DYNA Anwenderforum*. Bamberg, 2005.

Shuto, N., 1993. Tsunami Intensity and disasters. *Advances in Natural and Technological Hazards Research*, pp.197-216.

Smagorinsky, J., 1963. General circulationexperiments with the primitive equations. *Monthly weather review*, 91(3), pp.99-164.

Souli, M., 2010. ALE incompressible fluid in LS-DYNA. In *11th International LS-DYNA Users Conference*., 2010.

Souli, M., Ouahsine, A. & Lewin, L., 2000. ALE formulation for fluid-structure interaction problems. *Computer Methods in Applied Mechanics and Engineering*, pp.659-75.

Yasuda, T., Takayama, T., Mase, H. & Takeuchi, S., 2007. Stability of shelter tower at exertion of tsunami. *Annual Journal of Civil Engineering in the Ocean*, 23, pp.99-104. in Japanese.

Yeom, G., 2010. *Behavior of a container drifted by run-up tsunami and estimation method of its collison force*. PhD Thesis. Nagoya University.

Yeom, G., Nakamura, T. & Mizutani, N., 2009. Collision analysis of container drifted by runup tsunami using drift collision coupled model. *Journal of Disaster Research*, 4(6), pp.441-49.

Yim, C.S. & Zhang, W., 2009. A multiphysics multiscale 3-D computational wave basin model for wave impact load on a cylindrical structure. *Journal of Disaster Research*, 4(6), pp.450-61.

Zang, Y., Street, R.L. & Koseff, J.R., 1993. A dynamic mixed subgrid-scale model and its application to turbulent recirculating flows. *Physics and Fluids A*, 5(12), pp.3186-96.

Zhang, A. & Katsuyuki, S., 2007. A comparative study of numerical simulations for fluid-structure interaction of liquid-filled tank during ship collision. *Ocean Engineering*, pp.645-52.

Chathura Manawasekara

Doctoral Candidate, Nagoya University
Telephone: +819064695758; **Email**: chathuradm@hotmail.com
City Haitsu Higashiyama 604, Higashiyama-dori, Chikusa-ku, Nagoya, 464-0807, Japan

Education

- Doctor course in Civil Engineering (2010-present), Nagoya University
- Master of Science (2008-2010), University of Moratuwa, Sri Lanka
- Bachelor of Science in Engineering (2004-2008), University of Moratuwa

Publications

Journal Paper

1. Manawasekara, C., Aoki, S., Lee, K., Mizutani, N., Hirakawa, N. and Ashizawa, A. : "Effect of Three-Dimensionality on Tsunami Force Acting on a Structure", Journal of Japan Society of Civil Engineers, Series B3 (Ocean Engineering), JSCE, Vol. 69, No. 2, in press (June 28, 2013).
2. Manawasekara, C., Mizutani, N., Nakamura, T. and Aoki, S. : "Failure of Concrete Structure under Tsunami Loading", Journal of Japan Society of Civil Engineers, JSCE, (submitted, No. B2-E0005).
3. Aoki, S., Manawasekara, C., Mizutani, N., Hirakawa, S. and Ashizawa, A. : "Experimental Study on Tsunami Force acting on Tsunami Evacuation Buildings and Effect of Configurations of Building Structure", Journal of Japan Society of Civil Engineers, Series B2 (Coastal Engineering), JSCE, Vol. 69, No. 2 (2013) (Accepted).

Conference Proceedings:

1. C. Manawasekara, N. Mizutani, "Simulation of Tsunami Interaction with On-land Structure", Proc. 14th Intl. Summer Symp., JSCE, Nagoya, pp. 57-58, 2012.